February 2017

Master's Degree Thesis

Rain Attenuation Characteristics for Terrestrial and Satellite Links in the South Korea

Graduate School of Chosun University

Department of Information and Communication Engineering

Sujan Shrestha

Rain Attenuation Characteristics for Terrestrial and Satellite Links in the South Korea

February 24, 2017

Graduate School of Chosun University

Department of Information and Communication Engineering

Sujan Shrestha

Rain Attenuation Characteristics for Terrestrial and Satellite Links in the South Korea

Advisor: Prof. Dong-You Choi

This thesis is submitted to Graduate School of Chosun University in partial fulfillment of the requirements for a Master's degree in Engineering

October, 2016

Graduate School of Chosun University

Department of Information and Communication Engineering

Sujan Shrestha

This is to certify that the master's thesis of

Sujan Shrestha

has been approved by examining committee for the thesis requirement for the Master's degree in engineering.

Committee Chairperson _____

Prof. Seun-Jo Han

Committee Member_____

Prof. Jae-Young Pyun

Committee Member_____

Prof. Dong-You Choi

November, 2016

Graduate School of Chosun University

Table of Contents

List of Figures

List of Tables

Acronyms

ITU-R P. 837-6	:	Characteristics of precipitation for propagation modeling
ITU-R P. 618-12	:	Propagation data and prediction methods required for the design of earth-space telecommunication systems
ITU-R P. 530-16	:	Propagation data and prediction methods required for the design of terrestrial line-of-sight systems
ITU-R P. 838-3	:	Specific attenuation model for rain in prediction methods
ITU-R P. 311-15	:	Acquisition, presentation and analysis of data in studies of tropospheric propagation
CCDF	:	Complementary Cumulative Distribution Function
LOS	:	Line-Of-Sight
KMA	:	Korea Meteorological Administration
RRA	:	National Radio Research Agency
DSD	:	Drop Size Distribution
1-min. rain rate CCDF	:	1-minute rain rate CCDF
5-min. rain rate CCDF	:	5-minute rain rate CCDF

10-min. rain rate CCDF	:	10-minute rain rate CCDF
20-min. rain rate CCDF	:	20-minute rain rate CCDF
30-min. rain rate CCDF	:	30-minute rain rate CCDF
60-min. rain rate CCDF	:	60-minute rain rate CCDF
GIS	:	Advanced Geographic Information Systems
$\boldsymbol{R_1(P)}$	:	1-minute rain rate
$\boldsymbol{R_\tau(P)}$	:	τ-minute rain rate
$\boldsymbol{\rho_\tau(P)}$	:	conversion factor
ERSC	:	Excell Rainfall Statistics Conversion
$\boldsymbol{r}$	:	reduction factor
$\boldsymbol{\gamma_R}$	:	specific attenuation in dB/km
$\boldsymbol{d_{eff}}$	:	effective radio path length
$\boldsymbol{d}$	:	radio path length
$\boldsymbol{d_0}$	:	equivalent rain cell diameter
$\boldsymbol{R_{0.01}}$	:	rain rate at 0.01% of the time
$\boldsymbol{R_{eff}}$	:	effective rain rate
$\boldsymbol{R_{\%p}}$	:	rain rate at %p of the time
$\boldsymbol{A_{\%p}}$	:	attenuation at %p of the time

$A_{0.01}$	: attenuation at 0.01% of the time
DAH	: Dissanayake, Allnutt, Haidara
SAM	: Simple Attenuation Model
LNBC	: Low Noise Block Converter
$\varepsilon\,(P)_T$	: relative error percentage
SD	: Standard Deviation
RMS	: Root Mean Square
χ^2	: chi-square statistic
RSL	: Receive Signal Level
L_{fs}	: free space loss

Abstract

Rain Attenuation Characteristics for Terrestrial and Satellite Links in the South Korea

Sujan Shrestha
Advisor: Prof. Dong-You Choi, Ph.D.
Department of Information and
Communication Engineering,
Graduate School of Chosun University

Attenuation induced due to rain is a prime concern in transmission of microwave signals. The revolution observed in communication technology has resulted in a pressing need for larger bandwidth, higher data rate and better spectrum availability. This has focused the research community to investigate higher electromagnetic spectrum space. The effect of rain attenuation is more pronounce when signals are being transmitted at higher frequencies. To optimize the use of microwave (3~30 GHz) and millimeter wave (30~300 GHz), the three tiers of communication system as such receiver, transmitter, and transmission medium must be properly designed and configured. However, the transmission medium becomes an issue at this range of frequencies. The significant factor that accounts for the degradation of the signal quality at this range of frequencies is resulted due to the effect of rainfall. Scattering and absorption by rain at microwave and millimeter bands is the prime concern for system designers. The International Telecommunication Union Radio wave propagation models (ITU-R.P) were used in the investigation of the propagation impairments. The study is divided into three

parts. In the first part of this thesis, different rain rate computation methods will be presented. The experimental 1-minute rainfall amount data which are provided by Korea Meteorological Administration (KMA) of 93 different stations for a decade period from 2004 till 2013 are processed according to the prominent models and the suitable method is proposed. The analyses are primarily focus on nine major cities of the South Korea. The applicable rain rate contour plot at 0.01% of the time is developed using Kriging interpolation method through the advanced Geographic Information Systems (GIS) tools. Secondly, the study presents results of research into the interaction of rainfall with microwave propagation in 18, 38, and 75 GHz links in Icheon region of the South Korea. The study of rainfall characteristics allows for the estimation of rain induced attenuation in the presence of microwave and millimeter waves. The component of this work incorporate the study of rain drop size distribution and modeling of appropriate method for the estimation of rain attenuation in time percentage ranging from 1% to 0.001% of the time. In addition, the suitability of frequency and polarization scaling method as mentioned in ITU-R P. 530-16 are analyzed against the experimental database. Thirdly, study investigates the effect of propagation impairments such as rain on satellite communication link on earth-space path for frequencies of 12.25 and 20.73 GHz under circular polarization for Koreasat 6 and 19.8 GHz under vertical polarization for COMS1 (Communication, Ocean and Meteorological Satellite) in Mokdong station of the South Korea. The collection and analysis of meteorological data obtained for the period of 3 years from 2013 till 2015 as received from National Radio Research Agency (RRA) were performed to form statistics on diurnal, monthly and annual basis. The prominent propagation models applicable for slant path communication link were selected to calculate the attenuation distribution for a specified time percentage ranging from 1% to 0.001% of the time. The suitable technique is proposed which shows reliable estimation against the available local experimental database. Additionally, the regression coefficient used for the

calculation of specific rain attenuation and the frequency scaling method as mentioned in ITU-R P. 618-12 are studied. Finally, the results are statistically analyzed through the several error matrices as well as from ITU-R P. 311-15 recommendations.

요 약

국내 지상 및 위성 링크의 강우감쇠 특성에 관한 연구

Sujan Shrestha

지도교수: 최동유

조선대학교 대학원 정보통신공학과

강우로 인한 마이크로파 신호의 감쇠는 매우 중요한 문제이다. 통신기술은 넓은 대역폭, 높은 전송률 및 스펙트럼 가용성 등에 대한 필요성으로 인해 급속도로 발전하였다. 높은 주파수의 신호일수록 강우로 인한 감쇠는 더욱 두드러지며, 마이크로파(3 ~ 30 GHz)와 밀리미터파(30 ~ 300 GHz) 경우 수신기, 송신기 및 전송 매체의 적절한 설계와 구성이 필요하다. 높은 주파수 신호의 열화에 가장 중요한 인자는 강우로 인한 감쇠이다. 따라서 마이크로파 및 밀리미터파 대역의 강우로 인한 산란과 흡수는 시스템 설계자의 주요 관심사이며, 국제전기통신연합(ITU-R)의 전파예측 모델을 많이 활용하고 있다.

본 논문에서는 세 부분으로 나누어 연구를 수행하였다.

첫째, 강우율 산출을 위하여 기상청으로부터 2004 ~ 2013 년까지의 93 개 지역 1 분 강우량 데이터를 제공받아 기존 모델과 본 논문에서 제안한 방식을 통해 시간율에

따른 강우강도를 분석하였다. 0.01%의 시간율에 해당되는 강우율 등고선 플롯은 지리정보시스템 툴의 크리깅 보간법을 활용하였다.

둘째, 이천 지역에 설치되어 있는 18 GHz, 38 GHz 및 75 GHz 대역의 지상망을 대상으로 마이크로파와 강우량과의 상호 작용에 대해 연구하였으며, 강우 특성은 마이크로파와 밀리미터파의 강우로 인한 감쇠를 통하여 평가할 수 있다. 0.001% ~ 1%의 시간율에 대한 강우감쇠 평가를 위해 빗방울 크기 분포 분석과 적절한 방식의 모델링도 포함되어 있다. 또한 ITU-R P. 530-16 의 편파 스케일링 방법의 적합성을 판단하기 위하여 실제 측정한 데이터와 비교 및 분석하였다.

셋째, 목동 지역에 설치되어 있는 12.25 GHz 및 20.73 GHz 대역의 원형편파 특성을 갖는 무궁화 위성 6 호와 19.8 GHz 대역의 수직편파 특성을 갖는 COMS1 의 위성망에 대해 강우감쇠 특성을 연구하였다. 이에 대해 국립전파연구원(RRA)으로부터 3 년간(2013 년 ~ 2015 년)의 자료를 제공받아 연구를 수행하였다.

또한 ITU-R P. 618-12 의 주파수 스케일링 방법과 강우감쇠 예측값을 실측값과 회귀분석을 수행하였으며, ITU-R P. 311-15 강우감쇠에 대한 예측 방법에 대해서도 실측값과 통계적으로 분석하였다.

I. Introduction

A.Overview

In recent years, the implementation of millimeter radio communication systems has seen a remarkable increase. The utilization of millimeter waves for communication are attractive because it offers the promise of large bandwidth, provide ample radio frequency spectrum and high gain. Congestion at lower frequency bands and the increased use of digital techniques have made it necessary for communication service providers to move for higher frequency bands. However, atmospheric losses primarily caused by rain, impose some limitations on the application of millimeter waves. These waves are attenuated by atmospheric absorption and scattering which results in the degradation of signal amplitude and phase change. The method of predicting rain attenuation in terrestrial and satellite links, largely depend on the knowledge of 1-min. rain rate distribution. The estimation of rain attenuation need to be carried out at lower integration time, particularly, 1-min. interval, in accordance to International Telecommunication Union (ITU-R P.618-12[1] and ITU-R P. 530-16[2]). However, meteorological departments, all over the world, collect rain rate data at an hourly or longer integration time basis. Several efforts have been carried out by different groups working in the field to derive rain rate at shorter integration time. Generally, the conversion methods are grouped into three broad classes, namely, physical, analytical and empirical models[3]. The empirical methods are used extensively to convert higher integration time to lower equivalent because of its simplicity and experimental dependent. The prominent empirical methods are studied to discuss 1-min. rain rate pattern in the South Korea and ultimately, a new method is proposed that is seen to be suitable in

the local environment. The prediction of ITU-R P. 837-6[4] is studied, which is considered as a good approach in determination of 1-min. rain rate distribution. Furthermore, rain contour maps for rainfall rate at 0.01% of exceedence have been developed which shall be helpful for the system designers, site engineers and network planners in order to estimate appropriate fade margins due to rain attenuation. In this research, the contour map was developed using the advanced Geographic Information Systems (GIS) tools with the adoption of Kriging interpolation method that is used for spatial interpolation of rain rate values at 0.01% of time into a regular grid in order to obtain a highly consistent and predictable rainfall variation. In second step of research, rain attenuation is studied in microwave transmission system for 18, 38 and 75 GHz links set up in Icheon region. The lower frequency band, 18 GHz links for horizontal and vertical polarization are considered to study the effect of rain attenuation for two polarizations. Several prominent rain attenuation models are studied and the research proposed the simplified model of equivalent rain cell and additionally with the concept of an effective rain rate. Furthermore, the prediction error obtained from the application of ITU-R P. 530-16[2] approach have been studied and additional suitable margin are proposed for mentioned terrestrial links. The final step of research lies on the study of rain attenuation in the satellite communication links for 12.25, 19.8 and 20.73 GHz. The growing demand of advanced technology services such as broadband wireless access, local multipoint distribution service requires the use of millimeter and microwave communication systems that utilizes the Ku-band (14/12 GHz) and Ka-band (30/20 GHz)[5]. The higher frequency band namely, Ka-band are more attractive not only for the deployment of the new systems that are fruitful for advance communication technologies but also due to the congestion occurred in the lower frequency band. However, the links propagated through the higher frequency bands suffer more impairment due to rain, in terms of quality and

availability objectives. The severity of rain impairment increases with frequency and varies with regional location. In this regard, satellite communication system designers requires the need for reliable 1-min. rain rate data of high spatial resolution for various exceedance probabilities which in turns is used for the prediction of rain induced attenuation. This shall be helpful for predicting rain induced attenuation for designing in the absence of real-time measurement of rain attenuation. As in the previous cases, in order to determine suitable prediction models in the satellite communication links, we have considered the effective path length which is related to rain rate at 0.01% of the time with power law expression. In addition, the monthly and diurnal variation of rain rate and rain attenuation are studied which provides suitable values of regression coefficients for ITU-R P. 838-3[6] recommendation. The frequency scaling approach as mentioned in ITU-R P. 618-12[1] and ITU-R P. 530-16[2] recommendations are tested with the available experimental results. The performance of selected rain rate and rain attenuation models are tested mainly on Relative error percentage, Standard Deviation, Root Mean Square values and ITU-R P. 311-15[7] recommendation.

B.Objective of Research Project

The primary objective of study is to perform the prediction and comparative analysis on the results of rain attenuation and rain rate values collected in the South Korea. The 1-min. rain rates derived from the experimental 1-min. rainfall amount are compared with prominent empirical methods and research proposes the applicable contour maps for rain rate distribution at 0.01% of the time for the South Korea regions. In addition, the cumulative distribution of measured rain attenuation and rain rate are compared to applicable prominent prediction models for terrestrial and satellite communication links. Furthermore, the accuracy of the prediction of rain attenuation

are studied with existing frequency scaling method as presented in ITU-R P. 618-12[1] and ITU-R P. 530-16[2] as well as polarization scaling method as depicted in ITU-R P. 530-16[2].

C.Scope of Study

It indicates the basic guidelines and techniques required to meet the requirement of research which signifies that the work done stays within the intended study. As an initial step, the 1-min. rain rate distribution is studied by maintaining the 1-min., 5-min., 10-min., 20-min., 30-min. and 60-min. rain rate distribution pattern from available experimental 1-min. rainfall amount which is measured for a decade period from 2004 till 2013, as provided by KMA. Furthermore, the studies are performed to estimate propagation impairments induced by rain in terrestrial and satellite links at selected location in the South Korea for Icheon and Mokdong regions respectively whose database are provided by RRA for three year from 2013 till 2015.

D.Structure of Thesis

The organization of this thesis is maintained into five chapters which are outline as follows:

Chapter 1 gives the introduction of this research study which shows the overview, objective of research project, scope of study and the structure of thesis.

Chapter 2 focuses on the literature review which presents brief description on prominent 1-min. rain rate modeling methods as well as rain attenuation prediction approaches for terrestrial and satellite communication links and the new methods are generated for the South Korea regions. At the end to the chapter, the established frequency and polarization scaling of rain attenuation are discussed along with the uniqueness of each type of operating frequencies.

Chapter 3 explains the experimental methodology procedure of research project which signifies

data that were obtained from KMA for 1-min. rainfall amount and RRA for 1-min. rain rate distribution. The performance evaluations of prominent rain rate modeling have been performed through several statistical measures.

Chapter 4 discusses the attenuation induced by rain in terrestrial microwave links for 18, 38 and 75 GHz operating frequencies along with the experimental setup and evaluation of terrestrial rain attenuation prediction models.

Chapter 5 highlights the study of attenuation induced in slant path communication link for satellite communication system set up for 19.8, 12.25 and 20.73 GHz links. The performance evaluations are done for prominent rain attenuation prediction models applicable in slant path links for satellite communication.

Chapter 6 provides conclusion of the study, followed by recommendations for future work.

II. Literature Review

Rain rate modeling is a preferential component for estimating rain attenuation along a communication link. The attenuation induced due to rain is predicted from the mathematical combination of cumulative distribution of rain rate, which is a function of integration time. The primary causes of attenuation on electromagnetic wave propagation paths are resulted due to liquid water in the atmosphere in the form of rain. Hence, the simultaneous measurement of rain rate and rain attenuation is required on terrestrial line of sight paths between antennas located on the surface of Earth or between satellites and Earth terminals[3]. The main variable in the terrestrial link design are the available frequency band, the location of link end points, gains of antenna, transmitter power and receiver characteristics[8]. The rain is considered as a principal attenuating medium on slant paths for satellite communication links where the initial step in any attenuation prediction process is to obtain either the experimental 1-min. rainfall rate statistics for the mentioned site or an accurate prediction of those cumulative statistics. Furthermore, the slant path rain attenuation prediction model creates the effective path length over which the rain rate can be quantified and the required attenuation is calculated[9]. The following section review some contributions of many researchers in the area of 1-min. rain rate distribution, rain attenuation in terrestrial and microwave links.

A.1-min. Rain Rate Distribution

The conversion methods are grouped into two different approaches. The first approach involves the use of equivalent rain rates whereas second approach is based on the same probability of occurrence. The further research considers the latter approach for conversion purpose due to is

simplicity as compared to the former approach. Generally, the models covered include physical, analytical and empirical models. The brief overviews of the equal probability conversion techniques based on empirical nature are listed as follows:

A.1.Segal Method

This method was developed from high resolution rainfall records which are prepared at the Communications Research Centre for ten years of daily tipping bucket rain gauge charts of the 47 stations in Canada. The conversion method is expressed as[10]:

$$\boldsymbol{R_1(P) = \rho_\tau (P) R_\tau (P)} \quad \text{(A. 1)}$$

where conversion factor, $\boldsymbol{\rho_\tau (P) = aP^b}$, and parameters $\boldsymbol{a}$ and $\boldsymbol{b}$ are regression coefficients that are derived from statistical analysis of rainfall data.

A.2.Burgueno et al. Method

This method is derived from the 49 years of rainfall data measured at Barcelona, Spain. This used direct power law fit which is expressed as[11]:

$$\boldsymbol{R_1 (P) = a R_\tau^b (P)} \quad \text{(A. 2)}$$

where $\boldsymbol{a}$ and $\boldsymbol{b}$ represent the conversion variables obtained from statistical analysis of rainfall data.

A.3.Chebil and Rahman Method

This method is based on the experimental technique for estimating the precipitation rate conversion element by using the conversion process from 60-min. to 1-min. integration time, which is given as[12]:

$$\boldsymbol{\rho_{60}\,(P)} = \frac{\boldsymbol{R_1(P)}}{\boldsymbol{R_{60}\,(P)}} \tag{A. 3}$$

where $\boldsymbol{R_{60}\,(P)}$ is the precipitation rate in 60-min. integration time. $\boldsymbol{\rho_{60}\,(P)}$ is expressed as a mixed Power-Exponential Law, $\boldsymbol{\rho_{60}\,(P) = aP^b + ce^{(dP)}}$ with regression variables represented by $\boldsymbol{a}$, $\boldsymbol{b}$, $\boldsymbol{c}$, and $\boldsymbol{d}$ analyzed from statistical analysis of rainfall data. The applicability of this method has been further tested for other lower integration time intervals.

A.4.Logarithmic Model

This model was developed using the Electronics and Telecommunications Research Institute (ETRI) rainfall rate data measured through Optical Rain Gauge (ORG), where the research was performed to developed the conversion model with zero interception for logarithmic scale that shows efficient measure for 1-min. rainfall rate estimated data. The expression for this model is given as[13]:

$$\boldsymbol{\log[R_1(P)] = a \log[R_\tau\,(P)]} \tag{A. 4}$$

where $\boldsymbol{a}$ is the regression variable derived from statistical analysis of rainfall rate.

A.5.Exponential Model

The exponential model is expressed as:

$$\boldsymbol{R_1(P) = a\, exp\, [b\, R_\tau\, (P)]} \quad \text{(A. 5)}$$

where $\boldsymbol{a}$ and $\boldsymbol{b}$ are the regression coefficients obtained from statistical analysis of rain rate.

A.6.Global Coefficients Approach

The proposed global coefficients values are based on the power law conversion method which depicts the total and regional datasets. These coefficients extend its application to rain rate conversion methods in temperate, tropical and cold climates[14]. Applicability of these global coefficients and the new method for conversion of rain rate statistics with different integration time, adopted by Study Group 3 for the update of Recommendation P. 837-5, Annex 3[15] model performance is studied to yield 1-min. integration time from longer time rainfall rate statistics.

A.7.ITU-R P.837-6 Model

This model is classified as a physical based approach because the principles and philosophy of its conception address the conversion of statistics based on the physical process involved in the formation and development of rain and evolution of rain event in time. The prediction approach is based on the annual rainfall amount of convective type and stratiform type along with the probability of rainy 6 hour periods[4]. Excell Rainfall Statistics Conversion (ERSC) (henceforth Excell RSC) method is used for conversion of rainfall rate statistics from long to 1-min. integration time. The method is based on the simulated movement of rain cells over a virtual rain

gauge, with given integration time T, whose translation velocity depends both on the type of precipitation and on the observation period. The conversion of rainfall was obtained using a virtual rain gauge according to the local mean yearly wind velocity, which as extracted from the ERA-40 database. The rainfall model is described by the original Excell model that reproduce the local rainfall statistics by means of an ensemble of synthetic cells with rotational symmetry and exponential spatial distribution of rain intensity, $\boldsymbol{R}$. The schematical representation of the principles of the Excell RSC conversion model where virtual rain gauge experiences a variable rain rate over time due to the movement of rain cell is shown in[16]. The more theoretical concept of this model is clarified on the physical based methodology in[17] and on the update of Recommendation ITU-R P. 837-5, Annex 3.

B.Study of Rain Attenuation in Terrestrial Links

Microwave communication is considered as a significant technology in wireless communication. Rain attenuation results in outages that compromise the quality of signal and link availability rendering it as a prime factor to be considered in designing terrestrial link. The rain fade depth becomes noticeable at frequencies just above 5 GHz and severe at frequencies above 10 GHz [18]. Rain rate measurement is one of the key aspects of rain needed to estimate the amount of rain fade, which is frequency and location dependent. When designing Line-Of-Sight (LOS) microwave link operating at frequency above 10 GHz, the occurrence of rain along the transmission path is considered as a main impairment factor for microwave system degradation [19]. The performance of link can be determined with the knowledge of relevant link parameters as frequency, path length, antenna height. Furthermore, the attenuation on any given path depends on the value of specific attenuation, frequency, polarization, temperature[2]. The

method for the prediction of rain attenuation on microwave paths has been grouped into two categories[20]: the empirical method, which is based on measurement databases from stations in different zones within a given region and physical method, which make an attempt to reproduce the physical behavior involved in the attenuation process. However, when a physical approach is considered then all the input parameters needed for the analysis is not available. Empirical method is therefore the most used methodologies[5]. Several rain attenuation models are applied in different region of world which is detail in[21-24] that primarily focuses on the application of ITU-R P. 530-16[2]. Rain attenuation over a terrestrial path is defined as the product of specific attenuation (dB/km) and the effective propagation path length (km). The effective path length is determined from the knowledge of the link length and the horizontal distribution of the rain along the path. The rain attenuation $\boldsymbol{A}$ (dB) exceeded at $\boldsymbol{p}$ percent of time is calculated as:

$$\boldsymbol{A = \gamma_R d_{eff} = \gamma_R d \times r} \qquad \text{[dB]} \qquad \text{(B. 1)}$$

where $\boldsymbol{r}$ is the path reduction factor at the $\boldsymbol{p}$ time percentage and $\boldsymbol{d}$ is the radio path length in km. The recommendation of the ITU-R P.838-3[6] establishes the procedure of specific attenuation from the rain intensity. The specific attenuation, $\boldsymbol{\gamma_R}$ (dB/km) is obtained from the rain rate $\boldsymbol{R}$ (mm/hr) exceeded at $\boldsymbol{p}$ percent of the time using the power law relationship as,

$$\boldsymbol{\gamma_R = kR^{\alpha}} \qquad \text{(B. 2)}$$

where, $\boldsymbol{k}$ and $\boldsymbol{\alpha}$ depends on the frequency and polarization of the electromagnetic wave. The constants appears in recommendation tables of ITU-R P. 838-3[6] and also can be obtained by interpolation considering a logarithmic scale for $\boldsymbol{k}$ and linear for $\boldsymbol{\alpha}$. The values of these

coefficients are determined as functions of frequency, $\boldsymbol{f}$ (GHz), in the range from 1 to 1000 GHz. The $\boldsymbol{k}$ values can be either $\boldsymbol{k_H}$ or $\boldsymbol{k_V}$ and for $\boldsymbol{\alpha}$ can be either $\boldsymbol{\alpha_H}$ or $\boldsymbol{\alpha_V}$ for horizontal and vertical polarization respectively.

Owing to the applicability of prominent rain attenuation models, this research considered six established rain attenuation models which are analyzed on the data collected on 18, 38 and 75 GHz terrestrial links. We present a brief overview of applicable rain attenuation prediction models for terrestrial microwave links as well as the proposed estimation methods.

B.1.ITU-R P. 530-16 Model

The latest ITU-R P. 530-16 has been considered as a global model for prediction of the rain attenuation on terrestrial microwave link. The ITU-R recommendation (ITU-R P. 530-16, 2015) suggests the path attenuation exceeded for 0.01% of the time as the product of specific attenuation, $\boldsymbol{\gamma_R}$ (dB/km) and effective path length, $\boldsymbol{d_{eff}}$ for the consideration of time-space variability of rain intensity along the terrestrial path. Rain attenuation exceeded at 0.01% of the time percentage is calculated from the 1-min. rain intensity exceeded at same time percentage. The obtained value is scaled by the empirical formula to other percentages of time between 1% and 0.001% whose detail approach can be found in[2].

B.2.Da Silva Mello Model

This model uses the full rainfall rate distribution as input for predicting the rain attenuation cumulative distribution which considered the intercept of equivalent rain cell at any position with equal probability. The numerical coefficients that are derived for effective rain rate and equivalent rain cell diameter were obtained by multiple non linear regressions, using the measured data available in the ITU-R databanks[25]. Details of the model are fully reported in [26]. Furthermore, the dependence of reduction factor on link parameters was addressed through the introduction of correction factor, $\boldsymbol{r_p}$, to accommodate all percentage of time for available data[27]. This approach retains the general expression for $\boldsymbol{d_{eff}}$ and uses the full rainfall rate distribution at the links region as input for the prediction of the cumulative distribution of rain attenuation.

B.3.Moupfouma's Model

This approach for rain attenuation prediction is based on the use of rain intensity $\boldsymbol{R_{0.01}}$ (mm/hr) exceeded for 0.01% of time, and the determination of the percentage of time related to the exceedence of any given attenuation of interest. In addition, a terrestrial microwave link is described by its actual relay path length "*L*" which corresponds to the space between two ground stations. The detail description on the applicability of this model is described in[28].

B.4.Abdulrahman et al. Model

This method studied the relationship between path reduction factor and different link lengths by using the multiple non-linear regression techniques. In the analysis of the experimental data, the concept of equivalent rain cell has been retained where the relationship between equivalent rain cell diameter, $\boldsymbol{d_0}$, and the corresponding rain rate at 0.01% of the time, $\boldsymbol{R_{0.01}}$, is related. Detail description of model is described in[29].

B.5.Lin Model

The method gives empirical formulas for converting the distributions of 5-min. rain rates into the distributions of 11-GHz rain attenuation on any path length which has been deduced from experimental data gathered near Atlanta, Georgia and are further supported by experimental data from other United State of America locations. This approach is further detailed in[30].

B.6.Differential Equations Approach

This method presents the approach for prediction of rain attenuation on terrestrial radio links which was derived by differentiating measured rain attenuation with respect to rainfall rate. The results are presented in the form of slope, which in turn is used for predicting the expected rain attenuation at $\%\boldsymbol{p}$ of the time on a given link. The detail methodology is given in[31].

C.Study of Rain Attenuation in Satellite Communication Links

The prediction of rain induced attenuation starting from the cumulative distribution of rainfall intensity has been the subject of a major effort carried out by many researchers. The specific

attention is given to Ku and Ka bands which are of interest to communication systems designers in the South Korea because of its important application in broadband services and others. The higher frequency bands such as Ku (12/14 GHz) and Ka (20/30 GHz) are most effective in satellite communication and promise future demands of higher data rate services. In this concern, satellite communication plays a crucial role but the atmospheric propagation effects impair the availability and quality of satellite links during the service period[32]. The higher frequencies band has been preferable to provide Direct to Home (DTH) multi-media services[33]. Rain attenuation in satellite communication systems operating at Ka-band frequencies is more severe than usually experienced at lower frequency bands[34]. A number of mitigation techniques has been envisioned and experimented over the years, in the attempt to overcome the problem and to make Ka-band satellite applications as commercially viable as those at Ku-band[35]. Direct measurement of rain attenuation for all of the ground terminal locations in an operational network are not practical, so modeling and prediction methods must be used for better estimation of expected attenuation for each location[36]. The methods for the prediction of rain attenuation for a given path have been grouped into two categories, namely, physical and semi-empirical approaches. The physical approach considered the path attenuation as an integral of all individual increments of rain attenuation caused by the drops encountered along the path. Unfortunately, rain cannot be described accurately along the path without extensive meteorological database, which does not exist in most regions of the world[37]. In addition, when physical approach is used then all the input parameters needed for the analysis is not readily available[38]. Most prediction models therefore resort to semi empirical approaches which depend on the two factors namely, rain rate at a point on the surface of the earth and the effective path length over which rain can be considered to be homogeneous[39]. The attenuation on any given path depends on

the value of specific attenuation, frequency, polarization, temperature, path length and latitude [40]. When the comparative analyses of the various rain attenuation prediction models for earth space communication have been carried out against the measured results to predictions, the ITU-R P. 618[1] is preferred from both its inherent simplicity and reasonable accuracy, at least for frequencies up to approximately 55 GHz[35]. The short integration time rain rate is an essential input parameter required in prediction models for rain attenuation. In this regard, local prediction model for 1-min. rain rate is analyzed in the South Korea, where the modified polynomial shows the predictable accuracy for the estimation of 1-min. rain rate distribution[41, 42]. Similarly, rain attenuation had been studied for Koreasat-3 satellite from the database provided by the Yong-in Satellite Control Office where the ITU-R prediction model for earth space communication is analyzed[43, 44]. In this research, a technique for predicting the rain attenuation of Ku and Ka bands satellite signal during rain events at Mokdong-13 na-gil, Yangcheong-gu, Seoul, Republic of Korea has been presented which is analyzed from the database provided by National Radio Research Agency, RRA studied for earth space communication. The several prominent rain attenuation prediction methods have been studied in[45-53] where the performance of ITU-R method required for the design of earth-space telecommunication systems have been compared. The best possible estimates given by the available information can be provided by the use of prediction models due to sparse measured data. These measured distributions are compared with those predicted by method currently recommended by the International Telecommunication Union Radio communication Sector ITU-R P. 618-12[1], Unified[22], Dissanayake Allnutt and Haidara (DAH)[54], Simple Attenuation Model (SAM)[55], Crane Global[56], Ramachandran and Kumar[57], Gracia Lopez[58] and Karasawa[59] models. Although some research activities are performed for Ku-band satellite link in the South Korea region but fewer studies are done for

Ka-band link. A theoretical study of rain attenuation factor is been performed as mentioned in [60], which emphases on the need of more experimental data for better comparison with the existing rain attenuation models. The proposed technique utilizes power law relationship between the effective path length and rain rate at 0.01% of the time and predicts the attenuation values for other time percentage as per the ITU-R P. 618-12 extrapolation approach. The rainfall rate at 0.01% of the time is been useful parameter for estimation of rain induced attenuation on slant path which can be seen in[61]. The prediction approach requires the statistical features of the signal variation at the location obtained over a long term period, three years in the present case on earth-to-space propagation database at Ku and Ka band. This research studied the result of measured rain attenuation as compared with the cumulative probability distributions of existing prediction methods and proposes the suitable means to characterize the rain attenuation behavior for Ku and Ka band satellite communication links. The suitability in the Ka band has been mentioned in[62].

The attenuation prediction model consists of three methodologies, firstly, the calculation of specific attenuation[6]; secondly, the calculation of rain height[63] and thirdly, the attenuation calculation methodology. The recommendation of the ITU-R P.838-3[6] establishes the procedure of specific attenuation from the rain intensity. The specific attenuation, $\boldsymbol{\gamma}_{\mathbf{R}}$ (dB/km) is obtained from the rain rate $\boldsymbol{R}$ (mm/h) exceeded at $\boldsymbol{p}$ percent of the time using the power law relationship as,

$$\boldsymbol{\gamma}_{\mathbf{R}} = \boldsymbol{kR}^{\boldsymbol{\alpha}} \tag{C.1}$$

where, $\boldsymbol{k}$ and $\boldsymbol{\alpha}$ depend on the frequency and polarization of the electromagnetic wave. The

constants appear in recommendation tables of ITU-R P. 838-3[6] and also can be obtained by interpolation considering a logarithmic scale for $\boldsymbol{k}$ and linear for $\boldsymbol{\alpha}$. For the present location, values of two parameters $\boldsymbol{k}$ and $\boldsymbol{\alpha}$ at frequencies 12.25, 20.73 GHz under circular polarization are 0.024205, 1.151616; 0.10475, 1.010399857 respectively. In addition, there values are 0.094138726, 0.986283 respectively for 19.8 GHz under vertical polarization. Secondly, the mean annual rain height is determined through the recommendation of ITU-R P. 839-4[63] where the 0^0 C isotherm height above mean sea level is determined through the provided digital map. Thirdly, the attenuation calculation procedures differ as per the applicable methods. Several prominent methods for the calculation of rain attenuation in slant path have been developed and tested against the available data to relate the site climatic parameters to the signal attenuation statistics which are briefly described below:

C.1.ITU-R P. 618-12

ITU-R P. 618-12[1] provides estimates of the long term statistics of the slant path rain attenuation at a given location for frequencies up to 55 GHz. The required parameters are $\boldsymbol{R_{0.01}}$: point rain rate for the location in 0.01% of an average year (mm/hr); $\boldsymbol{h_s}$: height above mean sea level of the earth station (km); $\boldsymbol{\theta}$: Elevation angle (degree); $\emptyset$: Latitude of the earth station (degree); $\boldsymbol{f}$: frequency (GHz); $\boldsymbol{R_e}$: effective radius of the Earth (8,500 km).

The most widely accepted rain attenuation models for the planning and design of slant path radio systems are summarized in ITU-R P. 618-12[1]. The effective path length can be obtained using

equation C. 2(a), whereas the total rain attenuation at 0.01% of the time ($A_{0.01}$) can be calculated using equation C. 2(b):

$$L_E = L_R \, v_{0.01} \quad \text{[km]} \qquad \text{(C. 2(a))}$$

$$A_{0.01} = \gamma_R \, L_E \quad \text{[dB]} \qquad \text{(C. 2(b))}$$

The predicted attenuation exceedances for other time percentages of an average year can be acquired from the value of $A_{0.01}$ using the extrapolation approach as presented in equation (C. 2(c))[19]:

If $p \geq 1\%$ or $|\emptyset| \geq 36°$: $\beta = 0$

If $p < 1\%$ and $|\emptyset| < 36°$ and $\theta \geq 25°$: $\beta = -0.005(|\emptyset| - 36)$

Otherwise: $|\emptyset| < 36°$ and $\theta < 25°$: $\beta = -0.005(|\emptyset| - 36) + 1.8 - 4.25 \sin\theta$

$$A_p = A_{0.01} \left(\frac{p}{0.01}\right)^{-(0.655 + 0.033 \ln(p) - 0.045 \ln(A_{0.01}) - \beta(1-p)\sin\theta)} \qquad \text{(C. 2(c))}$$

This recommendation has been tested against available field results of the experimental links for earth space communication at 19.8 GHz for COMS1 and 12.25, 20.73 GHz for Koreasat 6 satellites.

C.2.Unified Method

This model uses the full rainfall rate distribution as input for predicting the rain attenuation cumulative distribution. The numerical coefficients that are derived for rain attenuation prediction were obtained by multiple nonlinear regressions, using the measured data available in the ITU-R databanks[25]. In this method, the model for the effective path length has been extended for slant path case by considering the rain height obtained from the recommendation ITU-R P.839-4[63]. Detail description of the model is described in[27]. The general expression for rain attenuation prediction is given as[27]:

$$A_{\%p} = k\left[1.763R^{0.753+\left(\frac{0.197}{L_S\mathrm{Cos}\theta}\right)}\mathrm{Cos}\theta + \frac{203.6}{L_s^{2.455}}R^{0.354+\left(\frac{0.088}{L_S\mathrm{Cos}\theta}\right)}\mathrm{Sin}\theta\right]^{\alpha}\frac{L_S}{1+\frac{L_S\mathrm{Cos}\theta}{119R^{-0.244}}} \quad \text{(C.3)}$$

C.3.Dissanayake Allnutt and Haidara (DAH) Model

This model is similar to ITU-R P. 618-12[1] since the rain related input to the model is the rain intensity at 0.01% of the time. This model is applicable across the frequency range 4-35 GHz and percentage probability ranges 0.001% to 10% of the time. In the DAH model, the rain height is relatively fixed to 5km, whereas, for ITU-R P.618-12[1], rain height varies depending on the latitude and longitude of the measurement site. The behavior of the DAH model can be modeled by the expressions in equation (C. 4), where $A_{\%p}$ and $A_{0.01}$ are attenuations for $p\%$ and 0.01% of the time respectively[54]:

$$A_p = A_{0.01}\left(\frac{p}{0.01}\right)^{-(0.655+0.033\ln(p)-0.045\ln(A_{0.01})-\beta(1-p)\mathrm{Sin}\theta)} \quad \text{(C. 4)}$$

where $\boldsymbol{\theta}$ is the elevation angle.

If $\boldsymbol{p} \geq 1\%$ or $|\emptyset| \geq 36°$: $z = 0$

If $\boldsymbol{p} < 1\%$ and $|\emptyset| < 36°$ and $\boldsymbol{\theta} \geq 25°$: $z = -0.005(|\emptyset| - 36)$

Otherwise: $|\emptyset| < 36°$ and $\boldsymbol{\theta} < 25°$: $z = -0.005(|\emptyset| - 36) + 1.8 - 4.25 \sin \boldsymbol{\theta}$

The detail methodology is given in[54].

C.4.Simple Attenuation Model (SAM)

SAM consists of three parts namely, the relationship between the specific attenuation and rain rate, statistics of the point rainfall intensity and spatial distribution of rainfall on earth-space communication links operating in the range of 10 to 35 GHz. The attenuation time series are calculated as[55]:

$$\boldsymbol{A}_{\boldsymbol{p}\%} = \boldsymbol{\gamma}\, \boldsymbol{L_s} \qquad \boldsymbol{R}_{\boldsymbol{p}\%} \leq \mathbf{10} \text{ mm/hr} \qquad \text{(C.5)}$$

$$\boldsymbol{L_s} = \frac{(\boldsymbol{H_R} - \boldsymbol{H_S})}{\boldsymbol{\sin \theta}} \qquad \text{(C.5 (a))}$$

where $\boldsymbol{A}_{\boldsymbol{p}\%}$ and $\boldsymbol{R}_{\boldsymbol{p}\%}$ are the attenuation and rain rate exceeded for $\boldsymbol{p}\%$ of time; $\boldsymbol{\gamma}$ is specific attenuation due to rainfall, $\boldsymbol{L}_{\boldsymbol{s}}$ is slant-path length up to rain height, $\boldsymbol{H}_{\boldsymbol{R}}$ is rain height above mean sea level, $\boldsymbol{H}_{\boldsymbol{s}}$ is station height, and $\boldsymbol{\theta}$ is elevation angle of the top of rain height.

In convective rainstorms, when $\boldsymbol{R}_{\boldsymbol{p}\%} > \mathbf{10}$ mm/hr a modified value of effective path length is used for determination of slant path attenuation as:

$$\mathbf{A}_{\mathbf{p}\%} = \boldsymbol{\gamma}\frac{\mathbf{1}-\exp[-\boldsymbol{\alpha}\mathbf{bln}(\mathbf{R}_{\mathbf{p}\%}/\mathbf{10})]\mathbf{L_s}\mathbf{cos}\boldsymbol{\theta}}{\boldsymbol{\alpha}\mathbf{bln}(\mathbf{R}_{\mathbf{p}\%}/\mathbf{10})\mathbf{cos}\boldsymbol{\theta}} \qquad \boldsymbol{R}_{p\%} > \mathbf{10}\text{mm/hr} \qquad \text{(C. 5(b))}$$

where b=1/22. Furthermore, the empirical expression for effective rain height $\boldsymbol{H}_{\boldsymbol{R}}$ is given as:

$$\boldsymbol{H}_{\boldsymbol{R}} = \begin{cases} \boldsymbol{H_0}; & \boldsymbol{R} \leq \mathbf{10}\ \text{mm/hr} \\ \boldsymbol{H_0} + \boldsymbol{log}\left(\frac{\boldsymbol{R}}{\mathbf{10}}\right); & \boldsymbol{R} > \mathbf{10}\ \text{mm/hr} \end{cases} \qquad \text{(C. 5(c))}$$

$\boldsymbol{H}_{\mathbf{0}}$ is the 0^0C isotherm height above mean sea level whose value is given by ITU-R P.839-4 [63]. The detail description on the applicability of this model is described in[55].

C.5.Crane Global Model

This model is developed by Crane which is based on the use of geophysical data to determine the surface point rain rate, point-to-path variations in rain rate, and the height dependency of the attenuation, given the surface point rain rate or the percentage of the year the attenuation value is exceeded. The model further relies on 0^0C isotherm height, $\boldsymbol{H}_{\mathbf{0}}$, and excessive precipitation events which showed a tendency toward a linear relationship between rain rate for $\boldsymbol{p}$% of the time exceeded, $\boldsymbol{R}_{\boldsymbol{p}}$, and $\boldsymbol{H}_{\mathbf{0}}$. Since, at high rain rates, the rain rate distribution function displays a nearly linear relationship between $\boldsymbol{R}_{\boldsymbol{p}}$ and $\mathbf{log}\,\boldsymbol{P}$, the interpolation model used for estimation of $\boldsymbol{H}_{\mathbf{0}}$from probability, $\boldsymbol{p}$, between 0.001% and 1% is of the form[56]:

$$\boldsymbol{H_0} = \boldsymbol{a} + \boldsymbol{b}\,\mathbf{log}\,\boldsymbol{P} \qquad \text{[km]} \qquad \text{(C. 6)}$$

The further step-by-step procedure can be found in[56, 64]. The mean slant path attenuation at each probability of occurrence, $\boldsymbol{p}$, for path projection of the slant path, D, is given as[56]:

$$\mathbf{H}_{\mathbf{P\%}} = \begin{cases} \dfrac{\mathbf{kR_p^{\alpha}}}{\mathbf{Cos\,\theta}}\left[\dfrac{\mathbf{e^{U\alpha D}-1}}{\mathbf{U\alpha}}\right]; & \mathbf{0 < D \le d} \\ \dfrac{\mathbf{kR_p^{\alpha}}}{\mathbf{Cos\,\theta}}\left[\dfrac{\mathbf{e^{U\alpha D}-1}}{\mathbf{U\alpha}} - \dfrac{\mathbf{X^{\alpha}e^{Y\alpha d}}}{\mathbf{Y\alpha}} + \dfrac{\mathbf{X^{\alpha}e^{Y\alpha D}}}{\mathbf{Y\alpha}}\right]; & \mathbf{d < D \le 22.5} \end{cases} \quad \text{[dB]} \qquad \text{(C. 6(a))}$$

where empirical constants for each probability, $\boldsymbol{p}$, of interest are:

$$\boldsymbol{H = 2.3R_P^{-0.17}; Y = 0.026 - 0.003\ln R_p\,; d = 3.8 - 0.6\ln R_p; U = \frac{\ln(Xe^{Yd})}{d}}$$

C.6.Ramachandran and Kumar Model

The modifications performed on this model are based on the elevation angle less than 60^0, at higher rain rate where multiple rain cells intersect the slant path, and the accumulation time factor at the breakpoints which is considered as an invariant. Using the rain-rate statistics, the breakpoint rain rate $\boldsymbol{R_B}$ and its exceedance, $\boldsymbol{p_{RB}}$ are first estimated. The attenuation exceedance, $\boldsymbol{p_{AB}}$ is calculated using the invariant accumulation time factor at the breakpoint. The attenuations at other exceedances are calculated separately for rain rates above and below the breakpoints using the modified expressions. The break point attenuation ($\boldsymbol{A_B}$) is computed as [57]:

$$\boldsymbol{A_B = kR_B^{\alpha}L_EC_f} \qquad 40^0 \le \boldsymbol{\theta} < 60^0 \qquad \text{(C. 7)}$$

where, $\boldsymbol{k}$, $\boldsymbol{\alpha}$ and the effective path length $\boldsymbol{L_E}$ are determined as per the recommendation of ITU-R P.618-12[1]. The correction factor, C_f is given as:

$$\boldsymbol{C_f} = \begin{cases} \boldsymbol{-0.002\theta^2 + 0.175\theta - 2.3}; & 40^0 \le \boldsymbol{\theta} < 60^0 \\ \boldsymbol{1}\,; & \boldsymbol{\theta} \ge 60^0 \end{cases}$$

R_B is assumed to occur at $R_{0.01}$ due to the lack of reliable and long term rainfall records. Hence, the attenuation at other percentages is computed as follows:

$$A_{\%p} = A_B \left(\frac{p-0.011}{0.01}\right)^{-(0.655+0.033\ln(p-0.011)-0.045\ln(A_B)-\beta(0.989-p)\sin\theta)} \quad [\text{dB}]$$

$$0.021 \leq p < 1 \qquad \text{(C. 7(a))}$$

$$A_{\%p} = A_B \left(\frac{p}{0.021}\right)^{0.5(0.655+0.033\ln p^2-0.03\ln p-0.045\ln A_B)-\beta(0.989-p)\sin\theta)} \quad [\text{dB}]$$

$$p \leq 0.021 \qquad \text{(C. 7(b))}$$

The detailed methodology is given in[57].

C.7.Gracia Lopez Model

This model features the suitable method for rain attenuation prediction to be used in satellite radio link which is tested over 77 satellite links placed in Europe, the US, Japan and Australia. The rain attenuation in a satellite link is given by[58]:

$$A_{\%p} = kR^{\alpha}L_s / \left\{a + \left[\frac{L_s(bR+cL_s+d)}{e}\right]\right\} \qquad \text{(C. 8)}$$

where R is the point rainfall intensity in mm/hr, k and α are the parameters depending on the frequency, polarization and elevation angle given by[6], L_s is the equivalent path length in km, given by

$$L_s = \frac{(H_R-H_S)}{\sin\theta} \quad [\text{km}] \qquad \theta \geq 5^0 \qquad \text{(C. 8(a))}$$

where $\boldsymbol{H_S}$ is the ground elevation from the sea level in km, $\boldsymbol{\theta}$ is the earth station elevation angle in degree, and

$$\boldsymbol{H_R} = \begin{cases} \mathbf{4}; & 0 < |\emptyset| < 36^0 \\ \mathbf{4 - 0.075}(|\emptyset| - \mathbf{36^0}); & |\emptyset| \geq 36^0 \end{cases}$$

with $\emptyset$, the latitude of the earth station in degree. The coefficients $\boldsymbol{a}$, $\boldsymbol{b}$, $\boldsymbol{c}$, and $\boldsymbol{d}$ are constants depends on the geographical area whose values are determined by regression techniques based on simultaneous rain attenuation and rain intensity measurement database. Coefficient $\boldsymbol{e}$ is a scaling factor where, $\boldsymbol{e}$ = 10000 and worldwide coefficients are $\boldsymbol{a}$ =0.7, $\boldsymbol{b}$ =18.35, $\boldsymbol{c}$ = -16.51, $\boldsymbol{d}$ =500.

C.8.Karasawa Model

This model primarily focuses on the lower probability exceedance levels where the rain attenuation is the function of time percentage, $\boldsymbol{p}$, and is given as[59]:

$$\boldsymbol{A_s = 10^{m+sq(p)}} \text{ [dB]} \qquad \text{for } 0.01 \leq \boldsymbol{p} \leq 1 \qquad \text{(C. 9)}$$

$$\boldsymbol{A_s = A_{0.01} - 1.74s10^{m+3.1s}(\log_{10}p + 2)} \text{ [dB] for } 0.001 \leq \boldsymbol{p} \leq 0.01 \qquad \text{(C. 9(a))}$$

where $\boldsymbol{q(x) = 2.33 - 0.847x - 0.144x^2 - 0.0657x^3}$

$$\boldsymbol{x = 1 + \log_{10}p}$$

$$\boldsymbol{m = 4.03 \log_{10} A_{0.1} - 3.03 \log_{10} A_{0.01}}$$

$$\boldsymbol{s = 1.30 \log_{10}\left(\frac{A_{0.01}}{A_{0.1}}\right)}$$

III. Distribution of 1-min. Rain Rate

A. Introduction

The rain rate integration time of longer period particularly 5-min., 10-min., 20-min., 30-min. and 60-min. are converted to 1-min. rain rate distribution with the application of prominent rain conversion models. The proposed models based on the polynomial relationship are studied in [41], [42] which is seems to be suitable for the South Korea regions. Furthermore, the brief description of experimental measurement of rain rate, models performance evaluation and concluding remarks are presented in the further section.

B. Experimental Set up of 1-min. Rainfall Amount and 1-min. Rain Rate

The experimental set up for the measurement of 1-min. rainfall amount are carried out by KMA over 93 different locations in the South Korea region, which lies in temperate zone with four distinct seasons as mentioned in Table 3.1.

Table 3.1. Seasonal climatic characteristic[65].

Month	January	February	March	April	May	June	July	August	September	October	November	December
Season	Winter		Spring			Summer			Fall			Winter
Weather Pattern	Cold		Mild			Warm			Serene			Cold
	Dry					Humid				Dry		
	Snow		Clear			Heavy rainfall				Clear		Snow

As indicated in Table 3.1, the seasonal climatic characteristic is grouped into four groups namely, winter, spring, summer and fall season. KMA have used tipping bucket rain gauge for the record of 1-min. rainfall amount and facilitate the digitization of telemetric observation signals which is installed in 93 stations across the South Korea. Figure 1 shows the internal

structure of rain gauge.

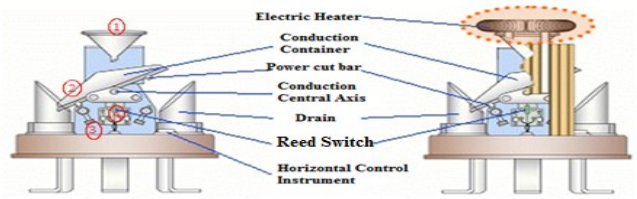

Figure 3.1: Tipping bucket rain gauge[17].

In the construction of tipping bucket rain gauge the conducting vessel size of 0.5mm is used to improve the shortcomings of the gutter. The bucket fills whenever the collected water is more than 0.5mm. The center of the bucket is shifted like a seesaw where it is in contact with the Reed Switch with the rotation axis that is operated by electrical pulse which is occurred due to tipping phenomenon. The measurement of 1-min. rainfall amount is recorded through the signal generated from Reed Switch. In order to measure the rainfall amount of 1-min. interval during snowfall, the heater is installed inside the sewer. The specification of tipping bucket rain gauge, experimental system for measuring 1-min. rainfall amount, the data extraction process along with the calculated rainfall rate statistics over various integration times are listed in[8]. The characteristic of study location for 1-min. rainfall amount are depicted in Table 3.2 where the terrestrial and satellite communication equipments are maintained in Icheon and Mokdong regions respectively. The simultaneous measurement of 1-min. rain rate distribution is described in section 4 and 5. The latitude, longitude and elevation values as well as rain rate of higher integration times that is calculated from experimental 1-min. rainfall amount are used in ITU-R P. 837-6 recommended software for the estimation of 1-min. rain rate from higher time integration instances as such 5-min., 10-min., 20-min., 30-min. and 60-min. rain rate distribution.

Table 3.2. Characteristics of study locations.

Station	Latitude (^{0}N)	Longitude (^{0}E)	Average Precipitation (mm)	Elevation (m)	Period (year)	Remark
Gwangju	$35^0$9’23.7”	$126^0$51’28.45”	above 300	about 47	10 (2004-2013)	KMA [70]
Daegu	$35^0$52’23”	$128^0$36’4.35”	above 200	about 45		
Daejeon	$36^0$21’4.55”	$127^0$23’4.37”	above 300	about 77		
Busan	$35^0$10’49.86”	$129^0$04’32.31”	above 300	about 71		
Seogwipo	$33^0$15’14.97”	$126^0$33’35.85”	above 200	about 24		
Seoul	$37^0$33’36”	$126^0$59’24”	above 300	about 86		
Ulsan	$35^0$32’18.5”	$129^0$18’40.89”	above 200	about 45		
Incheon	$37^0$27’14.4”	$126^0$43’55.2”	above 300	about 70		
Chuncheon	$37^0$52’54.24”	$127^0$43’49.17”	above 300	about 75		
Icheon	$37^0$16’46.72”	$127^0$26’04.07”	above 350	about 85		
Icheon	$37^0$08’49.2”	$127^0$32’56.4”	above 350	about 85	3 (2013-2015)	RRA [73]
Mokdong	$37^0$32’45.24”	$126^0$52’58.8”	above 350	about 55		

Furthermore, the calculated 1-min. rain rate distribution of nine prime location of the South Korea is depicted in Figure 3.2 which highlight the facts that the rain rate value at 0.01% of the time for Gwangju, Daegu, Daejeon, Busan, Seogwipo, Seoul, Ulsan, Incheon and Chuncheon regions are 90, 60, 79.8, 90, 90, 90, 65.4, 89.4 and 60 mm/hr respectively. It signifies that the 1-min. rain rate distribution at 0.01% of the time lies between 80 to 100 mm/hr for most of the prime locations in the South Korea.

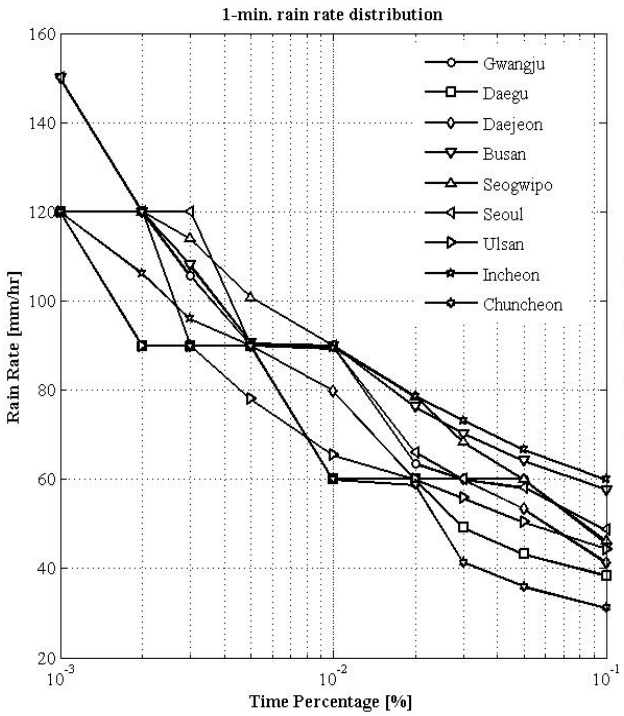

Figure 3.2: 1-min. rain rate distribution of various integration time percentage of the South Korea.

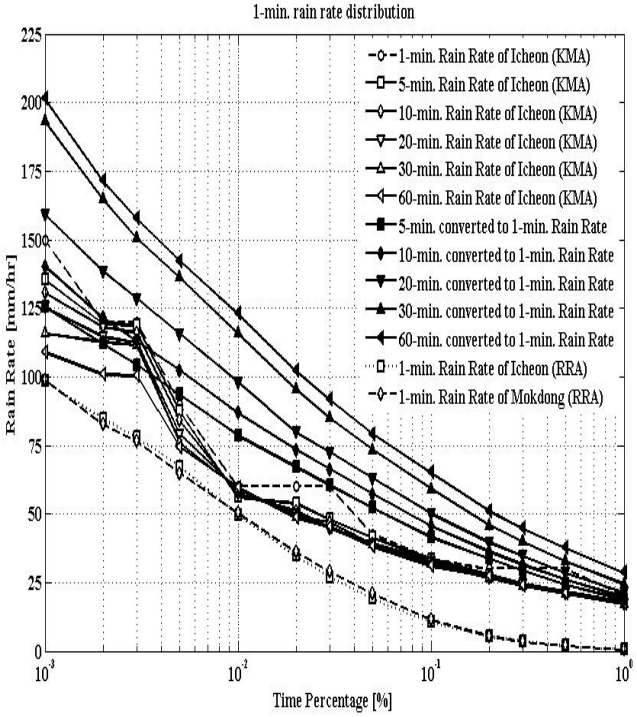

Figure 3.3: The rain rate distribution of various integration time percentages of Icheon and Mokdong regions of the South Korea.

Figure 3.3 shows the plot of 1-min., 5-min., 10-min., 20-min., 30-min. and 60-min. rain rate of Icheon region along with the converted 1-min. rain rate obtained from the higher time integration. Furthermore, it shows the plot of rain rate obtained for Icheon and Mokdong region provided by RRA. This figure highlights the facts that for lower time conversion particularly 5-min. and 10-min. to 1-min. ITU-R P. 837-6[13] gives the closer estimation against the measured 1-min. rain rate distribution whereas for higher time instances as such 20-min., 30-min. and 60-min. to 1-min. conversion shows the overestimation nature.

C.Proposed Model

The model proposed for study of 1-min. rain rate distribution for the South Korea is obtained from the curve fitting technique which is analyzed from the Matlab[41]. The separate studies

have been performed for the applicability of conversion methods in Daejeon site where the suitability of second and third order polynomial functions are analyzed[42]. Furthermore, the conversion methods are studied by using the 1-hour rain rate database without the use of 1-min. rain rate over this region[43]. The suitable models are expressed as:

Model 1 is expressed as:

$$\boldsymbol{R_1(P) = a\, e^{(a-b)}[R_\tau(P)]^4 + b\, e^{(b-a)}[R_\tau(P)]^3 + c\,[R_\tau(P)]^2 + d\,[R_\tau(P)]} \tag{3.1}$$

Model 2 is expressed as:

$$\boldsymbol{R_1(P) = a\, e^{(a-b)}\left[R_\tau(P)\right]^2 + b\, e^{(b-a)}[R_\tau(P)]} \tag{3.2}$$

Model 3 is expressed as:

$$\boldsymbol{R_1(P) = a\, e^{(a-b)}\left[R_\tau(P)\right]^2 + b\, e^{(b-a)}[R_\tau(P)] + c} \tag{3.3}$$

where, $\boldsymbol{R_1(P)}$ represents the rainfall rate in a 1-min. integration time with the possibility of occurrence $\boldsymbol{P}$, $\boldsymbol{R_\tau(P)}$ is the rainfall rate in τ-minutes integration time, and coefficients $\boldsymbol{a}$, $\boldsymbol{b}$, $\boldsymbol{c}$, and $\boldsymbol{d}$ are regression coefficients that are obtain through statistical analysis of rainfall data with the use of curve fitting technique derived from Matlab programming[66].

In addition, the mean 1-min. rain rate distribution is calculated from the selected nine prime locations of the South Korea regions whose regression coefficients values applicable for different conversion methods against the mean 1-min. rain rate distribution are calculated which are listed

in the Table 3.4.

Table 3.4. Estimated parameter values obtained from statistical program.

	Segal		Burgueno et al.		Chebil and Rahman				Logarithmic	Exponential		Global Coefficients		Second Order Polynomial Fit			Third Order Polynomial Fit			
T-min. to 1-min.	a	b	a	b	a	b	c	d	a	a	b	a	b	a	b	c	a	b	c	d
5-min. to 1-min.	1.03	-0.005367	1.36	0.948	1.134	-0.005801	-0.1138	27.41	1.018	34.54	0.01094	0.924	1.044	-0.005601	1.98	-32.49	-0.0001114	0.02288	-0.3016	24.45
10-min. to 1-min.	1.322	0.02072	5.872	0.6095	1.309	0.01953	-0.001517	129.5	1.016	52.41	0.005388	0.829	1.097	-0.008213	2.44	-47.31	-0.00007127	0.01392	0.4615	5.387
20-min. to 1-min.	1.464	0.03245	3.061	0.7583	12.79	0.0003768	-11.67	0.001617	1.016	38.93	0.009036	0.736	1.169	-0.006129	1.863	-19.97	0.0003082	-0.08317	7.852	-165
30-min. to 1-min.	1.201	0.005379	1.836	0.8889	-0.3521	0.7067	1.143	4.676	1.031	34.95	0.01124	0.583	1.265	-0.005853	1.944	-24.28	0.000204	-0.0546	5.613	-110.8
60-min. to 1-min.	0.9994	-0.02069	0.971	1.054	-1170	1.054	1.246	435.1	1.046	29.93	0.01438	0.509	1.394	-0.004187	1.893	-24.77	0.00000471	-0.005229	1.966	-26.4

Furthermore, the applicable methods are tested in Icheon regions in which 1-min. rain rate calculated from KMA database is used for further analyses whose generated regional coefficients are listed in Table 3.5. The rain rate values in 0.01% of the time is considered to be suitable time percentage for the calculation of rain induced attenuation[1] and is very crucial for system designers to obtain preliminary design of the satellite microwave link, satellite payload design and to have broad idea of rain attenuation for microwave engineers. The rain rate contour maps developed for 0.01% of the time is considered as preferential maps for most of the radio propagation[20]. Thus, the contour plot has been developed at 0.01% of the time using Kriging interpolation method for spatial interpolation of rain accumulation values into a regular grid in order to obtain a highly consistent and predictable rain rate variation. The input parameter used are the Latitude, Longitude, Altitude and 1-min. rain rate values at 0.01% of the time which is calculated for 1-min. rainfall accumulation of 40 stations. Furthermore, higher rain rate values exceeding 100mm/hr, at 0.01% of the time, is noted for Gangwon-do and Gyeonggi-do regions whereas for area with lower average annual precipitation such as Gyeongsangbu, Gyeongsangnam-do, the rain rate at 0.01% of the time, is between 50 mm/hr to 100 mm/hr. The fact that ITU-R P. 837-6 method overestimate rain rate values at 0.01% of the time in the South Korea is clearly revealed with the help of contour map as depicted in Figure 3.5.

Table 3.5. Regression coefficients for empirical conversion methods at different integration time.

Sites	T(min)	Segal		Burgueno et al.		Chebil and Rahman				Logarithmic	Exponential		Global Coefficients	
		a	b	a	b	a	b	c	d	a	a	b	a	b
Icheon	5	1.328	0.02261	1.324	0.9511	3.991	0.5065	1.032	-22.96	1.125	25.50	0.01316	0.924	1.044
	10	1.360	0.02232	1.387	0.9462	3.009	0.4432	1.049	-23.49	1.133	25.48	0.01352	0.829	1.097
	20	1.325	0.01682	1.301	0.9667	24.590	36.2200	1.137	10.44	1.140	25.06	0.01415	0.736	1.169
	30	1.293	0.01248	1.201	0.9904	5.359	0.6194	1.124	-17.89	1.144	24.35	0.01494	0.583	1.265
	60	1.200	-0.00082	0.884	1.0750	-1.673	4.9140	1.198	4.88	1.155	22.18	0.01724	0.509	1.394
	T(min)	Second Order Polynomial Fit			Third Order Polynomial Fit				Model 1					
		a	b	c	a	b	c	d	a	b	c	d		
	5	0.000909	0.8805	7.053	0.0000706	-0.01451	1.823	-8.372	0.0000008	-0.0001654	0.008	1.0290		
	10	0.000841	0.9177	6.841	0.0000959	-0.01944	2.116	-12.200	0.0000013	-0.0002591	0.0135	0.9698		
	20	0.001079	0.9351	6.331	0.0000998	-0.01927	2.096	-11.540	0.0000015	-0.0003064	0.0162	0.9369		
	30	0.001106	0.9850	4.742	0.0000685	-0.01212	1.697	-5.674	0.0000025	-0.0004893	0.0265	0.7684		
	60	0.004493	0.7017	10.120	0.0001660	-0.02587	2.285	-12.620	0.0000027	-0.0004529	0.0215	0.9019		

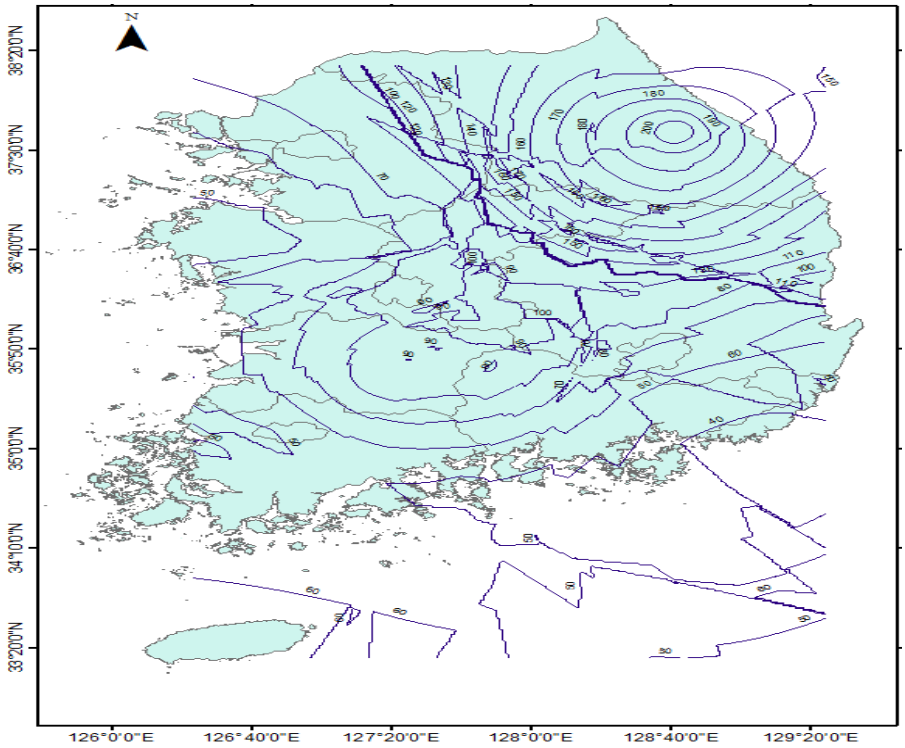

Figure 3.4: Contour plot for 1-min. rain rate at 0.01% of exceedance level.

D.Performance Evaluation

The goodness of fit for prominent rain rate conversion models are studied through several error analyses. The primarily used statistical measurement includes Mean, Standard Deviation (SD) and Root Mean Square (RMS) values of error probability, $\boldsymbol{\varepsilon}\ (\boldsymbol{P})$ where they are adopted for the

comparison to the performance of ITU-R P. 837-6[4]. The values for comparison of prediction methods are tabulated in fixed probability levels over decades where preferred values are 0.001%, 0.002%, 0.003%, 0.005%, 0.01%, 0.02%, 0.03%, 0.05%, and 0.1% of time. The mathematical expression for these error matrices as presented in[41] are depicted below:

Absolute percentage relative error figure is given as,

$$\boldsymbol{\varepsilon\,(P)_T} = \frac{\boldsymbol{R_e\,(P)_T - R_m\,(P)_T}}{\boldsymbol{R_m\,(P)_T}} \times \mathbf{100} \qquad [\%] \tag{3.4}$$

where, $\boldsymbol{R_e\ (P)_T}$ and $\boldsymbol{R_m\ (P)_T}$ are the rain rate values of the estimated and the measured T-minute integrated rainfall CDF, respectively, at the same probability level $\boldsymbol{P}$, in the percentage interval 10^{-3} % < $\boldsymbol{P}$ < 10^{-1} %.

The RMS is defined as,

$$\boldsymbol{RMS} = \left[\left(\frac{\mathbf{1}}{\boldsymbol{N}}\right) \times \sum_{\boldsymbol{i=1}}^{\boldsymbol{N}} (\boldsymbol{X_{est,i}} - \boldsymbol{X_{mea,i}})^{\mathbf{2}}\right]^{\mathbf{1/2}} \tag{3.5}$$

where $\boldsymbol{N}$ is the total number of available probability values, $\boldsymbol{X_{est}}$ and $\boldsymbol{X_{mea}}$ are the estimated and measured quantities respectively.

Similarly, standard deviation (SD) is calculated as,

$$\boldsymbol{SD} = \left[\left(\frac{\mathbf{1}}{\boldsymbol{N}}\right) \times \sum_{\boldsymbol{i=1}}^{\boldsymbol{N}} (\boldsymbol{\varepsilon(P)_i} - \boldsymbol{\mu})^{\mathbf{2}}\right]^{\mathbf{1/2}} \tag{3.6}$$

where N, is the total number of available probability values, $\boldsymbol{\varepsilon(P)_i}$ and $\boldsymbol{\mu}$ are each error value and arithmetic mean of error quantities respectively.

The calculated regression coefficient values along with the coefficient of determination $\boldsymbol{R^2}$ which are obtained from the curve fitting procedure of Matlab and the error matrices obtained after the use of regional coefficient sets and average coefficient values from the above listed error matrices are mentioned in[41]. The suitability of polynomial analyses is further analyzed in [42]. The values of $\boldsymbol{R^2}$ as obtained through statistical analysis whose results are calculated after averaging over nine selected prime sites are tabulated in Table 3.6.

Table 3.6. Coefficient of determination values as obtained after average over nine regions.

τ-min Integration Times	Burgueno et al.	Exponential	Second order Polynomial Fit	Third order Polynomial Fit
5-min. to 1-min.	0.965	0.931	0.976	0.980
10-min. to 1-min.	0.931	0.882	0.957	0.974
20-min. to 1-min.	0.935	0.873	0.944	0.971
30-min. to 1-min.	0.917	0.905	0.943	0.962
60-min. to 1-min.	0.864	0.821	0.927	0.949

As summarized in Table 3.6, the polynomial models have relatively higher correlation with the rainfall rate over the various integration times. Similarly, the $\boldsymbol{R^2}$ values as obtained through the statistical analysis done for Icheon region are tabulated in Table 3.7. The Table 3.7 depicts the higher correlation values obtained for Model 1 which highlight its effectiveness in the prediction of 1-min. rain rate. The chance of error is increased for exponential, Burgueno et al., Second and Third order polynomial fits which show relatively lower value of $\boldsymbol{R^2}$. The error variables obtained between the mean 1-min. rain rate of experimental result and estimated 1-min. cumulative distribution over all integration times and at 0.01% of the time are tabulated in Table 3.8 and Table 3.9 respectively.

Table 3.7. Coefficient of determination R^2 as obtained from statistical program.

Sites	5-min. to 1-min. R^2	10-min. to 1-min. R^2	20-min. to 1-min. R^2	30-min. to 1-min. R^2	60-min. to 1-min. R^2
Burgueno et al.					
Icheon	0.9882	0.9837	0.9818	0.971	0.9768
Exponential					
Gwangju	0.9138	0.9229	0.9281	0.9317	0.8993
Daegu	0.9497	0.8898	0.8978	0.7652	0.8373
Daejeon	0.9106	0.7917	0.9285	0.8821	0.8614
Busan	0.979	0.9746	0.9828	0.9918	0.9484
Seogwipo	0.9716	0.9304	0.9234	0.964	0.5423
Seoul	0.9575	0.9744	0.9623	0.9277	0.939
Ulsan	0.7542	0.608	0.3414	0.8732	0.7898
Incheon	0.9832	0.976	0.9466	0.9255	0.8589
Chuncheon	0.9597	0.8661	0.9434	0.8843	0.7137
Icheon	0.9703	0.9666	0.9646	0.9524	0.9735
Average	0.935	0.890	0.882	0.910	0.836
Second Order Polynomial Fit					
Icheon	0.9893	0.9846	0.9829	0.9716	0.9814
Third Order Polynomial Fit					
Icheon	0.993	0.9895	0.9865	0.9724	0.9852
Model 1					
Icheon	0.9943	0.9916	0.989	0.9749	0.9873

Table 3.8. Error obtained after testing over the interval [0.001% to 0.1%] against the mean 1-min. rain rate.

Methods	5 to 1 min			10 to 1 min			20 to 1 min			30 to 1 min			60 to 1 min		
	Error ε (%)	SD (%)	RMSE (%)	Error ε (%)	SD (%)	RMSE (%)	Error ε (%)	SD (%)	RMSE (%)	Error ε (%)	SD (%)	RMSE (%)	Error ε (%)	SD (%)	RMSE (%)
ITU-R P. 837-6	0.05	0.04	4.36	0.14	0.05	10.22	0.44	0.03	36.43	0.72	0.06	63.60	1.16	0.09	102.76
Segal	0.00	0.04	4.27	0.02	0.25	20.61	0.01	0.09	8.55	0.00	0.06	5.34	0.00	0.04	3.78
Burgueno et al.	0.01	0.04	3.77	0.03	0.15	10.61	0.01	0.08	6.20	0.01	0.06	4.49	0.01	0.04	3.89
Chebil and Rahman	0.00	0.04	4.33	0.02	0.25	20.73	0.00	0.11	10.42	0.00	0.06	5.68	0.00	0.04	3.54
Logarithmic	0.00	0.04	4.23	0.01	0.28	23.07	0.00	0.12	11.23	0.00	0.06	6.29	0.00	0.04	3.90
Exponential	0.02	0.10	7.32	0.05	0.21	14.64	0.02	0.11	7.68	0.02	0.10	6.62	0.02	0.08	6.07
Global Coefficients	0.03	0.04	5.91	0.18	0.26	39.52	0.42	0.24	51.00	0.58	0.20	61.38	1.18	0.22	113.09
Second Order Polynomial Fit	0.00	0.02	1.79	0.00	0.03	1.85	0.01	0.06	5.64	0.00	0.04	3.78	0.00	0.04	3.49
Third Order Polynomial Fit	0.00	0.01	1.15	0.00	0.01	0.81	0.00	0.05	3.10	0.00	0.04	2.98	0.00	0.04	3.49

Table 3.9. Error obtained after testing at 0.01% of the time against the mean 1-min. rain rate.

Methods	5 to 1 min		10 to 1 min		20 to 1 min		30 to 1 min		60 to 1 min	
	Error ε (%)	RMSE (%)	Error ε (%)	RMSE (%)	Error ε (%)	RMSE (%)	Error ε (%)	RMSE (%)	Error ε (%)	RMSE (%)
ITU-R P. 837-6	0.04	3.52	0.13	10.39	0.44	34.69	0.72	56.94	1.17	93.20
Segal	-0.04	3.40	-0.07	5.72	-0.13	9.98	-0.09	6.79	-0.06	4.63
Burgueno et al.	-0.04	2.84	-0.04	2.92	-0.10	7.76	-0.07	5.86	-0.06	4.39
Chebil and Rahman	-0.04	3.41	-0.07	5.74	-0.13	10.62	-0.09	6.79	-0.04	3.33
Logarithmic	-0.05	3.59	-0.09	7.24	-0.14	11.07	-0.09	7.15	-0.06	4.65
Exponential	-0.06	4.93	-0.05	4.02	-0.13	10.03	-0.10	8.03	-0.08	6.58
Global Coefficients	-0.01	1.16	0.06	4.73	0.20	15.62	0.40	31.87	1.01	80.43
Second Order Polynomial Fit	-0.01	0.46	0.01	0.51	-0.07	5.31	-0.05	3.81	-0.04	3.13
Third Order Polynomial Fit	-0.02	1.87	-0.02	1.42	-0.02	1.81	-0.02	1.67	-0.04	3.12

As depicted in Table 3.8, the ITU-R P. 837-6 and global coefficients methods generate higher error chances because of increased RMS values. In contrary, polynomial fit shows less error chances. Though the application of Segal, Burgueno et al., Chebil and Rahman, Logarithmic, Exponential methods show fair goodness but still the error chances remain higher because of higher RMS error values. The accuracy of polynomial nature is further tested at 0.01% of the time whose result is depicted in Table 3.9, which shows the similar nature for the selected rain rate conversion methods.

Similarly, the regional coefficients values as listed in Table 3.5 are tested in Icheon region whose error matrices are depicted in Table 3.10 and Table 3.11 for time percentage $0.001\% \leq \boldsymbol{P} \leq 1\%$ and in 0.01% of the time respectively. As shown in Table 3.10, Model 1 results less error percentages for all time conversion which are less than 1% which is justified by decreased value of SD and RMS error. Although, Segal, Burgueno et al., Chebil and Rahman, Second order polynomial fit show similar trend of relative error percentages in which Burgueno et al. results in lower error percentage. While applying Third order polynomial, the error chances get increased

for 30-min. to 1-min. conversion time. In contrast, exponential, global coefficients, logarithmic and ITU-R P. 837-6 generates higher relative error percentage. In addition, ITU-R P. 837-6 give less error chances for lower time conversion which is less than 13% for 5-, 10-min. to 1-min. whereas for higher time conversion, this error get increased. For instance, this approach results in relative error percentage of 3.32, 12.59, 24.64, 46.44 and 58.46 % for 5-, 10-, 20-, 30-, 60- to 1-min. conversion time respectively. Furthermore, Table 3.11 shows the results of evaluation in 0.01% of the time which highlights the suitability of Model 1 and exponential methods with lower error probabilities that is justified by decreased values of RMS error. In addition, Segal, Burgueno et al., Chebil and Rahman, Second and Third Order polynomial show similar pattern where error probabilities get increased for higher time conversion. For example, the relative error probabilities are 20.20, 19.43, 19.16, 13.27 and 11.44% for Segal, Burgueno et al., Chebil and Rahman, Second and Third Order polynomial respectively under 60-min. to 1-min. conversion time. In contrast, ITU-R P. 837-6, Logarithmic and global coefficients result in greater error probabilities which signifies that these models performance is relatively less efficient in Icheon.

Table 3.10. Average error obtained after testing over interval [0.001% to 1%].

Methods	5 to 1 min			10 to 1 min			20 to 1 min			30 to 1 min			60 to 1 min		
	Error ε (%)	SD (%)	RMSE (%)	Error ε (%)	SD (%)	RMSE (%)	Error ε (%)	SD (%)	RMSE (%)	Error ε (%)	SD (%)	RMSE (%)	Error ε (%)	SD (%)	RMSE (%)
ITU-R P. 837-6	3.32	17.32	10.87	12.59	17.56	11.35	24.64	19.35	17.46	46.44	23.27	32.81	58.46	24.26	38.61
Segal	0.70	8.55	4.69	0.78	8.43	5.43	0.85	8.72	5.66	0.80	9.04	7.20	1.04	9.61	6.61
Burgueno et al.	-0.38	8.09	4.39	-0.04	8.32	5.15	-0.21	8.69	5.43	-0.18	9.10	6.87	-1.54	10.17	6.15
Chebil and Rahman	0.70	8.16	4.35	0.78	8.33	5.18	0.92	8.79	5.60	0.70	8.78	6.96	1.03	9.50	6.80
Logarithmic	49.23	22.73	52.68	49.66	22.95	53.82	50.56	22.48	53.19	50.79	21.76	51.31	51.48	19.46	47.21
Exponential	6.46	20.10	6.95	6.49	20.07	7.37	6.41	19.68	7.58	6.26	18.95	8.79	4.75	15.97	6.56
Global Coefficients	0.07	10.48	7.54	7.64	14.43	16.31	24.20	20.48	33.19	41.47	29.53	53.23	95.86	47.60	106.55
Second Order Polynomial Fit	0.92	8.42	4.17	1.11	8.75	5.00	1.05	8.80	5.28	0.85	8.80	6.79	1.04	9.08	5.50
Third Order Polynomial Fit	0.36	8.12	3.38	0.46	9.03	4.14	0.54	9.29	4.68	56.35	391.47	453.80	0.55	9.15	4.91
Model 1	-0.01	7.8	3.03	0.04	8.5	3.7	-0.01	9.02	4.23	-0.29	10.07	6.39	0.07	9.05	4.55

Table 3.11. Relative Error obtained over the 0.01% of the time.

Methods	5 to 1 min		10 to 1 min		20 to 1 min		30 to 1 min		60 to 1 min	
	Error ε (%)	RMSE (%)	Error ε (%)	RMSE (%)	Error ε (%)	RMSE (%)	Error ε (%)	RMSE (%)	Error ε (%)	RMSE (%)
ITU-R P. 837-6	31.13	18.68	45.15	27.09	63.48	38.09	93.23	55.94	105.30	63.18
Segal	1.09	0.66	6.19	3.71	11.50	6.90	13.57	8.14	20.20	12.12
Burgueno et al.	1.92	1.15	6.96	4.17	11.60	6.96	13.79	8.28	19.43	11.66
Chebil and Rahman	0.05	0.03	5.23	3.14	11.83	7.10	12.31	7.39	19.16	11.50
Logarithmic	55.14	33.09	64.40	38.64	73.86	44.32	77.30	46.38	87.36	52.42
Exponential	-10.90	6.54	-7.55	4.53	-3.82	2.29	-1.84	1.10	3.38	2.03
Global Coefficients	3.43	2.06	17.79	10.67	44.02	26.41	69.34	41.60	153.38	92.03
Second Order Polynomial Fit	-0.90	0.54	4.05	2.43	8.67	5.20	11.40	6.84	13.27	7.96
Third Order Polynomial Fit	1.36	0.82	5.77	3.46	9.15	5.49	21.56	12.93	11.44	6.86
Model 1	3.36	2.01	8.53	5.12	12.14	7.29	12.98	7.79	13.79	8.27

The similar characteristic of models performance is observed while applying average coefficient sets as mentioned in[8] which is shown in Table 3.12 and Table 3.13 for all time percentage interval and at 0.01% of the time respectively.

Table 3.12. Calculated Mean Error after testing over the interval [0.001% to 1%] while using average coefficient sets.

Methods	5 to 1 min			10 to 1 min			20 to 1 min			30 to 1 min			60 to 1 min		
	Error ε (%)	SD (%)	RMSE (%)	Error ε (%)	SD (%)	RMSE (%)	Error ε (%)	SD (%)	RMSE (%)	Error ε (%)	SD (%)	RMSE (%)	Error ε (%)	SD (%)	RMSE (%)
ITU-R P. 837-6	3.32	17.32	10.87	12.59	17.56	11.35	24.64	19.35	17.46	46.44	23.27	32.81	58.46	24.26	38.61
Segal	1.57	10.21	7.85	9.41	12.45	14.82	44.14	17.19	42.54	48.16	19.91	47.27	39.45	18.60	38.16
Burgueno et al.	67.77	16.59	59.63	251.78	39.68	212.41	437.35	102.45	406.21	493.85	137.63	474.81	569.31	144.79	528.47
Chebil and Rahman	1.26	12.34	6.03	-341.56	50.78	248.25	-1.91	89.56	31.78	-175.46	85.35	109.68	4.08	17.94	9.50
Logarithmic	-1.65	9.24	5.58	-2.16	9.90	6.28	-1.10	10.02	6.41	2.05	10.50	8.32	3.99	10.37	7.10
Exponential	23.04	21.34	16.12	25.32	20.69	22.38	30.21	24.09	40.72	39.26	32.08	57.21	42.18	26.19	53.49
Global Coefficients	0.07	10.48	7.54	7.64	14.43	16.31	24.20	20.48	33.19	41.47	29.53	53.23	95.86	47.60	106.55
Second Order Polynomial Fit	-7.23	15.59	7.47	-1.87	14.21	9.65	18.05	14.21	21.01	37.66	26.72	37.35	29.25	15.38	24.99
Third Order Polynomial Fit	-2.73	10.11	6.49	-12.04	27.90	14.83	-14.46	63.84	44.64	-37.81	169.05	107.75	-75.24	103.50	39.89
Model 1	-3.53	11.17	6.68	-1.65	20.92	18.38	10.75	53.24	65.94	18.10	104.33	123.54	-185.93	198.27	350.90

As noted from Table 3.12, Model 1 generate low relative error probabilities for lower time conversion but the error probabilities get increased for higher time conversion especially 60-min. to 1-min. In addition, Logarithmic model result in less error chances which is justified from decreased SD and RMS values. In contrast, Segal, ITU-R P. 837-6, second and third order polynomial fits, global coefficients and exponential methods show relatively higher error probabilities whereas Burgueno et al. and Chebil and Rahman result in greater relative error percentages.

Table 3.13. Calculated Mean Error obtained over the 0.01% of the time while using average coefficient sets.

Methods	5 to 1 min		10 to 1 min		20 to 1 min		30 to 1 min		60 to 1 min	
	Error ε (%)	RMSE (%)	Error ε (%)	RMSE (%)	Error ε (%)	RMSE (%)	Error ε (%)	RMSE (%)	Error ε (%)	RMSE (%)
ITU-R P. 837-6	31.13	18.68	45.15	27.09	63.48	38.09	93.23	55.94	105.30	63.18
Segal	5.70	3.42	20.21	12.13	66.32	39.79	75.78	45.47	74.13	44.48
Burgueno et al.	73.20	43.92	282.80	169.68	526.76	316.06	614.16	368.50	759.00	455.40
Chebil and Rahman	3.15	1.89	-331.40	198.84	-28.15	16.89	-142.72	85.63	32.52	19.51
Logarithmic	1.41	0.85	6.04	3.62	12.12	7.27	17.71	10.63	25.56	15.34
Exponential	2.88	1.73	8.87	5.32	18.31	10.99	29.68	17.81	44.35	26.61
Global Coefficients	3.43	2.06	17.79	10.67	44.02	26.41	69.34	41.60	153.38	92.03
Second Order Polynomial Fit	1.03	0.62	10.18	6.11	18.59	11.15	23.85	14.31	36.15	21.69
Third Order Polynomial Fit	0.71	0.43	8.49	5.10	19.17	11.50	24.95	14.97	39.68	23.81
Model 1	0.75	0.45	9.16	5.49	17.46	10.48	15.28	9.17	-77.39	-46.43

As tabulated in Table 3.13, Logarithmic model shows less error percentage as compared to other approaches. Although Model 1 generates less relative error percentage for lower time conversion as such 5-, 10-, 20-, 30-min. to 1-min. but it get increased for higher time conversion, particularly 60-min. to 1-min. Interestingly, Segal, exponential, second and third order polynomial fits results in similar pattern of relative error percentage. Moreover, ITU-R P. 837-6, global coefficients, Burgueno et al. and Chebil and Rahman results in higher relative error probabilities.

E. Conclusions

The performance of ITU-R P. 837-6 and other prominent 1-min. rain rate estimation models are studied against the locally measured 1-min. rainfall amount provided by KMA from 2004 till 2013. The appropriate modified polynomial of fourth order is proposed that is observed to be suitable for the prediction of 1-min. rain rate distribution. Additionally, Logarithmic model show suitable performance for the better prediction of rain rate at 0.01% of time. The suitable contour maps for 0.01% of the time have been presented for the South Korea, which was developed using advanced Geographic Information Systems (GIS) tools with the adoption of Kriging interpolation estimator. The mean 1-min. rain rate distribution of nine prime locations is also studied. Furthermore, Icheon and Mokdong sites have been considered for the simultaneous measurement of rain rate and rain attenuation in 10second interval which is combined to 1-min. distribution. The experimental rainfall amount of 1-min. interval and the rain rate measurement results have been studied to measure the suitability of proposed models.

IV. Rain Attenuation in Terrestrial Links

A.Introduction

Rain attenuation for terrestrial links at 18 GHz horizontal and vertical, 38 and 75 GHz vertical polarizations has been calculated. In this study, two types of techniques are used. The results of this study show that the rain attenuation for vertically polarized signal is less than that of the horizontal polarization at all operating frequencies. Furthermore, the frequency and polarization scaling between distributions are also discussed.

B.Experimental Set up for Microwave Links

The concurrent measurement of rain attenuation and rainfall rate data were collected by National Radio Research Agency (RRA) at Icheon, South Korea. The experimental microwave links in 18, 38, 75 GHz are installed whose detail characteristics are listed in Table 4.1.

Table 4.1. Characteristics of study locations.

Station	Latitude (^{0}N)	Longitude (^{0}E)	Period	Region Climate
Khumdang (Korea Telecom, KT)	37.136	127.516	2013-2015	Temperate
Icheon (National Radio Research Agency, RRA)	37.147	127.549	2013-2015	Temperate
EMS Dong yoksang	37.197	127.426	2013-2015	Temperate

In Icheon, the climate is cold and temperate in which summers are much rainier than winters. The average rainfall is 1296 mm/year. For 18 GHz operation, one antenna at Khumdang, KT Station tower is vertically polarized and out of two antennas at Icheon, RRA Station tower, one antenna is vertically polarized and another is horizontally polarized in 3.2 km path length. Similarly, for 38 GHz operation, one antenna at Khumdang, KT Station tower and next at Icheon, RRA Station tower in 3.2 km path length is vertically polarized. In addition, for 75 GHz operation in 0.1km path length, one antenna at Icheon, RRA Station and next at EMS Dong yoksang Station is vertically polarized. These antennas were covered with radome to prevent wetting antenna conditions. These terrestrial links has availability of 99.95% and their specifications are given in Table 4.2.

Table 4.2. Specifications of the 18, 38 and 75 GHz links.

Microwave links	Descriptions	Specification
Common Features	Antenna type	Front-fed Parabolic
	Reception Method	Super heterodyne
	Modulation	QPSK
	Maximum Modulation Degree	8 bit/Hz (for 18 and 38 GHz links) 6 bit/Hz (for 75 GHz link)
	Size of Antenna for both transmit and receive side [m]	0.6
	Gain of Antenna for both transmit and receive side [dBi]	38.8 (for 18 GHz links) 45.1 (for 38 and 75 GHz links)
18 GHz (Link length= 3.2 km)	Frequency Band (GHz)	17.7 ~ 18.2
	Polarization (@ Khumdang, KT Station) Tower	Vertical
	Polarization (@ Icheon, RRA Station) Tower	Vertical for Antenna 1, Horizontal for Antenna 2
	Maximum Transmit Power	0.16 W (+22 dBm)
	BER Received Threshold (for Horizontal Polarization) [dBm]	-52.34
	BER Received Threshold (for Vertical Polarization) [dBm]	-32.81
	Half Power Beam width	1.9^0
38 GHz (Link length= 3.2 km)	Frequency Band (for 38 GHz)	38.316 ~ 38.936
	Polarization (@ Khumdang, KT Station) Tower	Vertical
	Polarization (@ Icheon, RRA Station) Tower	Vertical
	Maximum Transmit Power	0.063 W (+18 dBm)
	BER Received Threshold (for Vertical Polarization) [dBm]	-29.88
	Half Power Beam width	0.9^0
75 GHz (Link length=0.1 km)	Frequency Band (for 75 GHz)	71 ~ 76
	Polarization (@Icheon, RRA Station) Tower	Vertical
	Polarization (@EMS Dong yoksang Station) Tower	Vertical
	Maximum Transmit Power	0.005 W (+7 dBm)
	BER Received Threshold (for Vertical Polarization) [dBm]	-22.95
	Half Power Beam width	0.8^0

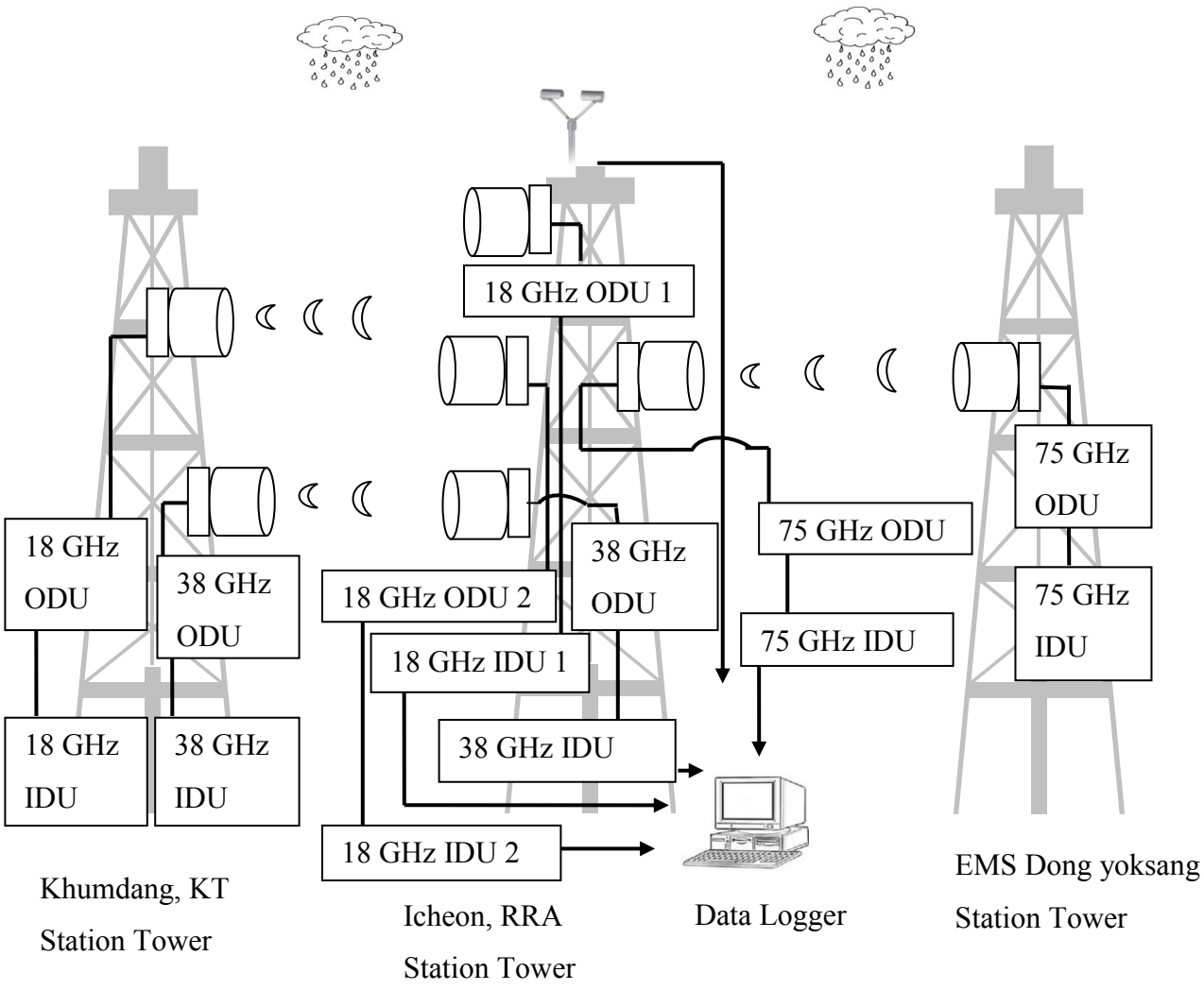

Figure 4.1: Experimental setup for rain attenuation and rain rate measurement

The received signal levels were sampled every 10 seconds and finally averaged over 1-min. Three years rainfall intensities with 99.95% of validity of all time, were collected by OTT Parsivel, a laser-based optical disdrometer for simultaneous measurement of particle size and velocity of all liquid and solid precipitation, for every 10 seconds interval which in turn is averaged over 1-min. as given in[44]. OTT Parsivel is a laser sensor that produces a horizontal strip of light in which the emitter and receiver are integrated into a single protective housing. The measured signal output voltage changes whenever a hydrometeor falls through the laser beam

anywhere within the measurement area. This will determine the particle size. In addition, to determine the particle speed, the duration of the signal is measured. A signal begins as soon as a precipitation particle enters the light strip and ends when it has completely left the light strip. After determining these two quantities, parsivel disdrometers bin measured particles into particle counts per velocity and diameter class. There are 32 velocity classes and 32 diameter classes, with varying widths. Parsivel determines the rain rate from the classification of precipitation particles. The corresponding software ASDO monitors the outdoor precipitation event to comfortable indoor evaluation with windows performance. The sensor on OTT Parsivel transmits all data to a PC through RS 485 interface which are stored in a powerful database and can be retrieved by browser with related date and time. An automatic heating system prevents ice buildup on the sensor heads. The heating system is adjusted by the temperature sensor which measures the temperature each second. The full list of procedure supported by Parsivel disdrometer can be found in[68, 69]. The schematic diagram for system set up is shown in Figure 4.1 which depicts that the two front-fed parabolic antennas are mounted on 35 m height Khumdang, KT Station tower for 18 and 38 GHz operation. The Out Door Unit (ODU) is connected to In Door Unit (IDU) via approximate 30 m coaxial cable. Similarly, four parabolic antennas are mounted on 20 m height Icheon, RRA Station tower in which one is in horizontal polarization and next in vertical polarization for 18 GHz operation. Similarly, remaining two parabolic antennas are vertically polarized for 38, 75 GHz operations. The ODU of these antennas are connected to separate IDU through coaxial cable. The data logger unit along with OTT Parsivel rain gauge is installed in Icheon, RRA Station where, rain gauge is set up at top of the tower. The receive signal level (RSL) for any terrestrial microwave link can be expressed as follows[19]:

$$\boldsymbol{RSL = P_T + G_T + G_R - L_{fs} - A_G - A_R - A_W - L_R - L_t} \quad (4.1)$$

where $\boldsymbol{P_T}$ (dBm) is the transmit power, $\boldsymbol{L_t}$ (dB) is the loss in the transmit system, $\boldsymbol{G_T}$ (dB) is the transmit antenna gain, $\boldsymbol{L_{fs}}$ (dB) is the free space loss, $\boldsymbol{A_G}$ (dB) is loss due to gaseous absorption, $\boldsymbol{G_R}$ (dB) is the receive antenna gain, $\boldsymbol{L_R}$ (dB) is the loss in receive systems, $\boldsymbol{A_R}$ (dB) is the excess attenuation due to rain on propagation path and $\boldsymbol{A_W}$ (dB) is the wet antenna loss on both antennas during rain ($\boldsymbol{A_{W,transmit} + A_{W,receive}}$). Among all the factors, free space loss, gaseous absorptions, and excess rain attenuation are all dependent on operating frequency, propagation path length, and the location of link. The free space loss can be obtained from the Friis expression:

$$\boldsymbol{L_{fs} = 32.4 + 20\, log_{10}\,(d_{km}) + 20\, log_{10}\,(F_{MHz})} \quad (4.2)$$

where $\boldsymbol{d_{km}}$ is path length in km and $\boldsymbol{F_{MHz}}$ is the operating frequency. Gaseous absorptions are negligible at frequencies below 30 GHz. For instance, the vapor absorption at 22 GHz is 0.16 dB/km. Therefore, the gaseous absorption A_G can be neglected in (4.1). Similarly, the losses in transmit ($\boldsymbol{L_t}$) and receive ($\boldsymbol{L_R}$) systems can also be neglected in (4.1) since it is not significant with respect to free space loss and excess attenuation due to rain. The wet antenna loss is also varied with antenna size, radomes materials so this loss has not been considered during calculation. Under clear sky condition, there is the continuous communication between Transmitter and Receiver section whose received signal level are continuously recorded in data logger. During raining condition, there is the fluctuation in this signal level. Hence, the corresponding path attenuation is calculated by finding the difference between the RSL during

clear sky conditions and the RSL during rain for horizontal and vertical polarized received signal as follows:

$$\boldsymbol{Attenuation\ (dB) = RSL_{clear\ sky} - RSL_{rainy}} \tag{4.3}$$

Monolithic Microwave Integrated Circuit (MMIC) with 12 VDC power supply and -10 dBm input signal which is build internally to the equipments support for the attenuation measurement with radio throughput of 367 Mbps. In order to counteract the effects such as scintillation, appropriate antenna size is chosen with suitable range of frequencies as 17.7 to 19.7 GHz along with the minimum received signal level threshold as mentioned in Table 4.2 are maintained at receiving side. In order to process raw data, similar approach as for determining 1-min. rain rate in[44] is adopted for determining the rain attenuation value for 1-min. interval. These data are combined in descending order and the required 1-min. rain rate and attenuation values along with rain cell diameter are determined from 1% to 0.001% of the time. For example, at 0.01% of the time, 1-min. rain rate and attenuation as well as rain cell diameter values are taken for about 158 $((3 \times 365 \times 24 \times 60 \times 0.01)/100) = 157.68 \approx 158)$ instance for 3-years measurement when combined together. These instances are obtained by multiplying the number of experimental year, number of days in a year, hour and minute in a day, with required time percentage.

The cumulative distribution of 1-min. rain rate calculated from the measured rain rate for 10 seconds intervals for three years (2013 till 2015) of the studied location is shown in Figure 4.2.

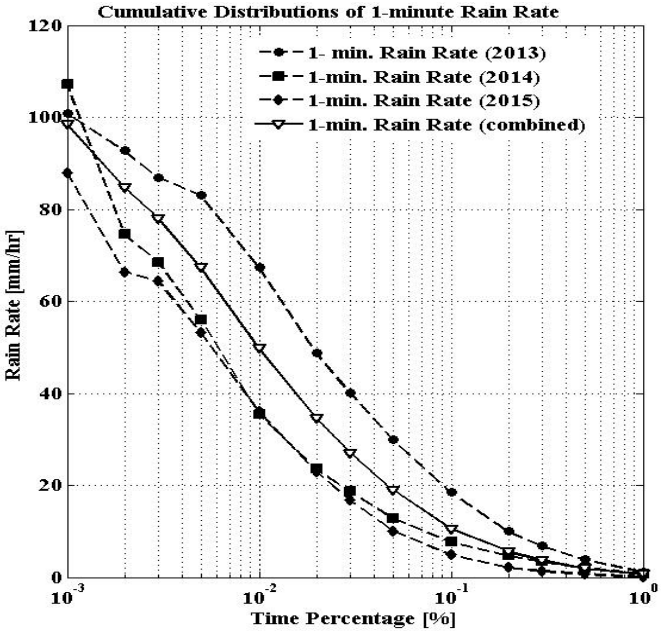

Figure 4.2: The rainfall rate distribution at Icheon.

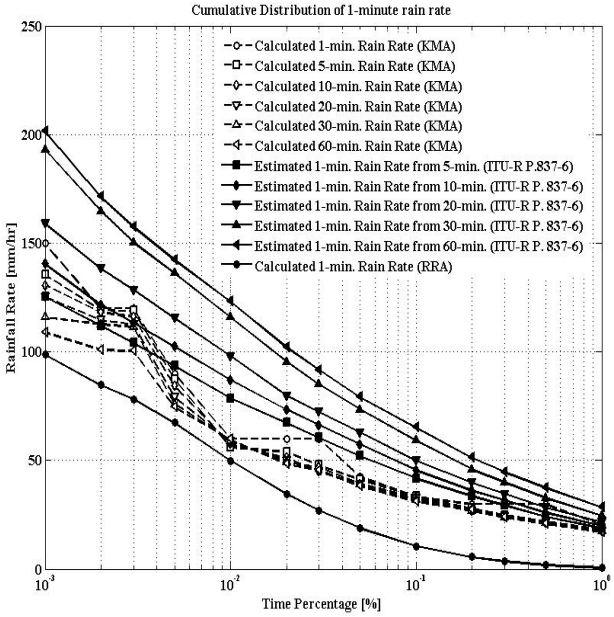

Figure 4.3: The rain rate distribution at Icheon from KMA and RRA database.

Figure 4.2 indicates the maximum rainfall rate occurred in 2013 but it decreases for successive years which might be due to the variability of rainfall occurrence in different seasons under mentioned periods. For instance, at 0.01% of the time, the obtained rainfall rate is 67.34 mm/hr in 2013 whereas, in 2014 and 2015, the values are 35.48 and 36.07 mm/hr respectively. The research considered the combined value of rainfall rate which indicate that at 0.01% of the time, the 1-min. rainfall rate value is 49.79 mm/hr for Icheon site. Furthermore, 1-min. rain rate values decreases and tends to be smaller for higher time percentages, for example, at 0.5% and 1% of the time the rain rate are observed to be 1.99 mm/hr and 0.65 mm/hr. Similarly, at lower time percentage 1-min. rain rate is increased, for example, at 0.001% of the time the rain rate obtained is 98.57 mm/hr. Similarly, the measured 1-min. rain rate as obtained from RRA is compared with the rain rate derived from the 1-min. rainfall amount experiment conducted by Korea Meteorological Administration (KMA)[70] in Icheon (37.27^0N, 127.45^0E) region, where the rain rate differ by about 10 mm/hr for 0.01% of the time which might be due to the different

experimental procedures. The detail operation of KMA experiment is mentioned in [41] [42]. Unfortunately, KMA experiment is conducted to measure only 1-min. rainfall amount where the measurement of rain attenuation is not conducted. However, this 1-min. rainfall amount experiment is significant for the comparison of 1-min. rain rate conducted by RRA. The experimental 1-min. rainfall amount are arranged and combined which are converted to higher time rain rate as 5-min., 10-min., 20-min., 30-min. and 60-min. following the approach as mentioned in[41], [20]. For instance, at 0.01% of the time, 1-min., 5-min., 10-min., 20-min., 30-min. and 60-min. rain rate are taken for about 526 ((10×365×24×60×0.01)/100) = 525.6 ≈ 526), 105 ((10×365×24×12×0.01)/100) = 105.12 ≈ 105), 53 ((10×365×24×6×0.01)/100) = 52.56 ≈ 53), 26 ((10×365×24×3×0.01)/100) = 26.28 ≈ 26), 18 ((10×365×24×2×0.01)/100) = 17.52 ≈ 18), 9 ((10×365×24×1×0.01)/100) = 8.76 ≈ 9) instance for 10-years measurement performed by KMA. These instances are obtained by multiplying the number of experimental year, number of days in a year, hour and minute in a day, with required time percentage. These values are taken as an input parameter along with the latitude and longitude information so as to obtained 1-min. rain rate from software recommended by ITU-R P. 837-6[4]. Additionally, this figure indicates that for higher time conversion, particularly, 20-, 30-, 60- min. to 1-min., ITU-R P. 837-6 shows the overestimation whereas for lower time conversion from 5- and 10-min. to 1-min., this model gives closer prediction against the calculated 1-min. rain rate values which are tabulated in Table 4.3 at 0.1%, 0.01% and 0.001% of the time.

Table 4.3. Calculated and predicted rain rate.

Time	Calculated Rain Rate (mm/hr)						Estimated Rain Rate (ITU-R P. 837-6) (mm/hr)				
Percentage	1-min.	5-min.	10-min.	20-min.	30-min.	60-min.	5- to 1-min.	10- to 1-min.	20- to 1-min.	30- to 1-min.	60- to 1-min.
0.1%	33.60	33.52	33.00	32.58	32.00	31.21	41.72	45.65	50.10	59.24	65.21
0.01%	60.00	56.25	57.54	58.95	59.12	59.65	78.68	87.09	98.09	115.94	123.18
0.001%	150.00	135.45	130.65	125.46	115.95	109.00	125.45	140.48	159.09	193.24	201.54

This signifies that the measured values of rainfall rate as provided by RRA is underestimated, which is used as an input data for the prominent prediction models that are derived from measurements in a significant number of links all over the world. This might be the reason that most of the prediction models generate lower values against the measured results. Hence, the rain rate measurement of longer duration is required for efficient analyses and the experimental system is still under progress. Figure 4.4 shows the rain attenuation for three different frequencies. At 18 GHz, the rainfall results in greater attenuation for horizontal polarization as compared to vertical polarization. During horizontal polarization, at 0.01% of the time, the obtained rain attenuation value is 32.57 dB and for vertical polarization at same percentage of time, the value is 21.88 dB. Similarly, the rain attenuation values get increased for lower time percentage which reached up to 50.83, 38.36 dB at 0.001% of the time for horizontal and vertical polarization respectively. Conversely, at higher time percentage as such for 1% of the time, the rain attenuation value gets decreased to 5.4, 0.41 dB respectively. It is observed that rain has greater effect in 75 GHz as compared to 38 and 18 GHz under vertical polarization. Interestingly, rain attenuation is greater at 18 GHz under horizontal polarization as compared to vertical polarization for 18, 38 and 75 GHz links. For instance, under horizontal polarization at 18 GHz we obtained 17.53, 32.57, 50.83 dB respectively at 0.1%, 0.01% and 0.001% of the time where as under vertical polarization for 18, 38, 75 GHz we obtained 11.59, 21.88, 38.36 dB; 10.53, 20.89, 38.44 dB; 16.11, 28.55, 40.48 dB respectively for same percentage of the time.

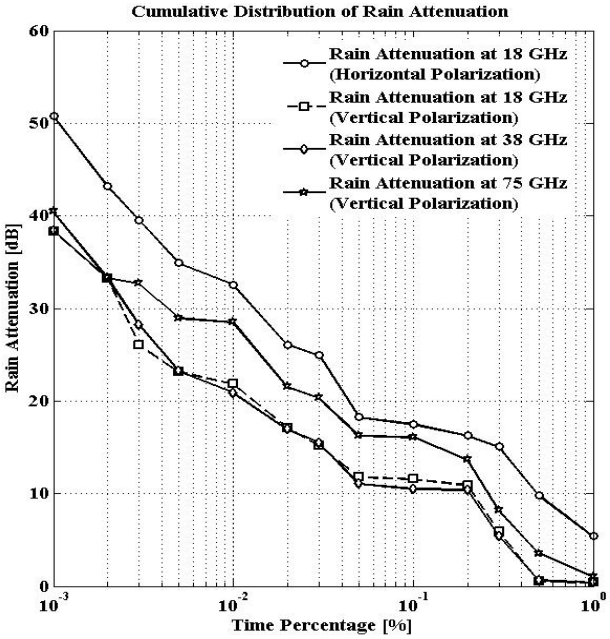

Figure 4.4: Distribution of rain attenuation at Icheon.

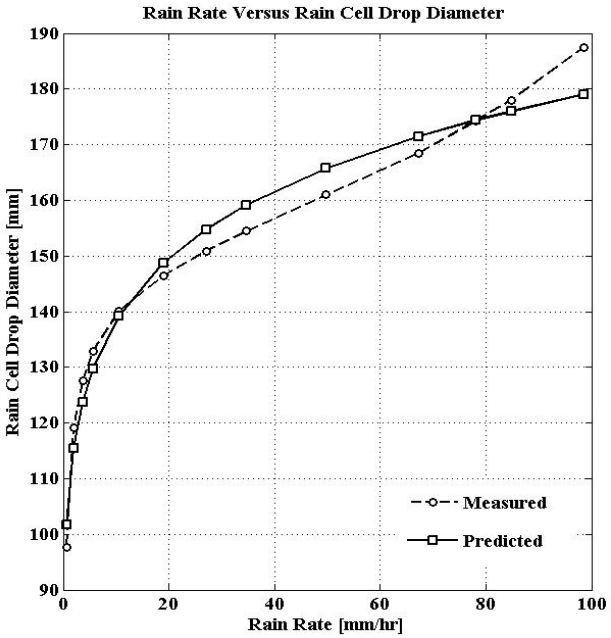

Figure 4.5: Distribution of rain rate against rain cell drop diameter.

Similarly, the plot of rain rate against rain cell drop diameter is depicted in Figure 4.5 which indicates the smaller rain cell diameter for lower rain rate whereas for higher rain rate, increase in rain cell drop diameter is observed. For instance, at 0.1%, 0.01%, 0.001% of the time, the observed rain rate are 10.58, 49.79, 98.57 mm/hr where rain cell drop diameter of 139.25, 165.77, 179.01 mm are noted. This profile is better estimated by power law equation which is expressed as,

$$\boldsymbol{d_0 = 106.8\, R_p^{-0.1125}} \tag{4.4}$$

where, $\boldsymbol{R_p}$ and $\boldsymbol{d_0}$ are the 1-min. rainfall rate and equivalent rain cell drop diameter. The regression value of $\boldsymbol{R^2}$ is 0.9738 which is close to unity which signifies its better accuracy for estimation of rain cell drop diameter. However, the $\boldsymbol{R_p^{-0.1125}}$ factor in the fitted expression is a

inverse $\mathbf{1/x}$ relationship which might not explain the shape of the curve with $\boldsymbol{x^{0.5}}$ family of curves. But these empirically derived coefficients values as obtained from the curve fitting procedure performed from Matlab program[66] which shows the preliminary step to characterize the relationship between rain cell drop diameter and 1-min. rain rate distribution.

C.Proposed Technique

In order to propose a suitable approach, we studied the relationship between the theoretical specific rain attenuation, $\boldsymbol{\gamma_{\%p}}$ as given by ITU-R P. 838-3[6] and effective specific rain attenuation, $\boldsymbol{\gamma_{eff}}$ which is obtained by dividing the experimentally derived rain attenuation values by the product of link distance and path correction factor. The methods as adopted in[27] has been used but with some variation on the effective rain rate. The empirical relationship between these two quantities is given by the following ratio:

$$\frac{\gamma_{\text{eff}}}{\gamma_{\%\text{p}}} = \frac{kR_{eff}^{\alpha}}{kR_{\%p}^{\alpha}} \tag{B.3}$$

Solving equation (8), we get the effective rain rate as,

$$R_{\text{eff}} = \left(\frac{1}{\text{k}}\gamma_{\text{eff}}\right)^{\frac{1}{\alpha}} = R_{\%\text{p}}\left(\frac{\gamma_{\text{eff}}}{\gamma_{\%\text{p}}}\right)^{\frac{1}{\alpha}} \tag{B.3 (a)}$$

Alternatively, effective rain rate can be expressed as a function of measured rain rate by power law as follows:

$$R_{eff} = aR_{\%p}^{b} \tag{B.3 (b)}$$

where $\boldsymbol{a}$ and $\boldsymbol{b}$ are derived empirically whose values are 18.24, 0.4318; 8.719, 0.6162 respectively for horizontal and vertical polarization. In order to generalize the proposed approached method, the experimental links performed at 38 and 75 GHz are been considered. Similar method is adopted to calculate the effective rain rate for these higher microwave links. The empirically derived values of a and b for 38 and 75 GHz links are 1.458, 0.7846 and 179.9, 0.655 respectively. Under the presence of effective specific rain attenuation, equation (B.3 (a)) has been used for derivation of effective rain rate. It is observed that effective path length is smaller than the actual physical path length, which leads to the introduction of path correction factor as mentioned in[71]. The path correction factor, $\boldsymbol{r}$, is given by:

$$\boldsymbol{r} = \frac{\mathbf{1}}{\mathbf{1}+\left(\frac{\boldsymbol{d}}{\boldsymbol{d_0(Rp)}}\right)} \qquad \text{(B. 3 (c))}$$

where $\boldsymbol{d}$, is the actual link distance and $\boldsymbol{d_0(R_p)}$ is equivalent rain cell diameter which is related through power law and the required coefficients are derived experimentally which depend on the 1-min. rain rate exceeded at $\%\boldsymbol{p}$ of the time.

In addition, proposed approach as represented by equation (B.3(b)) can be used to derive effective rain rate from 1-min. rain rate values for $\%\boldsymbol{p}$ time percentage. This approach is adopted for further analysis because it utilizes the full 1-min. rain rate distribution over $0.001\% \leq \%\boldsymbol{p} \leq 1\%$. Therefore, the attenuation exceeded at $\%\boldsymbol{p}$ of the time can be expressed as given in equation (B.3 (d)),

$$\textbf{Method 1: } A_{\%p} = \gamma_{\text{eff}}\, d_{\text{eff}} = k\,[R_{\text{eff}}(R_{\%\text{p}}, d)]^{\alpha}\left[\frac{d}{1+\left(\frac{d}{d_0(R_{\%p})}\right)}\right] \qquad \text{(B. 3 (d))}$$

However, the result is still preliminary and more data is needed to be collected for accurate results. Thus, there are many limitations for the utilization of this approach. More informative experiment should be involved with several longer paths along with other lower frequencies range as well as the study of rain attenuation in diverse locations of the South Korea. National Radio Research Agency (RRA) is planning for establishment of these systems in other locations in near future for better prediction of rain attenuation models. Hence, this approach shows suitability only in the mention location.

Furthermore, the difference in the prediction error obtained between the measured 1-min. rain attenuation values and predicted ITU-R P. 530-16 shows that the polynomial of second order is best least square regression that fits the ITU-R P. 530-16 prediction error against the 1-min. rain rate distribution for horizontal polarization which is given as:

$$\Delta A_{\%p} = \mathbf{a_1}\,\mathbf{R}_{\%\mathbf{p}}^{2} + \mathbf{a_2}\,\mathbf{R}_{\%\mathbf{p}} + \mathbf{a_3} \qquad \text{(B. 4)}$$

where, $\Delta A_{\%p}$ is the ITU-R P. 530-16 prediction error for horizontal polarization and $\mathbf{a_1}$, $\mathbf{a_2}$, $\mathbf{a_3}$ are regression parameters whose values depend on frequency and radio path length of the microwave link under consideration. In addition, for vertical polarization, the ITU-R P. 530-16 prediction errors are analyzed with the best least square regression of fourth order polynomials [74] whose expression is given by equation (B.5).

$$\Delta A_{\%p} = \mathbf{a_1}\, \mathbf{R}_{\%\mathbf{p}}^{\mathbf{4}} + \mathbf{a_2}\, \mathbf{R}_{\%\mathbf{p}}^{\mathbf{3}} + \mathbf{a_3}\, \mathbf{R}_{\%\mathbf{p}}^{\mathbf{2}} + \mathbf{a_4}\, \mathbf{R}_{\%\mathbf{p}} + \mathbf{a_5} \qquad \text{(B.5)}$$

where, $\Delta A_{\%p}$ is the ITU-R P. 530-16 prediction error for vertical polarization and $\mathbf{a_1}$, $\mathbf{a_2}$, $\mathbf{a_3}$, $\mathbf{a_4}$, $\mathbf{a_5}$ are regression parameters whose values depend on frequency and radio path length of the microwave link under consideration.

Table 4.4 shows the values of regression coefficients used for the estimation of ITU-R P. 530-16 prediction errors against the full 1-min. rain rate distribution over 0.001% ≤ %$\boldsymbol{p}$ ≤ 1% for 18, 38 and 75 GHz links.

Table 4.4. Regression coefficients for 18, 38 and 75 GHz links.

Frequency (GHz)	$\mathbf{a_1}$	$\mathbf{a_2}$	$\mathbf{a_3}$	$\mathbf{a_4}$	$\mathbf{a_5}$
Horizontal Polarization for 18 GHz	-0.003944	0.4698	4.73		
Vertical Polarization for 18 and 38 GHz	-0.0000008513	0.0002282	-0.01912	0.6344	1.474
Vertical Polarization for 75 GHz	-0.000001125	0.0003037	-0.02742	1.0540	2.063

Hence, in order to improve ITU-R P. 530-16 rain attenuation prediction model, it is proposed that for lower frequency particularly, for 18 GHz horizontal polarization, equation (B.4) should be added to the predicted values as shown in **Method 2 (a)**:

Method 2(a):

$$A_{\%predicted} = A_{0.01}\, \mathbf{C_1} p^{-(\mathbf{C_2}+\mathbf{C_3}\log_{10} p)} + [\mathbf{a_1}\, \mathbf{R}_{\%\mathbf{p}}^{\mathbf{2}} + \mathbf{a_2}\, \mathbf{R}_{\%\mathbf{p}} + \mathbf{a_3}] \qquad \text{(B.6)}$$

Similarly, for vertical polarization, the analyses have been performed by adding equations (B.5) separately on the ITU-R P. 530-16 rain attenuation prediction model for lower frequency

especially 18 GHz while for higher frequency, particularly, 38 GHz, this prediction error is subtracted over the percentages of time, $\boldsymbol{p}$, in the range 0.001% to 1% for the same link distance which is listed below in equation (B.7):

Method 2(b):

$$\boldsymbol{A_{\%predicted} = A_{0.01} C_1 p^{-(C_2 + C_3 \log_{10} p)} \pm [a_1 R_{\%p}^4 + a_2 R_{\%p}^3 + a_3 R_{\%p}^2 + a_4 R_{\%p} + a_5]} \quad \text{(B.7)}$$

where $\boldsymbol{A_{0.01}}$ is the estimated path attenuation exceeded for 0.01% of the time whose expression is defined in ITU-R P. 530-16[2] model along with C_1, C_2 and C_3 terms. Similarly, for 75 GHz operating frequency, the prediction error is added with similar expression as shown by Method 2. Appendix 1 shows the applicable formulas for existing six rain attenuation models for terrestrial links.

D.Performance Evaluation

The comparison between measured rain attenuation Complementary Cumulative Distribution Function (CCDF) against ITU-R P. 530-16 predicted values for several time percentages at equiprobable exceedance probability (0.001% ≤ $\boldsymbol{P}$ ≤ 1%) are plotted in Figure 4.6.

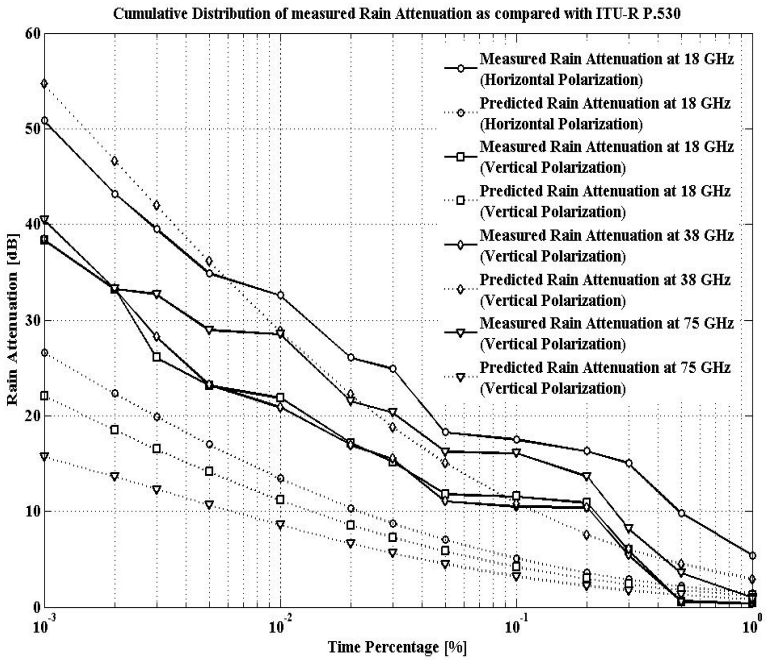

Figure 4.6: Cumulative distribution of measured rain attenuation versus ITU-R P. 530-16 predicted values.

The rain rate exceeded for 0.01% of the time, which is obtained from the RRA database as depicted in Figure 4.5 is used as an input rain rate for the prediction of ITU-R P. 530-16. The 1-min. rain attenuation statistics for 18, 38, 75 GHz are obtained by averaging the original 10 seconds measured values, because of which curves are not smooth enough. However, the results are useful for the preliminary study of attenuation induced by the rain in this region. We have arranged the measured rain attenuation statistics in 1-min. because the prominent rain attenuation prediction models predicts the 1-min. rain attenuation values from the 1-min. rain rate statistics. Figure 4.6 show that ITU-R P. 530-16 does not accurately estimate the rain attenuation CCDF even though this method gives fair well statistics at higher time percentage ($\boldsymbol{P} \geq 0.5\%$). At lower time percentage this method dramatically underestimates the measured rain attenuation except at 38 GHz where there is higher overestimation. For instance, at 0.01% of the time, the measured rain attenuation values are 32.57, 21.88, 20.89 and 28.55 dB for 18 GHz horizontal, 18, 38, 75 GHz vertical links respectively. While the corresponding ITU-R P. 530-16 estimated values are

13.47, 11.18, 28.83 and 8.59 dB respectively. Moreover, the deviations are more pronounced at higher frequencies; for example, the deviations are approximately 8 and 20 dB at 38 and 75 GHz respectively. The reason behind this difference could be the fact that the matrices used to obtain the parameters might have low spatial resolution. This indicates that ITU-R P. 530-16 method performance statistics does not shows good agreement with calculated 1-min. rain attenuation distribution from experimental 10-seconds measured rain attenuation values of the Icheon, South Korea. In this concern, there is the need for 1-min. rain attenuation prediction model that can give higher efficiency against the local 1-min. rain attenuation distribution. Under this aspect, the research presents new approach that shall be applicable in analyzing the 1-min. rain attenuation distribution pattern for terrestrial microwave links. As an initial step several prominent rain attenuation models as well as proposed approaches are analyzed against the calculated 1-min. rain attenuation distribution. These are shown from Figure 4.7(a) – 4.7(d) for 18 GHz horizontal, 18, 38, 75 GHz vertical polarization respectively.

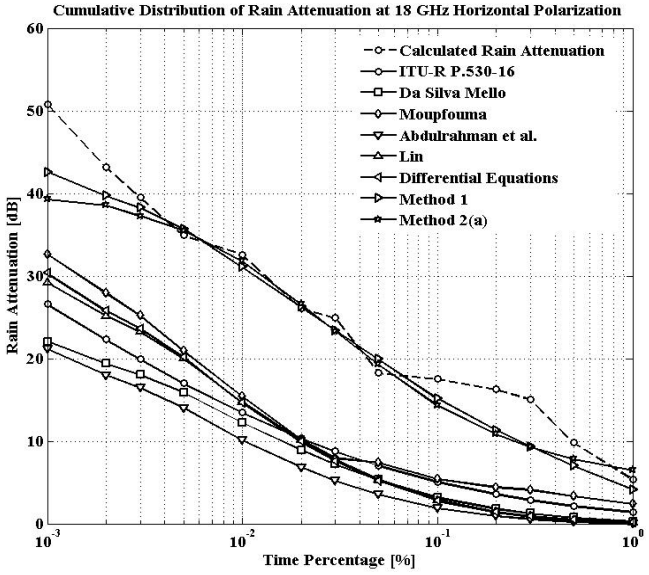

Figure 4.7(a): Cumulative distribution of rain attenuation compared under horizontal polarization with models prediction at 18 GHz.

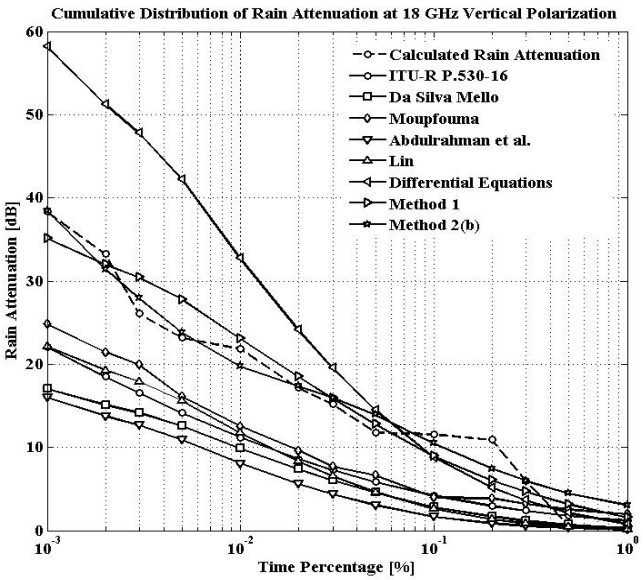

Figure 4.7(b): Cumulative distribution of rain attenuation compared under vertical polarization with models prediction at 18 GHz.

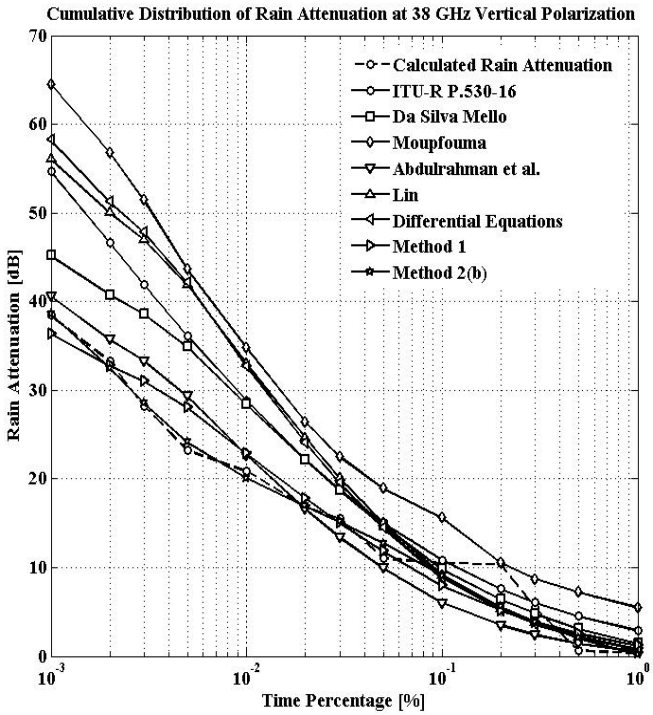

Figure 4.7(c): Cumulative distribution of rain attenuation compared under vertical polarization with models prediction at 38 GHz.

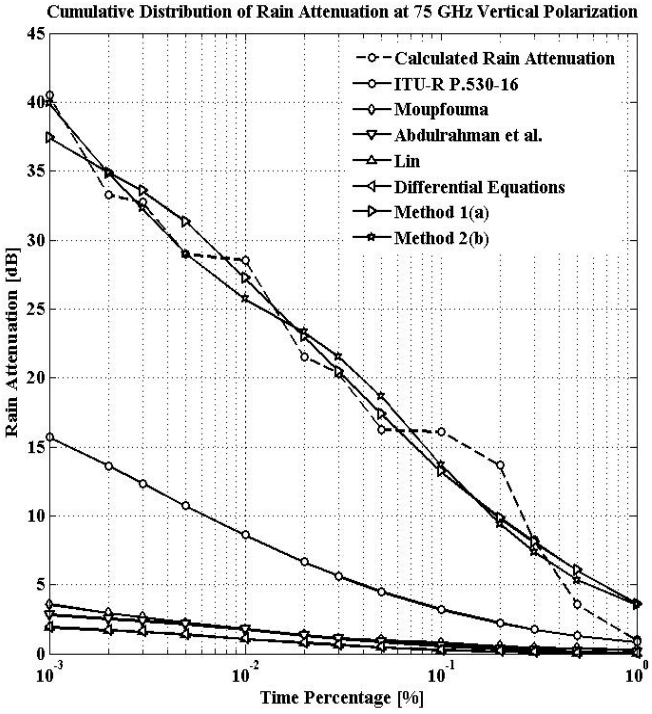

Figure 4.7(d): Cumulative distribution of rain attenuation compared under vertical polarization with models prediction at 75 GHz.

As noticed from Figure 4.7(a) and Figure 4.7(b), for 18 GHz under horizontal and vertical polarization, it is observed that the measured cumulative statistics of rain attenuation is underestimated by ITU-R P. 530-16. The underestimation becomes highly pronounced at lower time percentage. For instance, the calculated rain attenuation values are 17.53, 32.57, 50.83 dB and 11.59, 21.88, 38.36 dB respectively for horizontal and vertical polarization at 0.1%, 0.01%, 0.001% of the time while ITU-R P. 530-16 predicts 5.10, 13.47, 26.61 dB and 4.23, 11.18, 22.08 dB. Similar pattern is observed with the application of Da Silva Mello, Abdulrahman et al. and Lin which underestimate the measured cumulative statistics of rain attenuation. For instance, under horizontal and vertical polarization, Da Silva Mello model predicts 3.19, 12.24, 22.08 dB and 2.85, 9.89, 17.09 dB respectively at 0.1%, 0.01% and 0.001% of the time where as Abdulrahman et al. and Lin predicts 1.89, 10.12, 21.19 dB; 1.71, 8.09, 16.03 dB and 2.89, 14.75,

29.23 dB; 2.61, 11.78, 22.11 dB. More underestimation is observed from the application of Abdulrahman et al. In the same way, Lin and Differential Equations show underestimation for horizontal polarization whereas overestimation is observed for vertical polarization. For instance, Differential equations predicts 2.77, 14.61, 30.33 dB and 8.82, 32.71, 58.21 dB under horizontal and vertical polarization respectively for 0.1%, 0.01%, 0.001% of the time. Although Moupfouma underestimates the measured cumulative statistics of rain attenuation but this model predicts relatively higher rain attenuation values as compared to ITU-R P. 530-16, Da Silva Mello, Abdulrahman et al., Lin and Differential Equations approach. For instance, Moupfouma predicts 4.01, 13.22, 24.14 dB; 4.01, 12.55, 24.83 dB respectively at 0.1%, 0.01% and 0.001% of the time under horizontal and vertical polarization. The proposed approaches as Method 1, Method 2(a) and Method 2(b) give very close estimation to the calculated cumulative statistics of rain attenuation but these approaches overestimate at higher time percentages when $P \geq 0.5\%$. At this time percentage ITU-R P. 530-16, Da Silva Mello, Abdulrahman et al., Lin and Differential Equations approaches show the closer estimation for calculated rain attenuation values. As calculated, under horizontal and vertical polarization, the Method 1 estimates 15.18, 31.07, 42.59 dB; 8.93, 23.09, 35.09 dB whereas Method 2(a) estimate 15.18, 31.07, 42.59 dB for horizontal and Method 2(b) predicts 10.53, 19.77, 38.49 dB for vertical polarization respectively in 0.1%, 0.01%, 0.001% of the time. The better performance analyses of these methods are done from the error analysis.

As shown in Figure 4.7(c), most of the prediction models overestimate the calculated rain attenuation values. ITU-R P. 530-16 shows overestimation and is highly pronounced at lower time percentage. For instance, the calculated rain attenuation values are 10.53, 20.89, 38.44 dB respectively at 0.1%, 0.01% and 0.001% of the time and the corresponding prediction obtained

using ITU-R P.530-16 are 10.85, 28.83, 54.67 dB respectively. Similar pattern is observed with the application of Da Silva Mello and Abdulrahman et al. which overestimate the measured cumulative statistics of rain attenuation. For instance, Da Silva Mello predicts 9.86, 28.42, 45.19 dB respectively at 0.1%, 0.01% and 0.001% of the time where as Abdulrahman et al. predicts 6.03, 22.68, 40.66 dB respectively. More overestimation is observed from the application of Da Silva Mello. In the same way, Lin and Differential Equations show higher overestimation as compared to Da Silva Mello and Abdulrahman et al. For instance, Lin estimates 9.19, 33.04, 56.09 dB respectively at 0.1%, 0.01% and 0.001% of the time where as Differential Equations predicts 8.82, 32.71, 58.21 dB respectively. Moupfouma shows the highest overestimation against the measured cumulative statistics of rain attenuation as compared to ITU-R P. 530-16, Da Silva Mello, Abdulrahman et al., Lin, Differential Equations approach and the proposed methods. For instance, Moupfouma predicts 15.65, 34.85, 64.54 dB respectively at 0.1%, 0.01% and 0.001% of the time. Method 1 and Method 2(b) show the closer estimation to the calculated statistics of rain attenuation. As calculated, the Method 1 and Method 2(b) predicts 7.96, 22.84, 36.33 dB and 9.10, 20.09, 38.66 dB for 0.1%, 0.01% and 0.001% of the time respectively. Similarly, for 75 GHz as depicted in Figure 4.7(d), ITU-R P. 530-16, Moupfouma, Abdulrahman et al., Lin and Differential Equations approach show underestimation against the calculated rain attenuation values for 0.001 % $\leq \boldsymbol{P} \leq$ 1 % even though ITU-R P. 530-16 predicts higher rain attenuation values. For instance, the calculated rain attenuation values are 16.11, 28.55, 40.48 dB respectively at 0.1%, 0.01% and 0.001% of the time and the corresponding estimation obtained using ITU-R P. 530-16, Moupfouma, Abdulrahman et al., Lin and Differential Equations approach are 3.22, 8.59, 15.71 dB; 0.81, 1.78, 3.59 dB; 0.58, 1.74, 2.83dB; 0.29, 1.09, 1.94 dB; 0.29, 1.09, 1.95 dB respectively. Da Silva Mello model predict extremely higher rain attenuation

at lower time percentages when $\boldsymbol{P} \leq 0.1\%$ so this method is not depicted in graph. For instance, at 0.01% of the time, the model predicts rain attenuation of about 317.4 dB. Interestingly, Method 1 and Method 2(b) show the closer estimation to the calculated statistics of rain attenuation. As obtained, the Method 1 and Method 2(b) estimate 13.23, 27.23, 37.43 dB and 13.71, 25.74, 39.91 dB for 0.1%, 0.01% and 0.001% of the time respectively. Furthermore, the several error analyses supports for the better judgment of suitable methods.

The suitability of the proposed methods are done through the calculation of relative error variables ($\boldsymbol{\varepsilon\ (P)}$), Standard Deviation (STD), Root Mean Square (RMS), Chi-Square statistics values and ITU-R P. 311-15 recommendation where they are compared to the performance of the ITU-R P. 530-16, Da Silva Mello, Moupfouma and Abdulrahman et al., Lin and differential equations approach. Data for proposed approaches are tabulated at fixed probability levels when $0.001\% \leq \boldsymbol{P} \leq 1\%$ as recommended in ITU-R P. 311-15[7]. The relative error probability and Chi-Square statistic used to access the proposed methods are given by equation (4.5) and equation (4.6) respectively as:

$$\boldsymbol{\varepsilon\ (P)_T = \frac{A_{\%p,pedicted} - A_{\%p,measured}}{A_{\%p,measured}} \times 100} \tag{4.5}$$

Chi-Square statistic is defined as[72]:

$$\boldsymbol{\chi^2 = \sum_{i=1}^{N} \frac{(A_{\%p,predicted,i} - A_{\%p,measured,i})^2}{A_{\%p,predicted,i}}} \tag{4.6}$$

where, $A_{\%p,predicted}$ and $A_{\%p,measured}$ are the predicted and measured rain attenuation values respectively, at the same probability level P, in the percentage interval 10^{-3} % ≤ P ≤ 1 %. Similarly, for STD and RMS calculation, the approaches followed in[41] have been adopted. The evaluations with the logarithmic method have been performed as recommended by ITU-R P. 311-15[7].

The calculated error probabilities, standard deviation, root mean square and chi-square values of the test variable for each method are listed in Table 4.5 (a) – (d) for 18 GHz horizontal and 18, 38 and 75 GHz vertical polarization respectively.

Table 4.5(a). Percentage error obtained after testing over the interval [0.001% to 1%] for 18 GHz under horizontal polarization.

Methods (Horizontal Polarization)	Parameters	Time Percentage (%p)													ITU-R P.311-15		
		1	0.5	0.3	0.2	0.1	0.05	0.03	0.02	0.01	0.005	0.003	0.002	0.001	μ_v	σ_v	ρ_v
ITU-R P. 530-16	ε(P)	2.56	2.35	-0.67	-0.79	-0.71	-0.60	-0.66	-0.60	-0.60	-0.51	-0.43	-0.37	-0.38	-0.66	0.65	0.92
	STD	2.67	2.46	0.57	0.68	0.60	0.50	0.55	0.49	0.49	0.40	0.32	0.26	0.28			
	RMS	1.04	1.53	5.99	13.69	12.35	10.74	16.91	15.58	19.91	17.55	14.99	12.89	16.61			
	χ2	0.75	1.07	12.37	52.08	29.94	16.40	32.61	23.47	29.44	18.11	11.28	7.45	10.37			
Da Silva Mello	ε(P)	-0.31	0.14	-0.86	-0.89	-0.82	-0.70	-0.72	-0.66	-0.63	-0.54	-0.48	-0.45	-0.49	0.40	0.63	1.20
	STD	0.26	0.71	0.29	0.32	0.25	0.13	0.15	0.08	0.06	0.03	0.09	0.12	0.08			
	RMS	0.13	0.09	7.60	15.44	14.26	12.46	18.47	16.98	21.14	18.68	16.84	15.84	21.13			
	χ2	0.06	0.01	45.08	129.44	63.72	29.21	47.32	32.25	36.52	21.96	15.69	12.94	20.23			
Moupfouma	ε(P)	5.00	4.13	-0.53	-0.74	-0.69	-0.58	-0.69	-0.61	-0.54	-0.39	-0.28	-0.21	-0.24	-0.50	0.70	0.86
	STD	4.72	3.85	0.81	1.02	0.97	0.86	0.97	0.88	0.82	0.67	0.56	0.48	0.52			
	RMS	2.03	2.69	4.75	12.84	12.01	10.33	17.67	15.70	17.93	13.62	9.67	7.23	10.54			
	χ2	1.69	2.17	5.44	37.02	26.51	14.35	38.99	24.09	20.81	8.86	3.70	1.87	3.40			
Abdulrahman et al.	ε(P)	-0.77	-0.52	-0.93	-0.94	-0.89	-0.80	-0.80	-0.74	-0.70	-0.59	-0.53	-0.49	-0.51	-1.36	0.76	1.56
	STD	0.06	0.19	0.22	0.24	0.18	0.09	0.09	0.03	0.01	0.11	0.18	0.22	0.20			
	RMS	0.31	0.34	8.28	16.33	15.55	14.20	20.45	19.09	23.26	20.54	18.43	17.22	22.02			
	χ2	1.07	0.38	112.09	278.39	127.73	56.41	80.01	53.24	53.43	30.05	20.61	16.48	22.89			
Lin	ε(P)	-0.65	-0.27	-0.89	-0.91	-0.83	-0.70	-0.70	-0.61	-0.56	-0.42	-0.33	-0.28	-0.32	-1.00	0.71	1.23
	STD	0.07	0.31	0.32	0.34	0.26	0.12	0.12	0.03	0.02	0.15	0.24	0.29	0.25			
	RMS	0.26	0.17	7.95	15.82	14.56	12.38	17.86	15.78	18.63	14.53	11.66	10.01	13.98			
	χ2	0.49	0.06	67.18	170.16	73.34	28.37	40.77	24.56	23.54	10.54	5.85	3.98	6.69			
Differential Equations	ε(P)	-0.66	-0.29	-0.90	-0.92	-0.84	-0.71	-0.70	-0.62	-0.56	-0.42	-0.32	-0.27	-0.30	-1.01	0.73	1.25
	STD	0.08	0.28	0.32	0.34	0.26	0.13	0.13	0.04	0.02	0.16	0.26	0.31	0.28			
	RMS	0.27	0.19	7.99	15.88	14.68	12.57	18.09	16.02	18.78	14.39	11.26	9.41	12.88			
	χ2	0.53	0.08	70.74	178.95	77.69	30.35	43.13	25.91	24.14	10.27	5.36	3.43	5.47			
Method 1	ε(P)	9.23	9.74	0.05	-0.34	-0.13	0.12	-0.09	0.01	-0.07	0.03	0.10	0.13	-0.01	-0.02	0.01	0.02
	STD	7.78	8.30	1.39	1.79	1.57	1.32	1.53	1.43	1.51	1.41	1.35	1.32	1.46			
	RMS	3.75	6.34	0.46	5.95	2.27	2.14	2.25	0.35	2.31	1.15	3.35	4.51	0.62			
	χ2	3.39	5.75	0.02	3.13	0.34	0.23	0.22	0.01	0.17	0.04	0.29	0.51	0.01			
Method 2(a)	ε(P)	14.93	11.03	0.05	-0.37	-0.18	0.08	-0.09	0.03	-0.05	0.03	0.07	0.09	-0.09	0.18	0.56	0.59
	STD	12.97	9.06	1.91	2.34	2.14	1.88	2.06	1.94	2.01	1.94	1.90	1.87	2.05			
	RMS	6.08	7.18	0.43	6.44	3.09	1.50	2.36	0.69	1.57	0.93	2.38	3.32	3.89			
	χ2	5.69	6.58	0.02	3.82	0.67	0.12	0.24	0.02	0.08	0.02	0.15	0.29	0.38			

Table 4.5(b). Percentage error obtained after testing over the interval [0.001% to 1%] for 18 GHz under vertical polarization.

Methods (Vertical Polarization)	Parameters	Time Percentage (%p)													ITU-R P.311-15		
		1	0.5	0.3	0.2	0.1	0.05	0.03	0.02	0.01	0.005	0.003	0.002	0.001	μ_v	σ_v	ρ_v
ITU-R P. 530-16	ε(P)	1.96	2.18	-0.60	-0.73	-0.64	-0.51	-0.52	-0.50	-0.49	-0.39	-0.37	-0.44	-0.42	-0.52	0.53	0.74
	STD	2.07	2.29	0.48	0.61	0.52	0.39	0.41	0.39	0.38	0.28	0.25	0.33	0.31			
	RMS	0.80	1.24	3.55	7.95	7.36	6.00	7.91	8.55	10.70	9.06	9.57	14.69	16.28			
	χ2	0.53	0.85	5.24	21.18	12.81	6.16	8.59	8.52	10.24	5.81	5.54	11.65	12.01			
Da Silva Mello	ε(P)	-0.27	0.30	-0.79	-0.84	-0.75	-0.61	-0.60	-0.57	-0.55	-0.46	-0.46	-0.54	-0.55	-0.85	0.50	0.98
	STD	0.25	0.81	0.28	0.33	0.24	0.10	0.09	0.05	0.03	0.06	0.06	0.03	0.04			
	RMS	0.11	0.17	4.73	9.22	8.74	7.26	9.12	9.73	11.98	10.57	11.90	18.07	21.28			
	χ2	0.04	0.04	18.24	49.58	26.77	11.52	13.71	12.79	14.49	8.87	9.99	21.56	26.49			
Moupfouma	ε(P)	3.89	3.55	-0.46	-0.64	-0.65	-0.44	-0.49	-0.44	-0.43	-0.30	-0.24	-0.35	-0.35	-0.37	0.56	0.67
	STD	3.69	3.34	0.66	0.84	0.86	0.64	0.70	0.64	0.63	0.51	0.44	0.56	0.56			
	RMS	1.58	2.02	2.72	7.00	7.58	5.16	7.47	7.52	9.33	7.06	6.14	11.78	13.53			
	χ2	1.26	1.58	2.28	12.43	14.32	3.99	7.22	5.88	6.93	3.09	1.89	6.47	7.38			
Abdulrahman et al.	ε(P)	-0.74	-0.44	-0.90	-0.92	-0.85	-0.74	-0.71	-0.67	-0.63	-0.53	-0.51	-0.59	-0.58	-1.19	0.60	1.33
	STD	0.07	0.24	0.22	0.24	0.17	0.06	0.03	0.01	0.05	0.15	0.16	0.09	0.10			
	RMS	0.30	0.25	5.36	10.03	9.88	8.75	10.80	11.52	13.79	12.23	13.40	19.44	22.33			
	χ2	0.88	0.19	47.88	110.62	57.05	24.86	26.62	23.58	23.52	13.68	14.14	27.41	31.10			
Lin	ε(P)	-0.60	-0.13	-0.85	-0.87	-0.77	-0.61	-0.57	-0.51	-0.46	-0.33	-0.31	-0.42	-0.42	-0.83	0.55	1.00
	STD	0.08	0.39	0.32	0.34	0.25	0.08	0.04	0.01	0.07	0.20	0.21	0.11	0.10			
	RMS	0.25	0.08	5.03	9.54	8.98	7.18	8.63	8.80	10.10	7.55	8.18	13.92	16.25			
	χ2	0.38	0.01	27.48	65.24	30.89	11.08	11.35	9.29	8.65	3.65	3.74	10.04	11.94			
Differential Equations	ε(P)	1.03	2.75	-0.39	-0.53	-0.24	0.23	0.29	0.41	0.50	0.82	0.83	0.54	0.52	0.22	0.43	0.48
	STD	0.51	2.23	0.91	1.05	0.76	0.29	0.23	0.11	0.02	0.30	0.31	0.02	0.00			
	RMS	0.42	1.57	2.32	5.77	2.77	2.67	4.34	6.95	10.84	19.03	21.73	18.03	19.84			
	χ2	0.21	1.15	1.48	6.43	0.87	0.49	0.97	2.01	3.59	8.58	9.88	6.34	6.77			
Method 1	ε(P)	2.95	4.62	-0.21	-0.45	-0.23	0.08	0.05	0.08	0.06	0.20	0.17	-0.04	-0.09	0.08	0.38	0.39
	STD	2.40	4.06	0.76	1.00	0.78	0.47	0.51	0.47	0.50	0.35	0.39	0.59	0.64			
	RMS	1.20	2.63	1.26	4.87	2.66	0.97	0.70	1.36	1.22	4.61	4.34	1.22	3.27			
	χ2	0.89	2.16	0.34	3.91	0.79	0.07	0.03	0.10	0.06	0.77	0.62	0.05	0.31			
Method 2(b)	ε(P)	6.57	6.85	0.00	-0.32	-0.09	0.18	0.05	0.01	-0.10	0.03	0.07	-0.05	0.00	0.15	0.43	0.45
	STD	5.56	5.83	1.01	1.33	1.11	0.84	0.96	1.00	1.11	0.99	0.94	1.07	1.01			
	RMS	2.67	3.90	0.03	3.47	1.06	2.09	0.80	0.21	2.10	0.61	1.86	1.79	0.14			
	χ2	2.32	3.40	0.00	1.62	0.11	0.31	0.04	0.00	0.22	0.02	0.12	0.10	0.00			

As noted from Table 4.5(a) and 4.5(b), similar trend of statistical results are obtained for 18 GHz under horizontal and vertical polarization respectively. The ITU-R P. 530-16, Moupfouma, Abdulrahman et al., Lin models, Differential Equations, Method 1and Method 2(a), 2(b) show higher relative error when 0.5 % ≤ $\boldsymbol{P}$ ≤ 1 % which is justified from increased STD, RMS and Chi-Square values. In other hand, Da Silva Mello show lower relative error at same time percentage which is supported from lower STD, RMS and Chi-Square values. Thus, for higher time percentage when 0.5 % ≤ $\boldsymbol{P}$ ≤ 1 % Da Silva Mello model can be used. In addition, for lower time percentage, ITU-R P.530-16, Da Silva Mello, Moupfouma, Abdulrahman et al., Lin give higher relative error values which underestimate the measured cumulative rain attenuation statistics. Under horizontal and vertical polarization, ITU-R P. 530-16 shows relative error

percentage of 71%, 60%, 38%; 64%, 49%, 42% while it is 82%, 63%, 49%; 69%, 54%, 24%; 89%, 70%, 51%; 83% 56%, 32% and 75%, 55%, 55%; 65%, 43%, 35%; 85%, 63%, 58%; 77% 46%, 42% Da Silva Mello, Moupfouma, Abdulrahman et al., Lin at 0.1%, 0.01% and 0.001% of time respectively. Interestingly, Differential Equations give higher relative error values which underestimate and overestimate the measured cumulative rain attenuation statistics for horizontal and vertical polarization respectively. For instance, Differential Equations result in 84%, 56%, 30% and 24%, 50%, 52% for horizontal and vertical polarization respectively at 0.1%, 0.01% and 0.001% of the time. Additionally, Method 1 gives lower relative error percentage values as compared to Method 2(a), 2(b) which are justified from decreased STD, RMS and Chi-Square values. For instance, Method 1 show relative error percentage of 13%, 7%, 1%; 23%, 6%, 9% while it is 18%, 5%, 9%; 9%, 10%, 0% for Method 2(a), 2(b) at 0.1%, 0.01% and 0.001% of the time respectively. Thus, Method 1 is applicable for estimation of rain attenuation statistics at lower time percentage when 0.001 % ≤ $\boldsymbol{P}$ ≤ 0.3 % of the time. Furthermore, from the calculation of $\boldsymbol{\mu_v}$, as per the recommendation of ITU-R P.311-15[29], Method 1 and 2(a), 2(b) show relatively less values which are supported by lower values of $\boldsymbol{\sigma_v}$ and $\boldsymbol{\rho_v}$.

Table 4.5(c): Percentage error obtained after testing over the interval [0.001% to 1%] for 38 GHz under vertical polarization.

Methods (Vertical Polarization)	Parameters	Time Percentage (%p)													ITU-R P.311-15		
		1	0.5	0.3	0.2	0.1	0.05	0.03	0.02	0.01	0.005	0.003	0.002	0.001	μ_v	σ_v	ρ_v
ITU-R P. 530-16	ε(P)	6.21	5.76	0.11	-0.27	0.03	0.36	0.21	0.31	0.38	0.55	0.49	0.40	0.42	0.35	0.36	0.51
	STD	5.06	4.61	1.04	1.43	1.12	0.79	0.94	0.84	0.77	0.60	0.66	0.75	0.73			
	RMS	2.53	3.84	0.59	2.87	0.32	3.98	3.33	5.26	7.93	12.90	13.72	13.37	16.23			
	χ^2	2.18	3.27	0.06	1.08	0.00	1.05	0.59	1.25	2.18	4.59	4.49	3.83	4.82			
Da Silva Mello	ε(P)	2.54	3.68	-0.12	-0.39	-0.06	0.33	0.21	0.31	0.36	0.50	0.37	0.23	0.18	0.23	0.33	0.40
	STD	1.92	3.06	0.75	1.01	0.69	0.30	0.42	0.32	0.27	0.12	0.26	0.40	0.45			
	RMS	1.04	2.46	0.66	4.05	0.67	3.63	3.23	5.24	7.52	11.63	10.34	7.49	6.75			
	χ^2	0.74	1.93	0.09	2.57	0.05	0.89	0.56	1.24	1.99	3.88	2.77	1.38	1.01			
Moupfouma	ε(P)	12.59	9.85	0.60	0.01	0.49	0.71	0.45	0.56	0.67	0.88	0.82	0.71	0.68	0.59	0.37	0.70
	STD	10.36	7.61	1.63	2.22	1.74	1.52	1.78	1.67	1.56	1.35	1.41	1.52	1.55			
	RMS	5.12	6.56	3.28	0.09	5.12	7.85	7.03	9.50	13.95	20.39	23.21	23.55	26.10			
	χ^2	4.75	5.96	1.23	0.00	1.68	3.25	2.19	3.41	5.59	9.53	10.47	9.76	10.55			
Abdulrahman et al.	ε(P)	0.36	1.16	-0.55	-0.66	-0.43	-0.10	-0.13	-0.02	0.09	0.26	0.18	0.07	0.06	-0.11	0.41	0.43
	STD	0.34	1.14	0.57	0.69	0.45	0.13	0.15	0.04	0.06	0.24	0.16	0.05	0.04			
	RMS	0.36	1.16	0.55	0.66	0.43	0.10	0.13	0.02	0.09	0.26	0.18	0.07	0.06			
	χ^2	0.04	0.42	3.66	13.68	3.37	0.13	0.32	0.00	0.14	1.27	0.78	0.17	0.12			
Lin	ε(P)	0.92	2.33	-0.31	-0.48	-0.13	0.35	0.30	0.45	0.58	0.80	0.66	0.50	0.46	0.25	0.37	0.45
	STD	0.42	1.84	0.80	0.98	0.62	0.14	0.20	0.04	0.08	0.31	0.17	0.01	0.04			
	RMS	0.37	1.56	1.68	5.05	1.33	3.94	4.61	7.71	12.14	18.66	18.77	16.75	17.64			
	χ^2	0.18	1.09	0.74	4.73	0.19	1.03	1.06	2.41	4.46	8.31	7.49	5.61	5.55			
Differential Equations	ε(P)	1.03	2.20	-0.34	-0.51	-0.16	0.31	0.26	0.42	0.57	0.81	0.69	0.54	0.51	0.24	0.39	0.46
	STD	0.54	1.72	0.82	0.99	0.65	0.18	0.23	0.07	0.08	0.33	0.21	0.05	0.03			
	RMS	0.42	1.47	1.83	5.28	1.71	3.40	4.02	7.13	11.82	18.95	19.59	17.95	19.76			
	χ^2	0.21	1.01	0.92	5.39	0.33	0.79	0.83	2.11	4.27	8.51	8.02	6.29	6.71			
Method 1	ε(P)	1.92	2.82	0.29	0.50	0.24	0.07	0.03	0.05	0.09	0.21	0.10	0.02	0.05	0.03	0.35	0.36
	STD	1.60	2.50	0.60	0.82	0.56	0.25	0.35	0.26	0.22	0.11	0.22	0.33	0.37			
	RMS	0.78	1.88	1.57	5.27	2.58	0.76	0.44	0.89	1.94	4.78	2.77	0.51	2.11			
	χ^2	0.51	1.39	0.63	5.37	0.83	0.05	0.01	0.04	0.16	0.82	0.25	0.01	0.12			
Method 2(b)	ε(P)	-0.56	2.03	-0.29	-0.46	-0.14	0.15	-0.02	0.00	-0.04	0.04	0.01	-0.02	0.01	-0.06	0.29	0.29
	STD	0.61	1.98	0.35	0.52	0.19	0.09	0.08	0.06	0.09	0.01	0.04	0.08	0.05			
	RMS	0.23	1.36	1.61	4.84	1.43	1.63	0.34	0.04	0.81	0.92	0.32	0.80	0.22			
	χ^2	0.28	0.91	0.67	4.18	0.22	0.21	0.01	0.00	0.03	0.04	0.00	0.02	0.00			

As depicted by Table 4.5(c), ITU-R P. 530-16, Da Silva Mello, Moupfouma, Lin, Differential Equations, show higher relative error when 0.5 % ≤ $\boldsymbol{P}$ ≤ 1 % which is justified from increased STD, RMS and Chi-Square values. In other hand, Abdulrahman et al. show lower relative error at same time percentage which is supported from lower STD, RMS and Chi-Square values. Thus, for higher time percentage when 0.5 % ≤ $\boldsymbol{P}$ ≤ 1 % at 38 GHz, Abdulrahman et al. can be used. In addition, for lower time percentage, ITU-R P.530-16, Da Silva Mello, Moupfouma, Abdulrahman et al., Lin, Differential Equations give higher relative error values which overestimate the measured cumulative rain attenuation statistics. Interestingly, Abdulrahman et al. give lower values of overestimation. For instance, ITU-R P. 530-16 give relative error percentage of 3%, 38%, 42% while it is 6%, 36%, 18%; 49%, 67%, 68%; 43%, 9%, 6%; 13%

58%, 46%; 16%, 57%, 51% for Da Silva Mello, Moupfouma, Abdulrahman et al., Lin, Differential Equations at 0.1%, 0.01% and 0.001% of the time respectively. Additionally, Method 1, 2 (b) give lower relative error percentage values which is justified from decreased STD, RMS and Chi-Square values. For instance, Method 1 and 2(b) show relative error percentage of 24%, 9%, 5% and 14%, 4%, 1% at 0.1%, 0.01% and 0.001% of the time respectively. Thus, Abdulrahman et al., Method 1 and Method 2(b) shows suitability for the estimation of rain rate statistics when 0.001 % ≤ $\boldsymbol{P}$ ≤ 1 % of the time. These methods suitability is further judge from the lower values of $\boldsymbol{\mu_v}$, as per the recommendation of ITU-R P.311-15[7] which is supported by lower values of $\boldsymbol{\sigma_v}$ and $\boldsymbol{\rho_v}$.

Table 4.5(d): Percentage error obtained after testing over the interval [0.001% to 1%] for 75 GHz under vertical polarization

Methods (Vertical Polarization)	Parameters	Time Percentage (%p)													ITU-R P.311-15		
		1	0.5	0.3	0.2	0.1	0.05	0.03	0.02	0.01	0.005	0.003	0.002	0.001	μ_v	σ_v	ρ_v
ITU-R P. 530-16	ε(P)	-0.18	-0.64	-0.78	-0.84	-0.80	-0.72	-0.72	-0.69	-0.70	-0.63	-0.62	-0.59	-0.61	-1.12	0.40	1.19
	STD	0.48	0.02	0.13	0.18	0.14	0.07	0.07	0.04	0.04	0.03	0.03	0.06	0.04			
	RMS	0.18	2.27	6.45	11.44	12.89	11.78	14.71	14.89	19.95	18.28	20.38	19.68	24.77			
	χ2	0.04	3.96	23.52	58.74	51.59	30.81	38.41	33.35	46.30	31.21	33.68	28.44	39.07			
Da Silva Mello	ε(P)	-0.93	-0.83	-0.75	-0.66	-0.02	2.03	3.78	6.31	10.12	18.64	22.18	25.69	28.40	1.10	1.89	2.19
	STD	9.70	9.59	9.51	9.43	8.79	6.74	4.98	2.46	1.35	9.87	13.41	16.92	19.63			
	RMS	0.94	2.95	6.13	9.01	0.30	32.98	76.99	135.90	288.86	540.34	725.49	855.42	1149.62			
	χ2	12.36	14.01	17.99	17.38	0.01	22.09	60.89	117.31	262.88	512.83	694.18	823.37	1110.52			
Moupfouma	ε(P)	-0.72	-0.89	-0.95	-0.96	-0.95	-0.94	-0.94	-0.94	-0.94	-0.92	-0.92	-0.91	-0.91	-2.52	0.59	2.59
	STD	0.19	0.02	0.03	0.05	0.04	0.02	0.03	0.02	0.02	0.01	0.00	0.00	0.00			
	RMS	0.73	3.19	7.77	13.12	15.30	15.27	19.23	20.15	26.77	26.73	30.06	30.35	36.89			
	χ2	1.89	26.78	134.14	313.06	289.12	230.75	330.00	294.31	402.55	316.07	341.09	312.25	379.03			
Abdulrahman et al.	ε(P)	-0.92	-0.95	-0.97	-0.97	-0.96	-0.95	-0.94	-0.94	-0.94	-0.93	-0.93	-0.92	-0.93	-2.78	0.47	2.81
	STD	0.02	0.01	0.02	0.03	0.02	0.00	0.00	0.00	0.00	0.02	0.02	0.02	0.01			
	RMS	0.93	3.39	7.94	13.30	15.53	15.40	19.22	20.19	26.81	26.83	30.32	30.76	37.65			
	χ2	10.85	65.36	229.37	478.65	416.95	269.86	327.31	302.71	412.57	333.42	383.23	372.10	500.77			
Lin	ε(P)	-0.92	-0.95	-0.97	-0.97	-0.96	-0.95	-0.94	-0.94	-0.94	-0.92	-0.93	-0.92	-0.93	-2.76	0.47	2.80
	STD	0.02	0.01	0.02	0.03	0.02	0.00	0.00	0.00	0.00	0.02	0.02	0.02	0.01			
	RMS	0.93	3.39	7.94	13.30	15.53	15.38	19.20	20.17	26.78	26.80	30.28	30.72	37.61			
	χ2	10.66	64.37	226.00	471.84	411.14	265.07	321.59	297.44	405.68	327.95	377.14	366.26	493.31			
Differential Equations	ε(P)	-0.92	-0.95	-0.97	-0.97	-0.96	-0.95	-0.94	-0.94	-0.94	-0.92	-0.93	-0.92	-0.93	-2.76	0.47	2.80
	STD	0.02	0.01	0.02	0.03	0.02	0.00	0.00	0.00	0.00	0.02	0.02	0.02	0.01			
	RMS	0.93	3.39	7.94	13.30	15.53	15.38	19.20	20.17	26.78	26.80	30.28	30.72	37.61			
	χ2	10.66	64.25	225.64	471.02	410.26	265.41	321.95	297.70	405.83	327.86	376.88	365.92	492.59			
Method 1	ε(P)	2.57	0.70	0.01	0.28	0.18	0.07	0.01	0.07	0.05	0.08	0.03	0.05	0.08	0.07	0.27	0.28
	STD	2.34	0.47	0.24	0.51	0.41	0.16	0.22	0.16	0.28	0.15	0.20	0.18	0.30			
	RMS	2.57	0.70	0.01	0.28	0.18	0.07	0.01	0.07	0.05	0.08	0.03	0.05	0.08			
	χ2	1.87	1.03	0.00	1.48	0.63	0.07	0.00	0.09	0.07	0.17	0.02	0.07	0.26			
Method 2(b)	ε(P)	2.54	0.50	-0.10	-0.31	-0.15	0.14	0.06	0.08	-0.10	0.00	-0.01	0.05	-0.01	0.05	0.27	0.27
	STD	2.33	0.29	0.31	0.52	0.36	0.06	0.15	0.12	0.30	0.21	0.22	0.16	0.22			
	RMS	2.56	1.78	0.83	4.26	2.40	2.36	1.21	1.79	2.81	0.02	0.43	1.60	0.57			
	χ2	1.84	0.59	0.09	1.93	0.42	0.29	0.07	0.14	0.31	0.00	0.01	0.07	0.01			

As shown in Table 4.5(d), Da Silva Mello, Moupfouma, Abdulrahman et al., Lin, Differential Equations, Method 1(a) and Method 2(b) show higher relative error when 0.5 % ≤ $\boldsymbol{P}$ ≤ 1 % which is justified from increased STD, RMS and Chi-Square values. In other hand, ITU-R P. 530-16 shows lower relative error at same time percentage which is supported from lower STD, RMS and Chi-Square values. Thus, for higher time percentage when 0.5 % ≤ $\boldsymbol{P}$ ≤ 1 % ITU-R P. 530-16 method can be used. In addition, for lower time percentage, when 0.001 % < $\boldsymbol{P}$ < 0.3 %, ITU-R P.530-16, Da Silva Mello, Moupfouma, Abdulrahman et al., Lin, Differential Equations give higher relative error values which underestimate the measured cumulative rain attenuation statistics. Interestingly, Da Silva Mello shows greater overestimation against the calculated rain attenuation statistics at lower time percentage particularly when $\boldsymbol{P}$ ≤ 0.05% of the time. ITU-R P. 530-16, Moupfouma, Abdulrahman et al., Lin, Differential Equation give relative error percentage of 80%, 70%, 61%; 95%, 94%, 91%; 96%, 94%, 93%; 96%, 94%, 93%; 96%, 94%, 93% at 0.1%, 0.01% and 0.001% of the time respectively. Furthermore, Method 1, Method 2(b) gives lower relative error percentage values which are justified from decreased STD, RMS and Chi-Square values. For instance, Method 1 and Method 2(b) show relative error percentage of 18%, 5%, 8% and 15%, 10%, 1% at 0.1%, 0.01% and 0.001% of the time respectively. Thus, Method 1 and Method 2(b) give better estimation of rain attenuation statistics at lower time percentage when 0.001 % ≤ $\boldsymbol{P}$ ≤ 0.3 % of the time. In addition, the lower values of $\boldsymbol{\mu_v}$ support the suitability of proposed technique and ITU-R P. 530-16 which is justified from decreased values of $\boldsymbol{\sigma_v}$ and $\boldsymbol{\rho_v}$.

The further research are performed on the frequency and polarization scaling methods that provide an alternative to rain attenuation models which are considered to be excellent predictors

and a means for determining what to expect at a frequency and polarization for which there is no data. This research analyses the approaches presented in ITU-R P. 530-16[2] where the frequency scaling formula is adopted for estimation of rain attenuation at 38 GHz link under vertical polarization from the calculated 18 GHz rain attenuation values. Similarly, polarization scaling is performed for the estimation of rain attenuation for 18 GHz horizontal and vertical polarizations and for 38, 75 GHz under horizontal polarization. Further experimental analyses need to be carried out for the validation of estimated rain attenuation statistics at 38 and 75 GHz under horizontal polarization. The predicted values are shown in Figure 4.8.

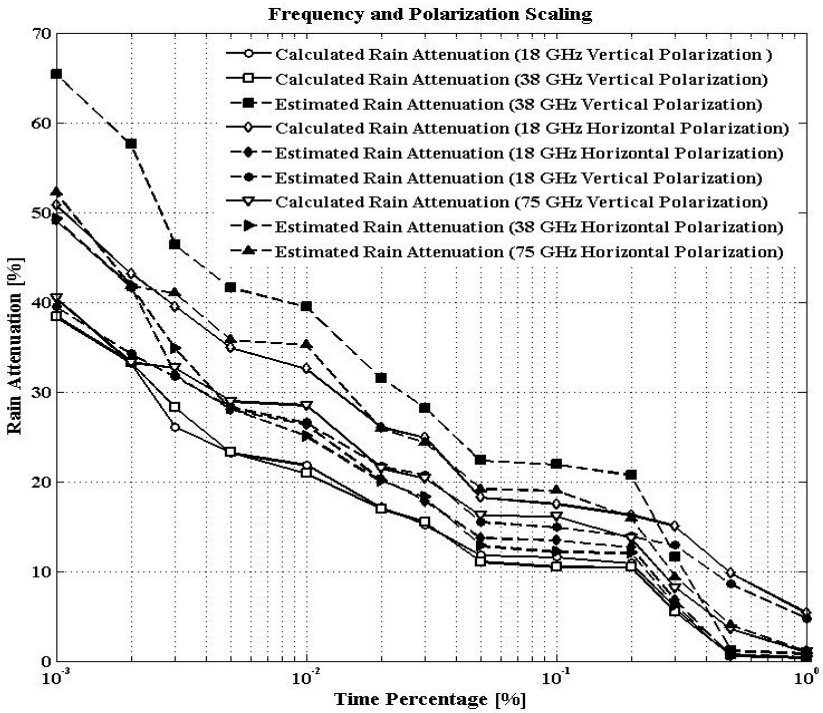

Figure 4.8: Cumulative distribution of calculated and estimated rain attenuation obtained after frequency and polarization scaling for various integration times.

As noticed from Figure 4.8, for estimated 38 GHz under vertical polarization, it is observed that the measured cumulative statistics of rain attenuation for 38GHz link is over estimated. For instance, the calculated rain attenuation values at 38GHz link are 10.53, 20.89, 38.44 dB

respectively at 0.1%, 0.01% and 0.001% of the time and the estimated values after frequency scaling are 21.91, 39.48, 65.42dB respectively. Similarly, the estimated rain attenuation statistics for 18 GHz under horizontal polarization is relatively underestimated while over estimation is observed for predicted 18 GHz under vertical polarization. For instance, the calculated rain attenuation values at 18GHz horizontal and vertical polarization are 17.53, 32.57, 50.83 dB; 11.59, 21.88, 38.36 dB respectively at 0.1%, 0.01% and 0.001% of the time while the estimated values after polarization scaling are 13.46, 26.35, 49.12 dB; 14.92, 26.58, 39.52 dB respectively. The better performance analyses are judge through the error matrices presented in Table 4.6.

Table 4.6: Percentage error obtained after testing over the interval [0.001% to 1%] after frequency and polarization scaling.

Methods	Parameters	Time Percentage (%p)													ITU-R P. 311-15		
		1	0.5	0.3	0.2	0.1	0.05	0.03	0.02	0.01	0.005	0.003	0.002	0.001	μ_v	σ_v	ρ_v
ITU-R P. 530-16 (Frequency Scaling- Estimated 38 GHz)	ε(P)	1.07	0.77	1.13	0.99	1.08	1.01	0.82	0.86	0.89	0.79	0.64	0.73	0.70	0.58	0.12	0.59
	STD	0.19	0.12	0.25	0.10	0.20	0.13	0.06	0.02	0.01	0.09	0.24	0.15	0.18			
	RMS	0.44	0.51	6.18	10.30	11.37	11.24	12.69	14.59	18.58	18.36	18.11	24.28	26.98			
ITU-R P. 530-16 (Polarization Scaling- Estimated 18 GHz Horizontal	ε(P)	-0.92	-0.94	-0.55	-0.22	-0.23	-0.25	-0.28	-0.22	-0.19	-0.20	-0.19	-0.03	-0.03	-0.60	0.82	1.01
	STD	0.59	0.61	0.22	0.11	0.10	0.08	0.04	0.11	0.14	0.13	0.13	0.29	0.29			
	RMS	4.95	9.20	8.27	3.61	4.07	4.51	7.07	5.79	6.22	6.85	7.63	1.50	1.71			
ITU-R P. 530-16 (Polarization Scaling- Estimated 18 GHz Vertical)	ε(P)	10.70	14.03	1.17	0.27	0.29	0.31	0.37	0.26	0.22	0.22	0.21	0.03	0.03	0.42	0.45	0.62
	STD	8.54	11.87	1.00	1.89	1.87	1.85	1.79	1.90	1.95	1.94	1.95	2.13	2.13			
	RMS	4.35	7.99	6.95	2.97	3.33	3.68	5.59	4.54	4.71	5.12	5.58	1.06	1.16			

As noticed from Table 4.5, the predicted 38 GHz rain attenuation statistics obtained after applying frequency scaling technique shows the higher relative error chances for all time percentage when 0.001 % ≤ $\boldsymbol{P}$ ≤ 1 % of time. For instance, obtained relative error percentages are 108%, 89% and 70% for 0.1%, 0.01% and 0.001% of time. Similarly, predicted rain attenuation statistic obtained by using polarization scaling scheme at 18GHz under horizontal and vertical polarization depict increasing relative error chances for higher time percentage and decreasing relative error probability for lower time percentage. For instance, the predicted rain attenuation statistics in 18 GHz under horizontal polarization and vertical polarization show the

relative error percentage of 23%, 19%, 3% and 29%, 22%, 3% for 0.1%, 0.01% and 0.001% of the time respectively.

E.Conclusion

The comparison of rain attenuation was made with the calculated rain attenuation distribution and six preexisting models for terrestrial microwave links. Three different operating frequencies as such 18, 38 and 75 GHz are considered for the analyses of rainfall effect. The local environmental propagation effect in microwave links have been investigated by considering the rain attenuation and rain rate data, collected over three years during 2013-2015 in mentioned operating frequencies. As first approach to this open research problem, a novel statistical analysis has been proposed to predict the time series of rain attenuation in microwave links in the South Korea. The measured rain attenuation distribution at 0.01% of the time is 50 mm/hr in the mentioned region. It was found that at higher time percentage when 0.5 % ≤ $\boldsymbol{P}$ ≤ 1 %, for 18 GHz microwave link under horizontal and vertical polarization, Moupfouma and ITU-R P. 530-16 methods shows better estimation of rain attenuation whereas for lower time percentage 0.001 % ≤ $\boldsymbol{P}$ ≤ 0.5 % , Moupfouma, Method 2(a) and Method 2(b) give reasonable estimation. In addition, under 38 GHz link, for 0.001 % ≤ $\boldsymbol{P}$ ≤ 1 % of the time, Abdulrahman et al., Method 1 and Method 2(b) show the better prediction which signifies their suitability. Similarly, for 75 GHz link, ITU-R P. 530-16, Method 1 and Method 2(b) show the better prediction for 0.001 % ≤ $\boldsymbol{P}$ ≤ 1 % of the time whereas for higher time percentage, when 0.5 % ≤ $\boldsymbol{P}$ ≤ 1 %, ITU-R P. 530-16 give suitable estimation. The prediction of rain attenuation statistics for 18, 38 and 75 GHz microwave links which is justified from the lower values of relative error, Standard Deviation,

Root Mean Square, ITU-R P. 311-15 and Chi-Square calculation. In addition, frequency and polarization scheme are analyzed as per the recommendation of ITU-R P. 530-16 where the validation of this approach is performed by comparing with experimental data through error matrices. Thus, the research presents the comparison of measured data with the six preexisting rain attenuation models and their categorization for the best fitting approach. On the whole, the better estimation of rain attenuation can be determined by relating the effective rain rate with 1-min. rain rate distribution and by better modeling the prediction error obtained from ITU-R P. 530-16 as a function of 1-min. rain rate distribution.

V. Rain Attenuation in Satellite Communication Links

A.Introduction

Rain Attenuation for satellite communication at 12.25 and 20.73 GHz circular and 19.8 GHz vertical polarization has been calculated. Simultaneously, the rain rate at 10 second interval are measured which is averaged to 1-min. distribution. In this study, we have proposed the applicable technique to calculate rain attenuation in slant path for satellite communication in Ku and Ka bands. The result of this study shows that rain attenuation get increased for Ka band frequencies. Furthermore, the frequency scaling techniques between distributions are also discussed. The characterization of rain specific attenuation along with diurnal and monthly variation of rain rate and rain attenuation on Ka band are studied. A monthly variation of the coefficients has been indicted and the empirical measured data was compared with the ITU-R P. 838-3 derived regression coefficients. The result indicates the significance of the ITU-R recommended regression coefficients of rain specific attenuation. Moreover, the statistics analyzed to 6 hour contiguous periods of the day are also shown.

B.Measurement of Rain Attenuation in Slant Path

The experimental setup is installed at Korea Radio Promotion Association building, Mokdong-13 na-gil, Yangcheong-gu, Seoul, Republic of Korea ($37^0$32’45.25” N, $126^0$52’58.8”E) by National Radio Research Agency, RRA. The beacon receiver measures the level of Ku and Ka bands beacon of the Koreasat 6 satellite at 12.25 and 20.73 GHz respectively using 1.8 m antenna whose specification is detailed in Table 5.1. Similarly, another beacon receiver is installed at

same place to measure the Ka band beacon at 19.8 GHz from COMS 1 using similar sized antenna whose specification are depicted in Table 5.2. Both the receivers, sample the data at an interval of 10 seconds which are averaged over 1-min. distribution for further statistical analyses. Satellite links have availability of 99.95% and the schematic for the setup is shown in Figure 1. In addition, an optical disdrometer, OTT Parsivel, is used to measure the rain rates which operate simultaneously with the monitoring system of satellite beacon signal whose specification is also given in Table 5.1. These antennas were covered with radome to prevent wetting antenna conditions. The received signal levels were sampled every 10 seconds and finally averaged over 1-min.The three years rainfall intensities with 99.95% of the validity of all time, were collected by OTT Parsivel, a laser-based optical disdrometer for simultaneous measurement of particle size and velocity of all liquid and solid precipitation, for every 10 seconds. The same disdrometer is used for terrestrial links also whose descriptions are mentioned in section 4.

Table 5.1. Specifications of the 12.25 and 20.73 GHz links for Koreasat 6 satellite link.

Type	Descriptions	Specification
System Location	Location	37.5447^0N, 126.8833^0E
	Elevation angle	45^0
	Azimuth angle	197.5^0
	Sea level [km]	0.055
Receiver Antenna	Antenna type	Off-set parabolic
	Frequency Band [GHz]	10.95 ~ 31
	Beacon signal level for clear sky @12.25 GHz	-80.5 dBm
	Beacon signal level for clear sky @20.73 GHz	-38.7 dBm
	Polarization	Circular
	Gain	55dB±2dB
Optical Disdrometer	Type	OTT Parsivel
	Measuring area	$54cm^2$
	Range of measurement particle size	0.2 to 25 mm
	Range of measurement velocity	0.2 to 20 m/s
	Precipitation Intensity	0.001 to 1200 mm/hr
	Operating Temperature range	-40^0C to $+70^0$C

Table 5.2. Specifications of the 19.8 GHz link for COMS1 satellite link.

Type	Descriptions	Specification
System Location	Location	37.5459^0N, 126.883^0E
	Elevation angle	46.5^0
	Azimuth angle	177.8^0
	Sea level [km]	0.055
Receiver Antenna	Antenna type	Off-set parabolic
	Frequency Band [GHz]	10.95 ~ 31
	Beacon signal level for clear sky	-73.4 dBm
	Polarization	Vertical
	Gain	55dB±2dB

The schematic diagram for system set up is shown in Figure 5.1.

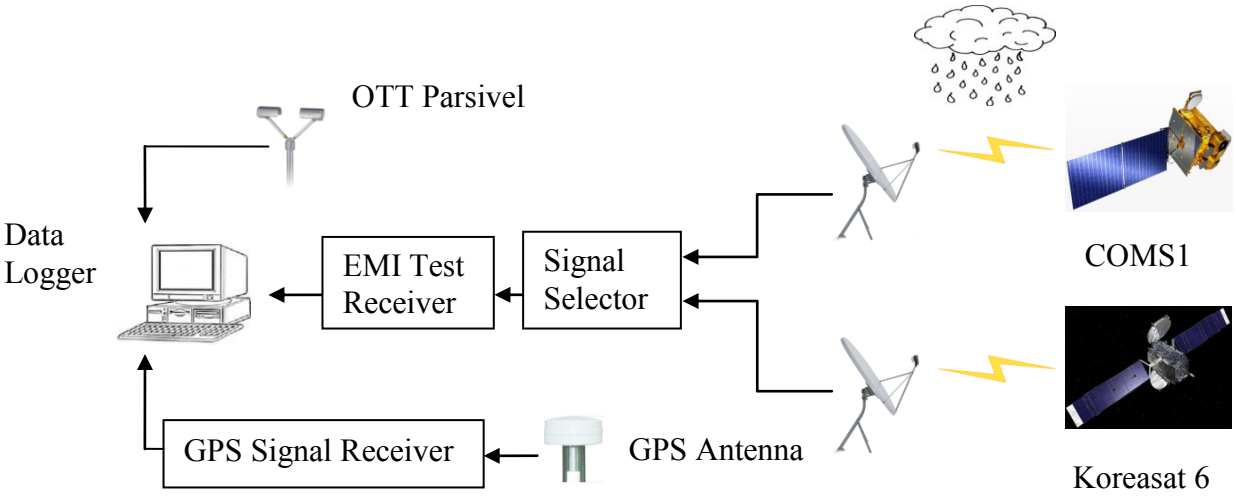

Figure 5.1: Experimental setup for rain attenuation and rain rate measurement.

As depicted in Figure 5.1, the off-set parabolic antenna is faced towards Koreasat 6 and COMS 1 satellites. The circularly polarized beacon signal at 12.25, 20.73 GHz from Koreasat 6 and vertically polarized singal at 19.8 GHz were down converted using separate Low Noise Block Converter (LNBC). The noise figure and bandwidth of LNBC are 1.5 dB and 1000 MHz respectively. The output of LNBC is passed through a 4 dB signal splitter (signal selector) and fed into a spectrum analyzer (EMI Test Receiver) via RG-11 coaxial cable, at a sampling rate of 1 sample every 10 seconds interval. The output of spectrum analyzer was sent to the computer via General purpose interface bus (GPIB) cable and then stored using a data logger at a sampling rate of 0.1samples/sec. The beacon signal level was used to provide a reference level (in dBm), which is the average signal power received under clear-sky conditions. During rain, the attenuation was estimated by measuring the excess attenuation over the clear weather values at respective rain rates. The raw data were converted from quantization levels to beacon receive signal level (RSL) in dBm. GPS Antenna records the position whose information is also recorded in data logger through GPS signal receiver. Further, the rainfall rate is recorded simultaneously

with the satellite signal with a sampling interval of 10 seconds. Figure 5.2 (a), Figure 5.2 (b) and Figure 5.2 (c) show the sample record of simultaneous measurements of received signal level and rain rate for 12.25, 20.73 and 19.8 GHz respectively.

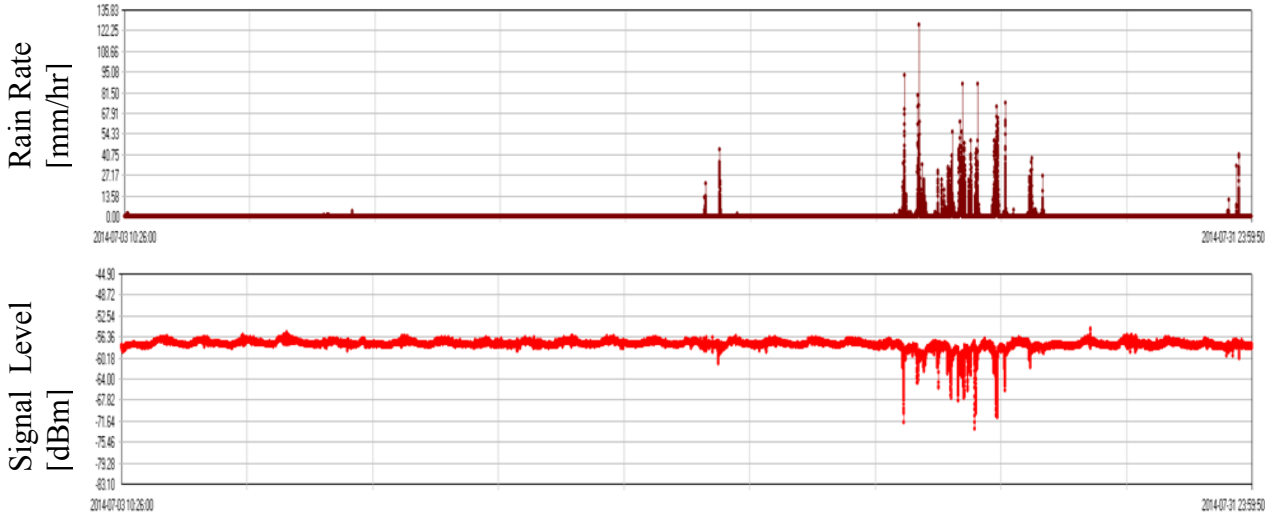

Figure 5.2 (a): Variation of 12.25 GHz signal level during a rain event.

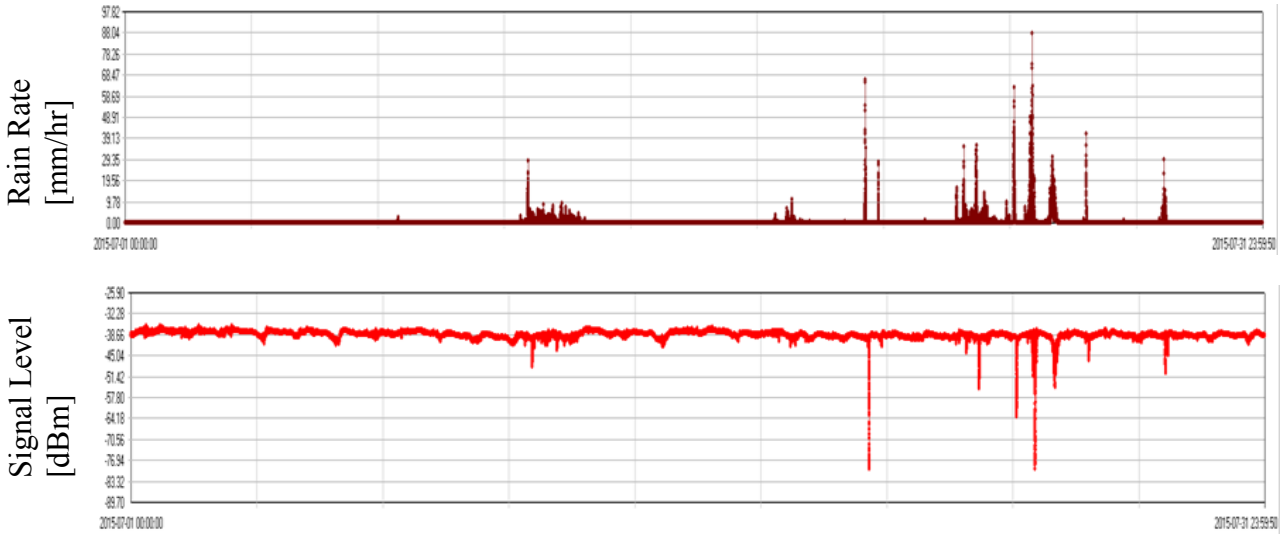

Figure 5.2 (b): Variation of 20.73 GHz signal level during a rain event.

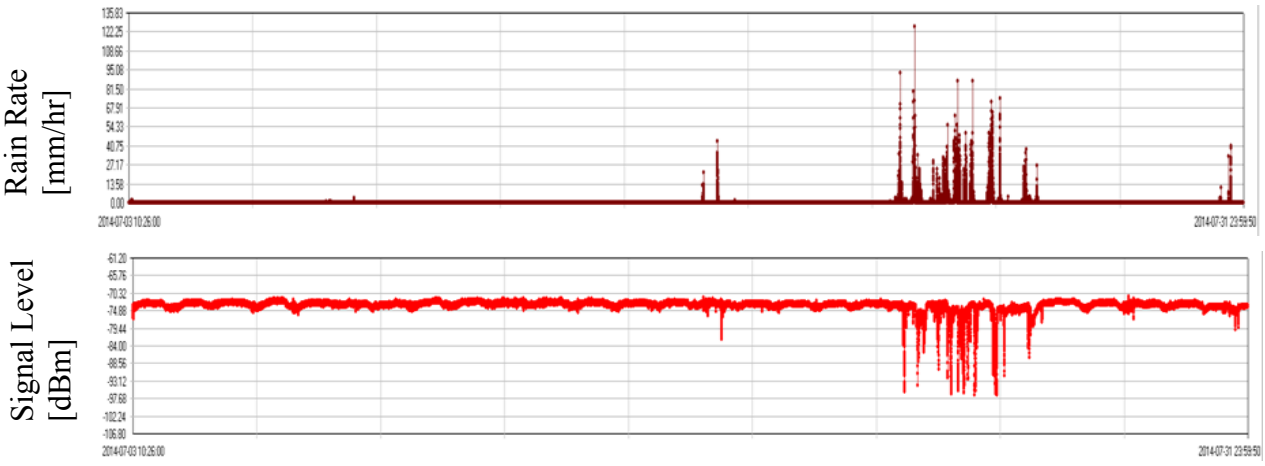

Figure 5.2 (c): Variation of 19.8 GHz signal level during a rain event.

Thus, the corresponding path attenuation is calculated by finding the difference between the RSL during clear sky conditions and the RSL during rain for circularly and vertically polarized received signals at various rain rates as follows:

$$\boldsymbol{Attenuation\ (dB) = RSL_{clear\ sky} - RSL_{rainy}} \tag{5.1}$$

The slant path attenuation exceedances for other percentages of the time for the average year were obtained using statistical methods. The calculated path attenuation and received rain rate data for 10 seconds interval are averaged to 1-min. following the procedure as presented in[44], which give the method for estimation of 1-min. rain rate and the similar approach is adopted for determination of 1-min. rain attenuation. These data are combined in descending order and the required 1-min. rainfall rate and attenuation values are determined for 5% to 0.001% of the time. In this paper for comparison with other prominent rain attenuation models, these data are arranged for 1% to 0.001% of the time. For example, at 0.01% of the time, 1-min. rain rate and attenuation values are taken for about 158 ((3×365×24×60×0.01)/100) = 157.68 ≈ 158)

instance for 3-years measurement. Similarly, for each year of measurement the values for about 53 ((1×365×24×60×0.01)/100) = 52.56 ≈ 53) instance was considered at the same percentage of the time. These instances are obtained by multiplying the number of experimental year, number of days in a year, hour and minute in a day, with required time percentage. The yearly occurrences of 1-min. rain rate and rain attenuation from 2013 till 2015 along with the cumulative distribution of 1-min. rain rate and rain attenuation for these years when sorted together, are shown in Figure 5.3 (a) and 5.3 (b) respectively. Figure 5.3 (a) indicates that the maximum rainfall occurred in 2013 but it decreases for successive years which might be because of invariability in rainfall occurrence in different seasons under mentioned periods. For instance, at 0.01% of the time, the obtained rainfall rate is 67.02 mm/hr in 2013 whereas, in 2014 and 2015, the values are 38.14 mm/hr and 30.19 mm/hr respectively. The study considered the analysis done for the combined values of rainfall rate which indicate that at 0.01% of the time, the 1-min. rain rate value is 50.35 mm/hr for Mokdong site. Furthermore, 1-min. rain rate values decrease and tend to be smaller for higher time percentages, for example, at 0.5% and 1% of the time the rain rate are observed to be 1.95 mm/hr and 0.54 mm/hr respectively. Similarly, at lower time percentage 1-min. rain rate is increased, for example, at 0.001% of the time, the rain rate observed is 98.74 mm/hr. Figure 5.3 (b) shows the rain attenuation for 12.25, 19.8 and 20.73 GHz frequencies which are obtained on the yearly basis and when combined together from 2013 till 2015. The rain rate is greater in 2013 and 2014 which resulted in higher rain attenuation values of 10.8, 12.3 dB; 12.3, 11 dB; 12.1, 10.2 dB respectively for 0.01% of the time. For further analysis, this study considered the combined values of rain attenuation which indicates the lower attenuation values at higher time percentages and higher values at lower time

percentage. For instance, the attenuation values of 7.9, 10.7, 19 dB; 6.2, 11.6, 25.1 dB; 5.7, 11.3, 18.9 dB are observed for 0.1%, 0.01% and 0.001% of the time respectively.

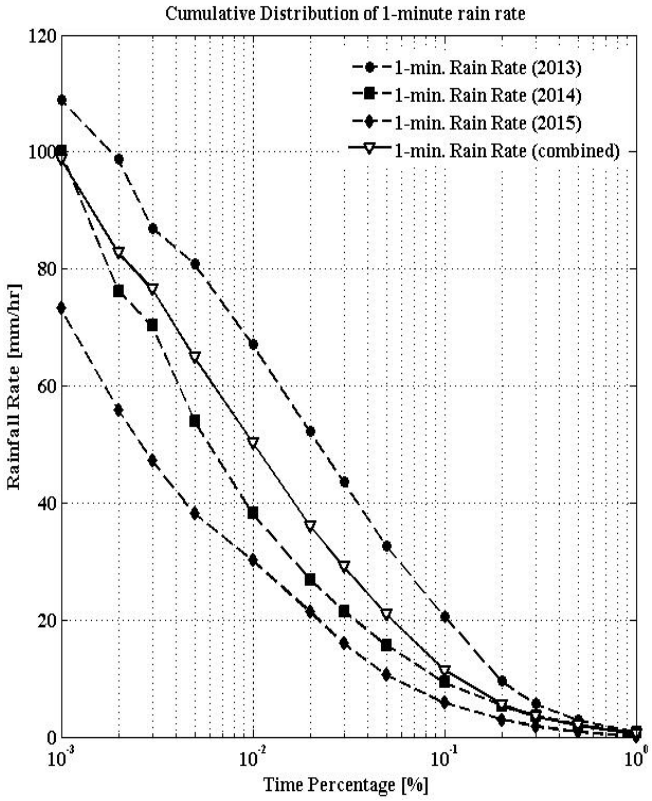

Figure 5.3 (a): The rain rate distribution at Mokdong.

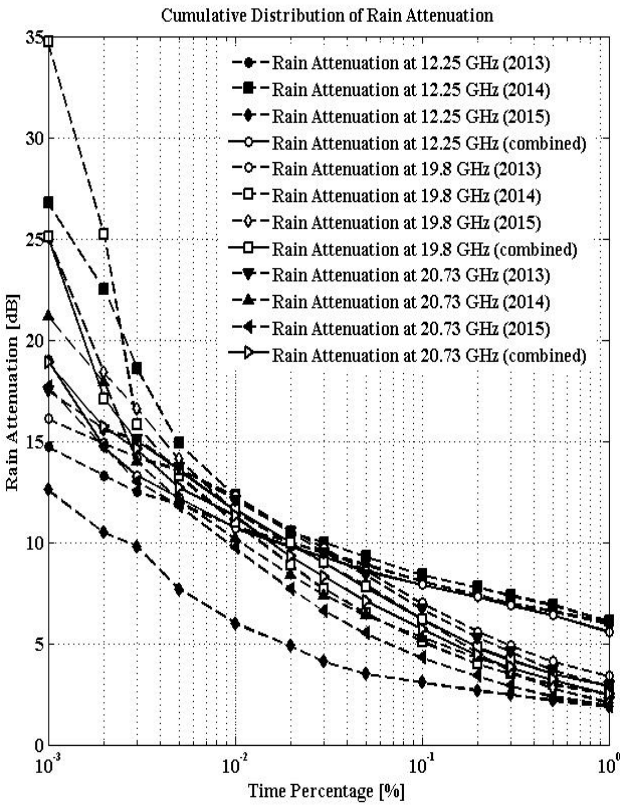

Figure 5.3 (b): Distribution of rain attenuation at Mokdong.

Furthermore, the relation between rain attenuation and rain rate is shown in Figure 5.4 for three years of measurement along with the combined values. This figure indicates that there is the positive correlation between the rain rate and rain attenuation. Additionally, the experimental procedure carried out by Korea Metrological Administration (KMA) is studied for better analyses of 1-min. rain rate statistics. Figure 5.5 show the cumulative distribution of rainfall rate for 1-min., 5-min., 10-min., 20-min., 30-min. and 60-min. for near location namely Icheon (37.27^0N, 127.45^0E), which are obtained from the experimental 1-min. rainfall amount database provided by Korea Meteorological Administration (KMA) from 2004 to 2013.

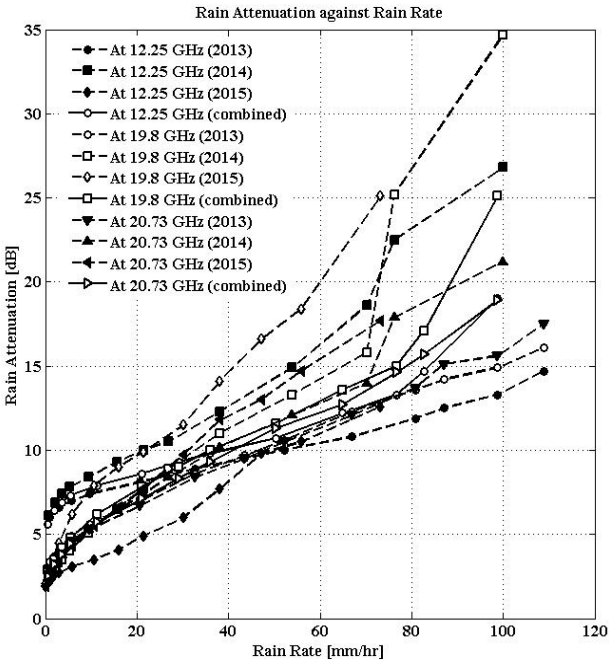

Figure 5.4: Rain attenuation versus rain rate.

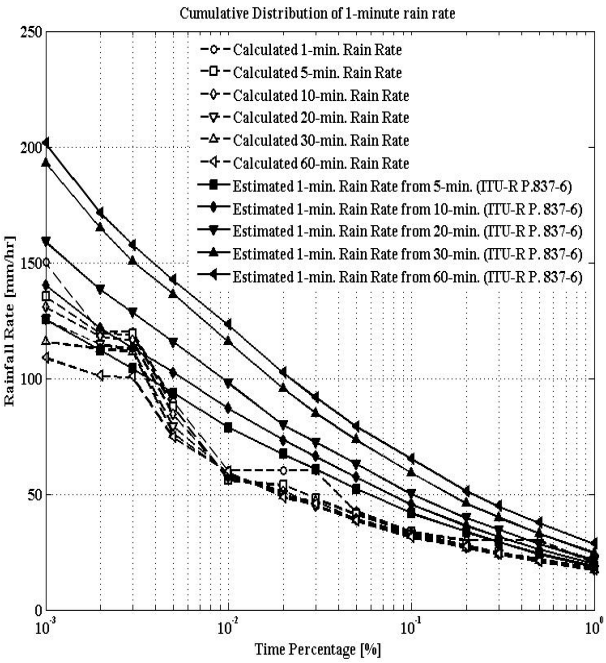

Figure 5.5: The rain rate distribution of various integration times.

Tipping bucket rain gauge is used to record the 1-min. rainfall amount whose detail operation are detailed in[41]. These experimental 1-min. rainfall amounts are arranged and combined which are converted to higher time rain rate as 5-min., 10-min., 20-min., 30-min. and 60-min. following the approach as given in[41, 20]. There is a slight variation on the 1-min. rain rate as compared to higher integration times because the experiment is done for the calculation of 1-min. rainfall amount rather than 1-min. rainfall rate. These values are taken as an input parameter along with the latitude and longitude information of the Icheon site so as to generate the estimated 1-min. rainfall rate from software recommended by ITU-R P. 837-6[4] which are also shown in Figure 5.5. This indicates that for higher time conversion particularly for 20-min., 30-min. and 60-min.to 1-min., ITU-R P. 837-6 shows the overestimation. Similarly, for lower time conversion from 5-min. and 10-min. to 1-min., ITU-R P. 837-6 gives closer estimation against the calculated 1-min. rain rate whose values are tabulated in Table 3 at 0.1%, 0.01% and 0.001% of the time.

Table 5.3. Calculated and estimated rain rate.

Time Percentage	Calculated Rain Rate (mm/hr)						Estimated Rain Rate (ITU-R P. 837-6) (mm/hr)				
	1-min.	5-min.	10-min.	20-min.	30-min.	60-min.	5- to 1-min.	10- to 1-min.	20- to 1-min.	30- to 1-min.	60- to 1-min.
0.1%	33.60	33.52	33.00	32.58	32.00	31.21	41.72	45.65	50.10	59.24	65.21
0.01%	60.00	56.25	57.54	58.95	59.12	59.65	78.68	87.09	98.09	115.94	123.18
0.001%	150.00	135.45	130.65	125.46	115.95	109.00	125.45	140.48	159.09	193.24	201.54

This signifies the need of measurement for rainfall rate provided by RRA with longer duration. The experimental records for rainfall rate and rain attenuation are in progress. Furthermore, RRA is planning to setup the experimental links in other prime locations of the South Korea for accurate estimation of rain attenuation.

The procedure used to obtain slant path attenuation exceedances for other time instances are detailed in[62] along with the cumulative distribution of 1-min. rain rate for each year and when combined together. Figure 5.6 (a), (b), (c) and Figure 5.7 (a), (b), (c) represents the monthly variation of rain attenuation and rain rate for three consecutive years 2013, 2014 and 2015 respectively for 19.8 GHz link.

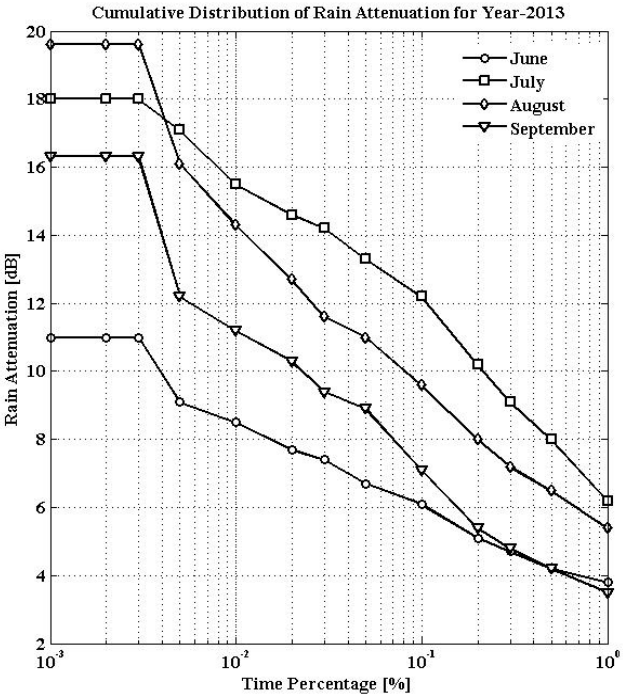

Figure 5.6 (a): Distribution of rain attenuation for 2013.

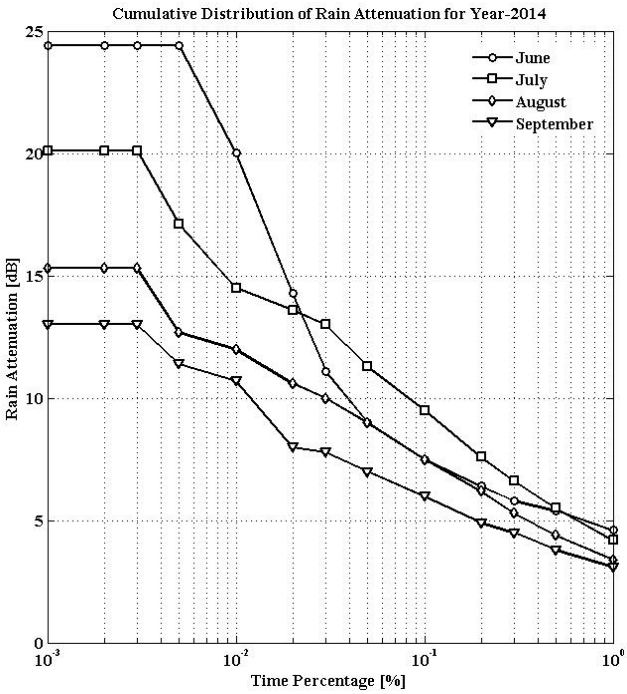

Figure 5.6 (b): Distribution of rain attenuation for 2014.

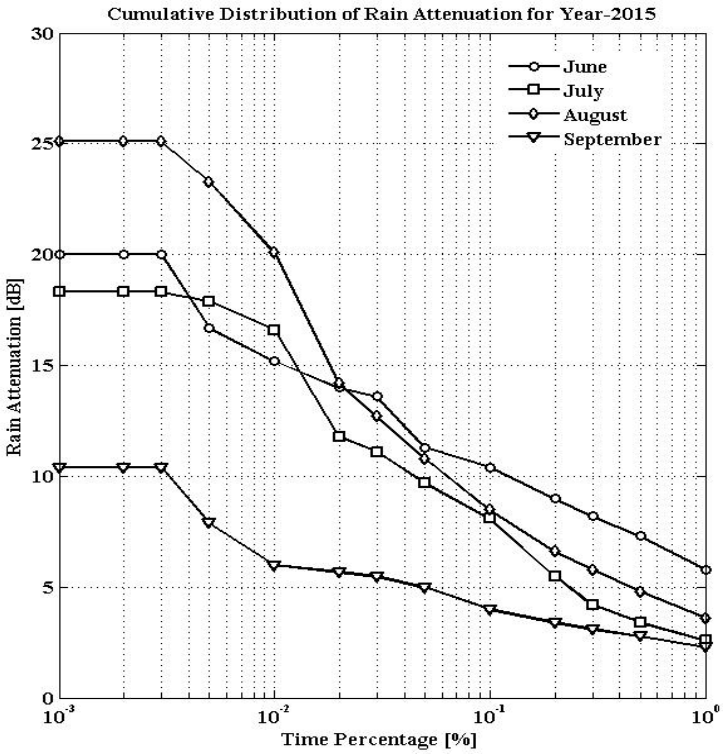

Figure 5.6 (c): Distribution of rain attenuation for 2015.

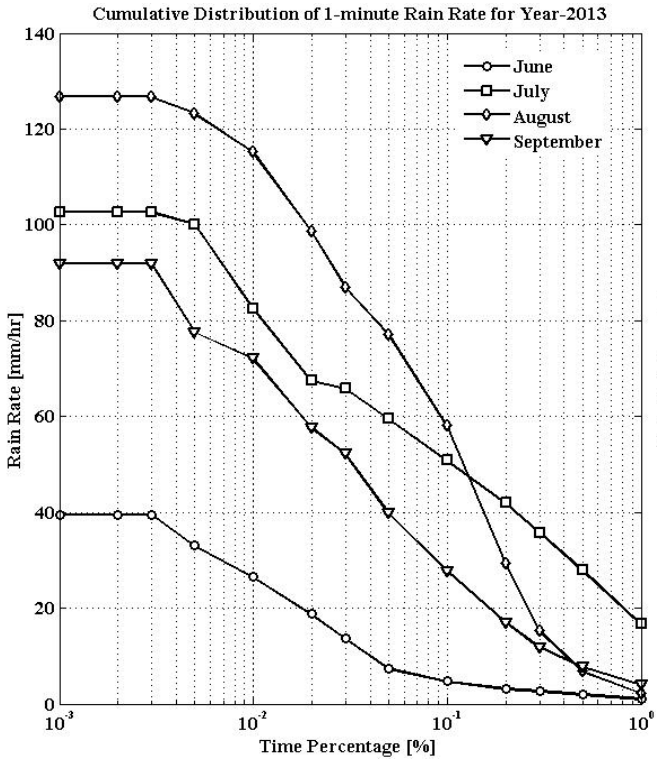

Figure 5.7 (a): Rainfall rate distribution for 2013.

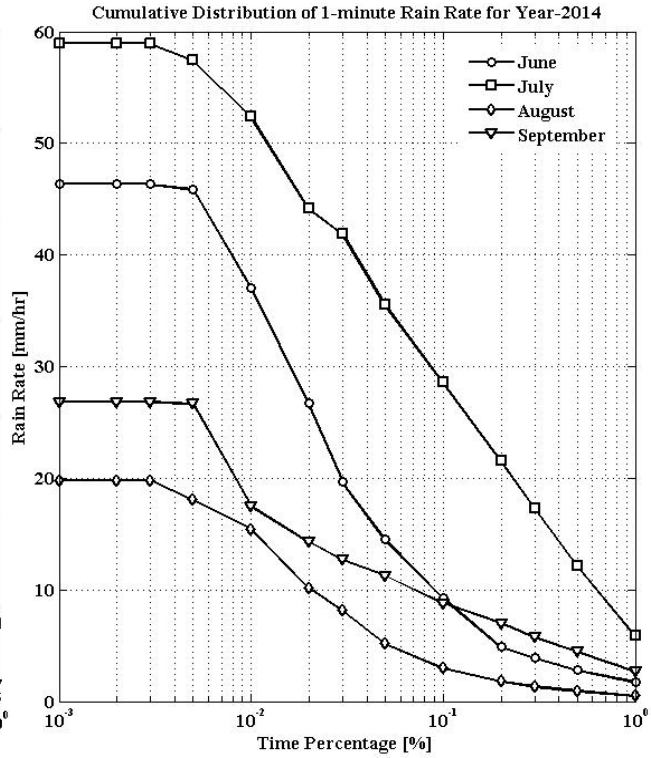

Figure 5.7 (b): Rainfall rate distribution for 2014.

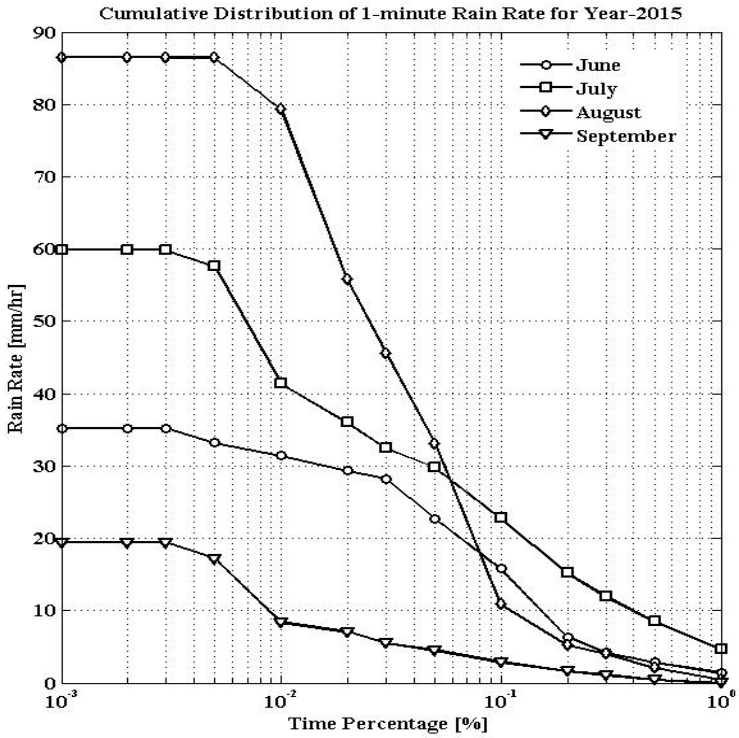

Figure 5.7 (c): Rainfall rate distribution for 2015.

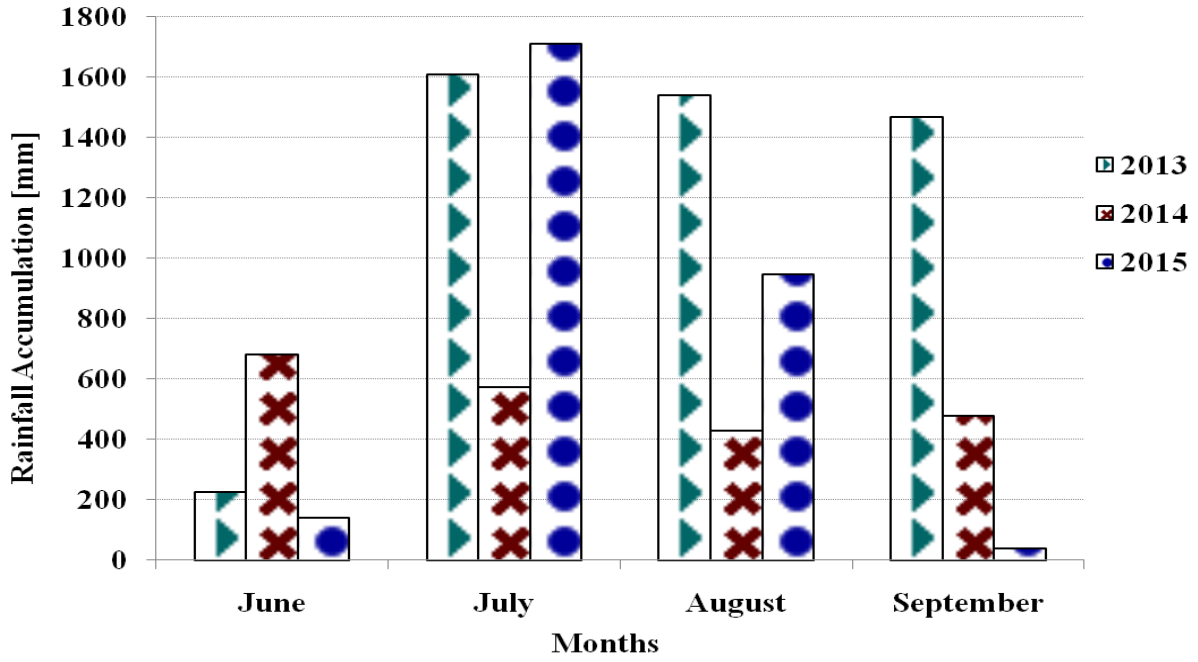

Figure 5.8: Monthly average of rainfall amount for three years of measurement.

The relative trend of better curves are shown in 2013 where as for successive two years, the higher attenuation values are observed, particularly in the month of June and August respectively. This might be because of the measurement of data that had been performed for 5-second instances which have been combined for 1-min. distribution. Similarly, the 1-min. rain rate distribution is higher in the month of July and August expect for 2014 where, rain rate is observed to be lower in the month of August. The arrangement of rain rate against rain attenuation indicates that there is the better positive correlation between the rain rate and rain attenuation in 2013. Thus, this year have been taken for the study of diurnal variation of rain attenuation and rain rate. The mentioned months have been considered because in this time period, the rainfall is observed to be greater over this region. The average monthly rainfall accumulation for the three years of measurement is shown in Figure 5.8 which reveals that

maximum average monthly rainfall accumulation is observed in the month of July and August. In addition, month wise variability of rain rate and rain attenuation is studied further to generalize the use of regression, coefficients $\boldsymbol{k}$ and $\boldsymbol{\alpha}$ value for the better estimation against the measured rain attenuation statistics.

C.Proposed Technique

In order to propose a suitable approach, we studied the relationship between slant path rain attenuation and effective path length exceeded at 0.01% of the time. The empirical relationship between these two quantities is given as,

$$\boldsymbol{A_{0.01} = kR_{0.01}^{\alpha} \times L_{eff}} \quad \text{[dB]} \qquad \text{(C. 8)}$$

where parameters $\boldsymbol{k}$ and $\boldsymbol{\alpha}$ are determined from ITU-R 838-3[6] which depend on frequency and wave polarization. The effective path length, $\boldsymbol{L_{eff}}$, can be more conveniently estimated from the ratio of measured rain attenuation to rain rate, at equal probability level for 0.01% of the time which is given as,

$$\boldsymbol{L_{eff} = \frac{A_{0.01}}{kR_{0.01}^{\alpha}}} \qquad \text{(C. 8(a))}$$

This method is applied on the experimental databanks of rain intensity and rain attenuation database provided by National Radio Research Agency, RRA for three years spanning from 2013 till 2015 and the successive years database is still under developmental phase. A curve fitting technique was employed to obtain the empirical expression between effective path length and rain rate for 0.01% of the time. Hence, the expression obtained for effective path length is used

in equation (C. 8) for calculating slant path attenuation exceeded at 0.01% of the time. The regression analysis of the experimental data has shown that $\boldsymbol{L_{eff}}$ is related to $\boldsymbol{R_{0.01}}$ by the following power law as,

$$\boldsymbol{L_{eff} = 0.001261 \times R_{0.01}^{1.997}} \qquad \text{(C. 8(b))}$$

An empirical expression for calculating, $\boldsymbol{A_{0.01}}$, is proposed by substituting (C. 8(b)) into (C. 8) as follows,

$$\boldsymbol{A_{0.01} = 0.001261 \times k \times R_{0.01}^{\alpha+1.997}} \qquad \text{(C. 8(c))}$$

The rain attenuation exceeded for other time percentages, $\boldsymbol{P}$, in the range 0.001% to 1% of the time of an average year, can be estimated by the extrapolation equation as stated in equation (C. 2(c)). The proposed technique shows the initial step for the determination of slant path attenuation. However, it lacks the detail parameters such as reduction factor for inhomogeneity nature of rain which require more experimental data considering the various values of effective path length and actual path length.

D.Performance Evaluation

The analysis presented above is applied here to numerically illustrate the relation between estimated and measured rain attenuation. To this end, the Complementary Cumulative Distribution Function (CCDF) for rain attenuation at 12.25, 19.8 and 20.73 GHz along with the ITU-R P. 618-12 predicted values are shown in Figure 5.9 in several time percentages, $\boldsymbol{P}$, at equiprobable exceedance probability (0.001% ≤ $\boldsymbol{P}$ ≤ 1%). As shown in figure, for 12.25 GHz

link, ITU-R P. 618-12 model predictions shows a close value at 0.01% of the time but differ significantly against the rain attenuation CCDF in lower and higher time percentage. At lower time percentage the difference in prediction is relatively lower as compared to higher time percentage. For instance, the calculated 1-min. rain attenuation values are 7.9, 10.7, 19 dB while the corresponding ITU-R P. 618-12 estimates 3.73, 11.14, 23.49 dB for 0.1%, 0.01% and 0.001% of the time respectively. Similarly, for 19.8 and 20.73 GHz links, ITU-R P. 618-12 model prediction differs significantly for the rain attenuation CCDF even though this model gives fair good estimation at higher time percentage ($\boldsymbol{P} \geq 0.5\%$). At lower time percentage this model dramatically overestimates the 1-min. rain attenuation values. For instance, at 0.01% of the time, the calculated 1-min. rain attenuation values are 11.6 and 11.3 dB for 19.8 and 20.73 GHz respectively. While the corresponding ITU-R P. 618-12 estimated values are 20.02 and 26.09 dB respectively. Moreover, in $\boldsymbol{P} \leq 0.01\%$ of the time, the deviations are more pronounced. For instance, the deviations are approximately 18 and 32 dB for 19.8 and 20.73 GHz for 0.001% of the time respectively. The reason behind this difference could be the fact that the matrices used to obtain the parameters might have low spatial resolution. This indicates that ITU-R P. 618-12 model performance statistics does not show good agreement with calculated 1-min. rain attenuation distribution from experimental 10-seconds measured rain attenuation values. In this concern, there is the immediate need for 1-min. rain attenuation prediction model that can give the higher estimation for local 1-min. rain attenuation distribution. Under this aspect, the study presents the new approach that shall be applicable in analyzing the 1-min. rain attenuation distribution pattern for instantaneous attenuation over the earth-space path. As an initial step several prominent rain attenuation models as well as proposed approach are analyzed against the

calculated 1-min. rain attenuation distribution. These are shown in Figure 5.10(a), (b) and (c) for 12.25, 19.8 and 20.73 GHz satellite communication links respectively.

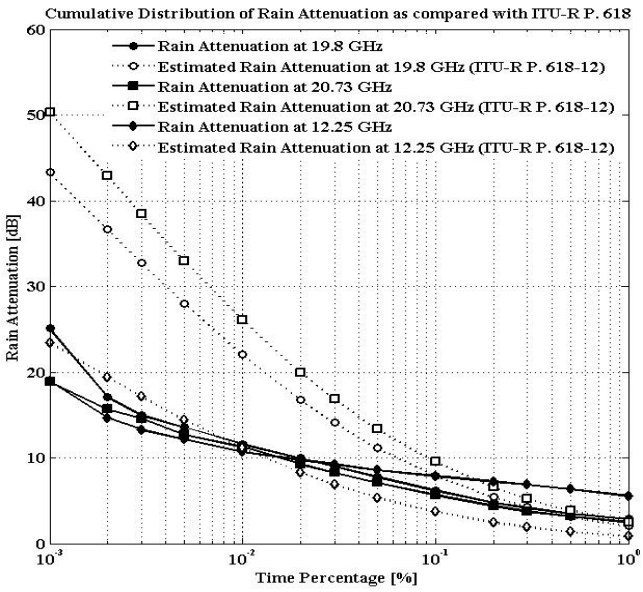

Figure 5.9: Cumulative distribution of rain attenuation as compared with ITU-R P. 618-12.

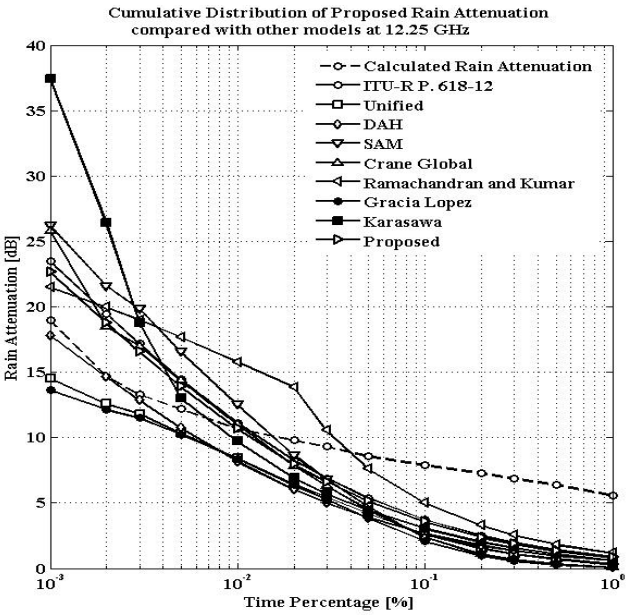

Figure 5.10(a): Cumulative distribution of proposed rain attenuation compared with models at 12.25 GHz.

As noticed from Figure 5.10 (a), for 12.25 GHz, it is observed that the measured cumulative statistics of rain attenuation is preferably predicted by ITU-R P. 618-12 and the proposed approach at 0.01% of the time and they show the similar pattern for other time percentage but the chances of overestimation and underestimation are greater for lower and higher time percentages respectively. For instance, the calculated rain attenuation values are 7.9, 10.7, 19dB at 0.1%, 0.01%, 0.001% of the time while ITU-R P. 618-12 and proposed approach predict 3.73, 11.14, 23.49 dB and 3.56, 10.7, 22.67 dB respectively. A similar pattern is observed with the application of Crane Global and SAM methods which overestimate and underestimate the measured rain attenuation values at lower and higher time percentage respectively. Interestingly, Crane Global give closer estimation against the measured rain attenuation for lower time percentage when $\boldsymbol{P} < 0.01\%$ of the time. For instance, Crane Global predicts 2.39, 11.05, 25.84

dB respectively at 0.1%, 0.01% and 0.001% of the time where as SAM predicts 2.37, 12.52, 26.2 dB respectively. DAH, Unified and Gracia Lopez show underestimation against the measured cumulative statistics of rain attenuation for all time percentage but the closer prediction is obtained by the application of DAH method for lower time percentage when $\boldsymbol{P} < 0.01\%$ of the time. Considerable underestimation is observed by this method at lower time percentage when $\boldsymbol{P} > 0.01\%$ of the time. For instance, DAH, Unified and Gracia Lopez estimate 2.66, 8.19, 17.84dB; 2.63, 8.42, 14.55dB and 2.09, 8.41, 13.64dB respectively at 0.1%, 0.01% and 0.001% of the time. Karasawa shows preferable estimation at 0.01% of the time but greater overestimation and underestimation are observed for lower and higher time percentage respectively as compared to other methods. Additionally, Ramachandran and Kumar give the better estimation for higher time percentage but overestimation is noted on lower time percentage. For instance, Karasawa, Ramachandran and Kumar estimate 3.07, 9.72, 37.45dB and 5, 15.79, 21.48dB respectively at 0.1%, 0.01% and 0.001% of the time. The better performance analyses of these methods are done from error calculation in further part.

As depicted in Figure 5.10 (b) and Figure 5.10 (c), for 19.8 and 20.73 GHz, similar statistical nature is observed. It is observed that the measured cumulative statistics of rain attenuation is overestimated by ITU-R P. 618-12. The overestimation becomes highly pronounced at lower time percentage. For instance, the calculated rain attenuation values are 6.2, 11.6, 25.1 dB; 5.7, 11.3, 18.9 dB at 0.1%, 0.01% and 0.001% of the time respectively for 19.8 and 20.73 GHz links while ITU-R P. 618-12 predicts 7.91, 22.02, 43.29 dB; 9.53, 26.09, 50.37 dB. A similar pattern is observed with the application of DAH and Crane Global models which overestimate the measured rain attenuation values, particularly when $\boldsymbol{P} \leq 0.1\%$ of the time. Interestingly, these

models give closer estimation against the measured rain attenuation for higher time percentage when $\boldsymbol{P} > 0.1\%$ of the time. For instance, in 19.8 and 20.73 GHz links, DAH model predicts 7.06, 19.88, 39.50 dB; 8.43, 23.33, 45.57 dB respectively at 0.1%, 0.01% and 0.001% of the time where as Crane Global model predicts 5.67, 21.56, 48.57 dB; 7.12, 27.60, 60.09 dB. The lower values of overestimation are noticed from the application of DAH model. In the same way, SAM shows a relatively greater overestimation of rain attenuation for lower time percentage when $\boldsymbol{P} \leq 0.1\%$ of the time as compared to all methods except Ramachandran and Kumar model. While it underestimates the measured rain attenuation for $\boldsymbol{P} > 0.1\%$ of the time which is very similar to Crane Global model. Similarly, Ramachandran and Kumar model shows greater overestimation throughout the time percentage for $10^{-3}\ \% \leq \boldsymbol{P} \leq 1\ \%$ which indicates that this model gives poor estimation against the measured statistical values of rain attenuation. For instance, SAM, and Ramachandran and Kumar estimates 6.01, 25.75, 49.01 dB; 7.27, 31.89, 61.36 dB and 13.23, 37.76, 49.05 dB; 16.08, 44.94, 57.85 dB respectively at 0.1%, 0.01% and 0.001% of the time for 19.8 and 20.73 GHz links. Unified and Gracia Lopez show closer estimation for calculated cumulative statistics of rain attenuation and closest is obtained with the application of Gracia Lopez. For instance, Unified and Gracia Lopez estimate the rain attenuation of 6.70, 17.89, 28.47 dB; 7.99, 22.07, 35.61 dB and 5.33, 16.87, 24.58 dB; 6.40, 20.91, 30.86 dB for 0.1%, 0.01% and 0.001% of the time respectively. Karasawa shows preferable estimation for higher time percentage when $\boldsymbol{P} > 0.1\%$ of the time but greater overestimation is observed for lower time percentage as compared to other methods. As calculated, Karasawa shows the rain attenuation values of 6.15, 19.46, 75.01 dB and 7.64, 24.18, 93.19 dB for 0.1%, 0.01% and 0.001% of the time in 19.8 and 20.73 GHz links respectively. Interestingly, proposed approach gives relatively

lower overestimation to the calculated cumulative statistics of rain attenuation at lower time percentages when $\boldsymbol{P} \leq 0.01\%$. In addition, for higher time percentage when $\boldsymbol{P} > 0.01\%$ of the time, this method give the closer prediction to the calculated cumulative statistics of rain attenuation. For instance, proposed approach estimate the rain attenuation of 4.87, 14.19, 29.20 dB and 6.08, 17.36, 34.97 dB for 0.1%, 0.01% and 0.001% of the time respectively in 19.8 and 20.73 GHz links. The several error analyses support for further judgment of suitable methods.

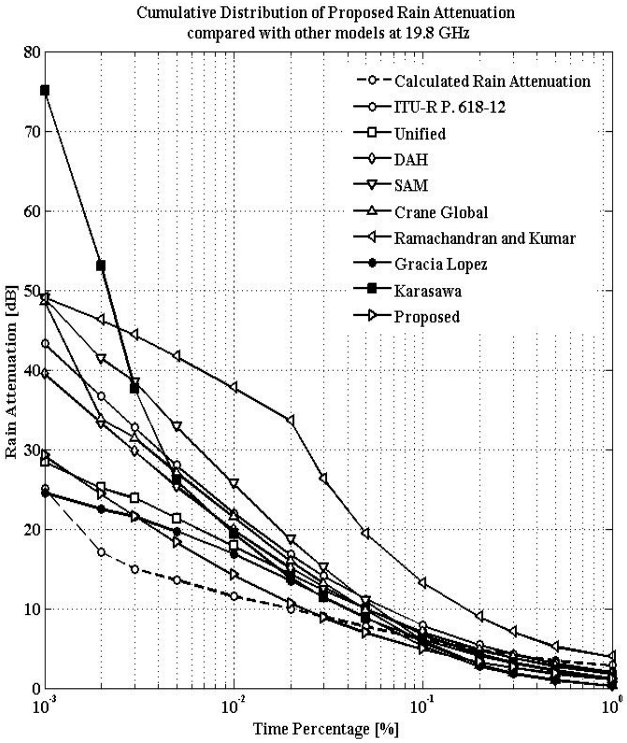

Figure 5.10 (b): Cumulative distribution of proposed rain attenuation compared with models at 19.8 GHz.

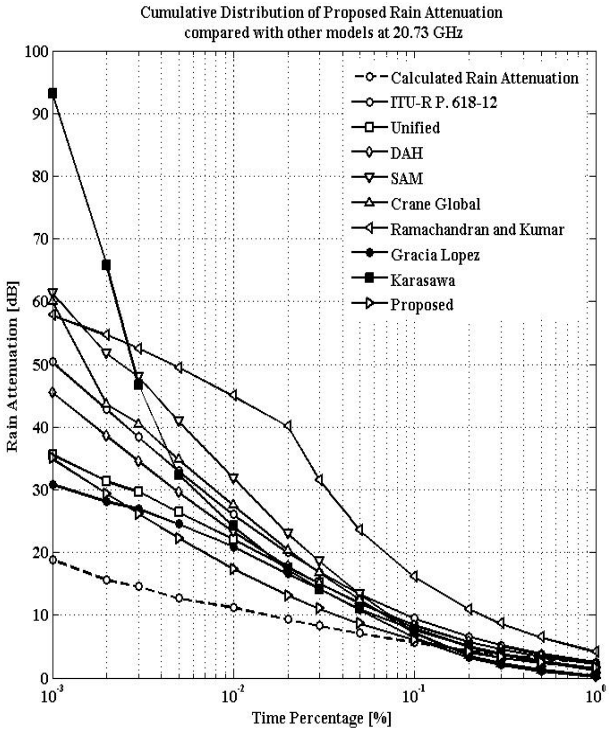

Figure 5.10 (c): Cumulative distribution of proposed rain attenuation compared with models at 20.73 GHz.

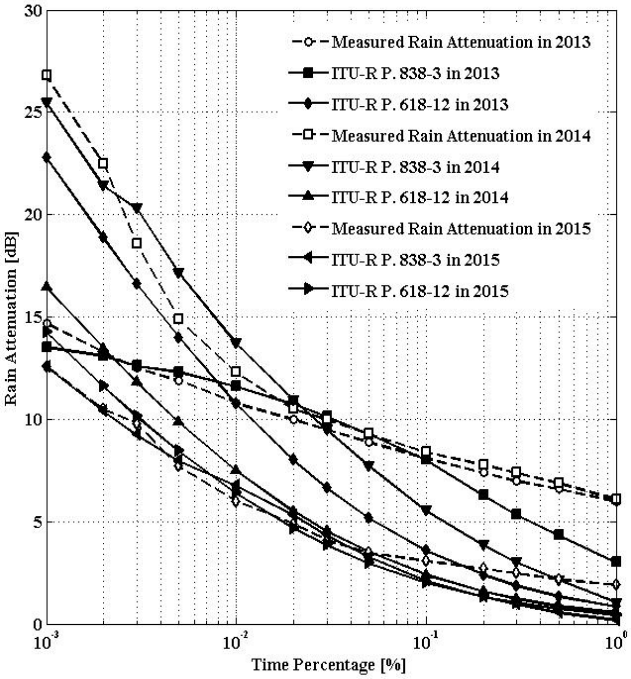

Figure 5.11: Comparison between empirical measured data and ITU-R P. 618-12 at 12.25 GHz.

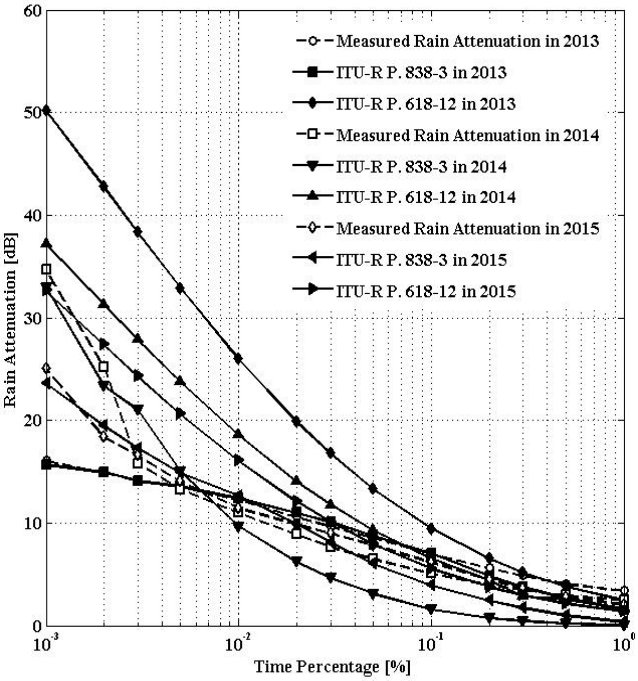

Figure 5.12: Comparison between empirical measured data and ITU-R P. 618-12 at 19.8 GHz.

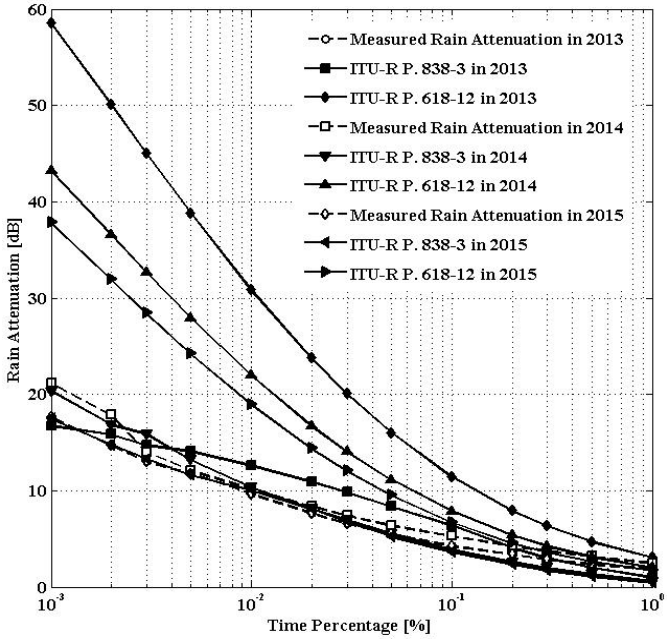

Figure 5.13: Comparison between empirical measured data and ITU-R P. 618-12 at 20.73 GHz.

The comparison of attenuation obtained from empirically generated k and α along with the ITU-R P. 618-12 prediction method are graphically shown in Figure 5.11, 5.12, 5.13 under 12.25, 19.8 and 20.73 GHz for 2013, 2014 and 2015 years respectively. As noticed from these figures, it is observed that the measured cumulative statistics of rain attenuation is overestimated by ITU-R P. 618-12 for Ka-band operation as compared to Ku-band. The overestimation becomes highly pronounced at 20.73 GHz. The attenuation obtained after using the empirically derived k and α for specific attenuation, γ_R when multiplied with predicted L_{eff} generate the better estimation against the measured attenuation values for Ku and Ka band frequencies. For instance, in 12.25 GHz, the calculated attenuation values are 8.10, 10.80, 14.70 dB; 8.40, 12.30, 26.80 dB; 3.10, 6.00, 12.60 dB for 2013, 2014, 2015 respectively at 0.1%, 0.01% and 0.001% of the time while ITU-R P. 618-12 predicts 3.59, 10.78, 22.80 dB; 2.41, 7.50, 16.48 dB; 2.02, 6.39, 14.27 dB. Similarly, the product of specific rain attenuation obtained from proposed empirical coefficients k and α, along with predicted L_{eff} results in 8.02, 11.61, 13.53 dB; 5.56, 13.72, 25.51 dB; 2.13, 6.76, 12.59 dB for same time percentages. In addition, in 19.8 GHz, the calculated attenuation values are 7.00, 12.30, 16.10 dB; 5.10, 11.00, 34.70 dB; 6.20, 11.50, 25.10 dB for 2013, 2014, 2015 respectively at 0.1%, 0.01% and 0.001% of the time while ITU-R P. 618-12 predicts 9.51, 26.03, 50.28 dB; 6.57, 18.61, 37.22 dB; 5.59, 16.07, 32.64 dB. Similarly, the product of specific rain attenuation obtained from proposed empirical coefficients k and α, along with predicted L_{eff} results in 9.51, 26.03, 50.28 dB; 1.63, 9.71, 33.04 dB; 3.95, 12.63, 23.61 dB for same time percentages. Furthermore, in 20.73 GHz, the calculated attenuation values are 6.70, 12.10, 17.50 dB; 5.30, 10.20, 21.20 dB; 4.30, 9.70, 17.70 dB for 2013, 2014,

2015 respectively at 0.1%, 0.01% and 0.001% of the time while ITU-R P. 618-12 predicts 11.48, 30.88, 58.59 dB; 7.90, 22.00, 43.24 dB; 6.71, 18.97, 37.87 dB. Similarly, the product of specific rain attenuation obtained from proposed empirical coefficients k and α, along with predicted L_{eff} results in 6.40, 12.67, 16.79 dB; 3.89, 10.39, 20.37 dB; 3.61, 10.05, 17.44 dB for same time percentages. The further error analyses support for the judgment of mentioned approaches.

Rain rate is plotted against the rain attenuation values arranged for time percentage 1% to 0.001% after applying power law so as to generate regression coefficients, k and α. These values are listed in Table 5.4.

Table 5.4. Regression coefficients for three satellite links.

Satellite Links	Year	Expression for L_{eff}	R^2	k	α
12.25 GHz	2013	$5.022\ R^{-0.318}$	0.6539	0.6167	0.6323
	2014	$4.739\ R^{-0.326}$	0.5926	0.2783	0.9692
	2015	$3.488\ R^{-0.2794}$	0.5677	0.1778	0.9805
20.73 GHz	2013	$5.022\ R^{-0.318}$	0.6539	0.2207	0.8974
	2014	$4.739\ R^{-0.326}$	0.5926	0.1727	1.024
	2015	$3.488\ R^{-0.2794}$	0.5677	0.3456	0.9017
19.8 GHz	2013	$5.022\ R^{-0.318}$	0.6539	0.3242	0.8015
	2014	$4.739\ R^{-0.326}$	0.5926	0.0201	1.596
	2015	$3.488\ R^{-0.2794}$	0.5677	0.3266	0.9854

The correlation coefficient, R^2, is greater in 2013 for mentioned three links which indicates the better estimation of rain attenuation from rain rate statistics. This might be due to the use of higher rain rate values at 0.01% of the time. The effective length as obtained from SAM approach is plotted against the respective year wise rain rate values whose relationship is

established by the power law. In addition, the measured rain rate is divided by estimated L_{eff}, which is again plotted against the rain rate measurement so as to obtain the required regression coefficients, k and α for specific attenuation, γ_R at different rain rate. The rain attenuation is thus calculated with the product of empirically generated k and α values, with the estimated, L_{eff}. Similarly, the k and α as derived from the procedure explained in ITU-R P. 838-3, are used to obtained attenuation values for ITU-R P. 618-12 extrapolation approach.

In further study, the Complementary Cumulative Distribution Function (CCDF) for rain attenuation of three years at 19.8 GHz, calculated with the ITU-R P. 618-12 prediction with the use of k and α value as recommended by ITU-R P. 838-3 and attenuation obtained from the product of effective path length and specific attenuation values as calculated with the use of empirically generated regression coefficients k and α are shown in Figure 5.14 (a), (b) and (c) in several time percentages, P, at equiprobable exceedance probability ($0.001\% \leq P \leq 1\%$).

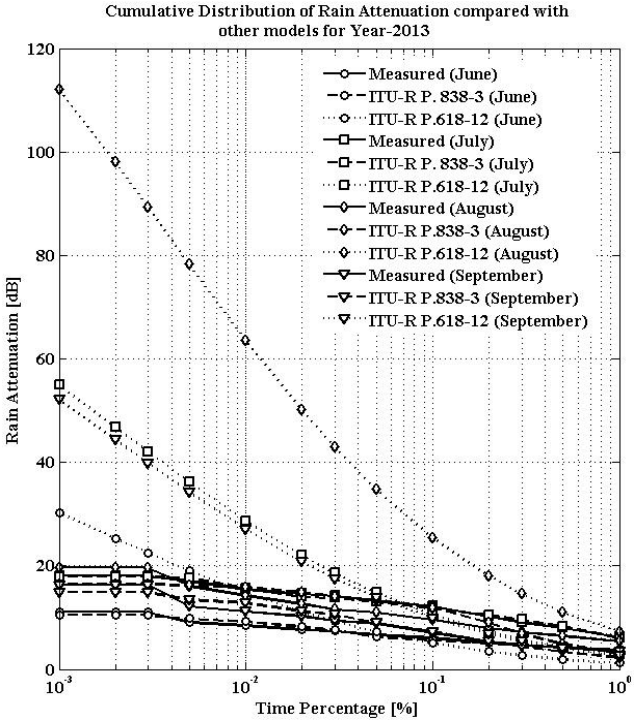

Figure 5.14(a): Distribution of rain attenuation as compared with other models for 2013.

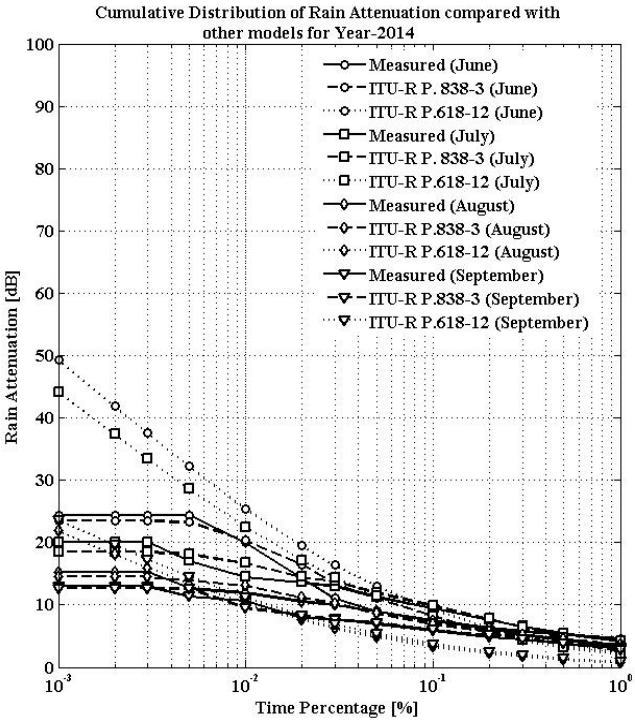

Figure 5.14(b): Distribution of rain attenuation as compared with other models for 2014.

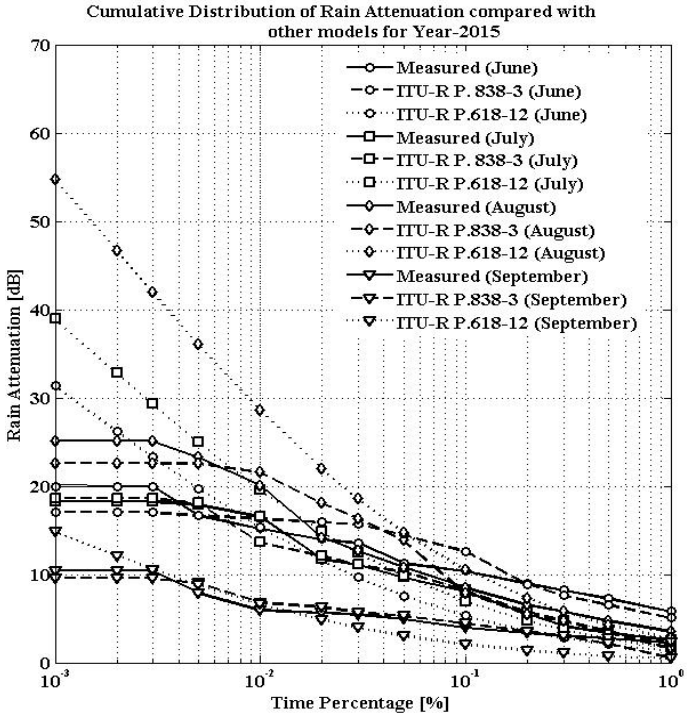

Figure 5.14(c): Distribution of rain attenuation as compared with other models for 2015.

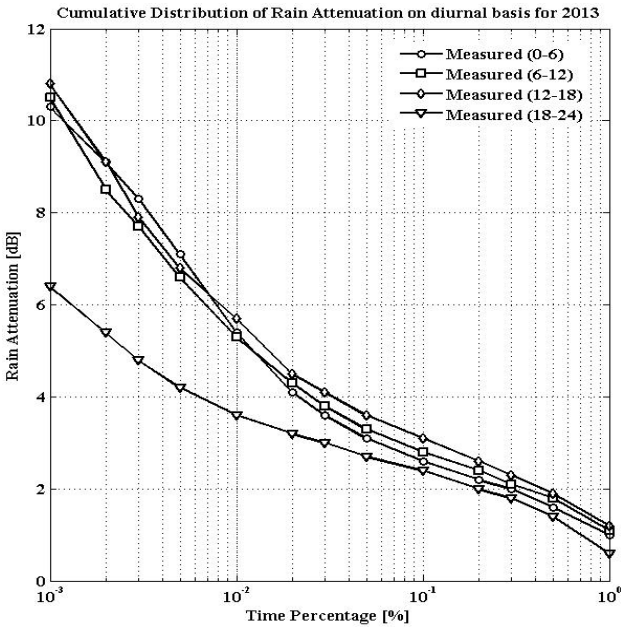

Figure 5.15(a): Distribution of rain attenuation based on diurnal variation for 2013.

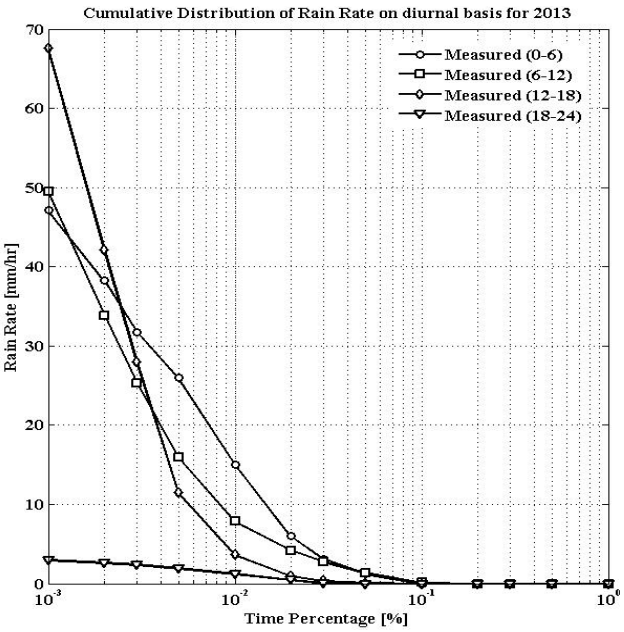

Figure 5.15(b): Distribution of rain rate based on diurnal variation for 2013.

As shown in Figure 5.14(a), ITU-R P. 618-12 models shows overestimation against the measured values except for the month of June where it shows closer values. Interestingly, the overestimation is less for successive two years as depicted by Figure 5.14(b) and Figure 5.14(c). The better analyses can be determined by the values of error matrices in further part. Figure 5.15(a) presents the diurnal rain attenuation pattern which depicts the less attenuation values during late night time from 18 to 24 hours whereas for other time instances there are the higher attenuation values for 2013. Similarly, the diurnal rain rate distribution is shown in Figure 5.15(b) which highlight the similar facts where there is the less values of rain rate for late night time from 18 to 24 hours whereas for other time instances, there is the higher values of ran rate. We have maintained the duration of 24 hour with four intervals such as 0-6, 6-12, 12-18 and 18-24.

Table 5.5. Regression coefficients for Ka band satellite links.

Satellite Links	Year	Month	Expression for L_{eff}	R^2	k	α
19.8 GHz	2013	June	$3.8420\ R^{-0.11640}$	0.8382	0.9269	0.1753
		July	$6.2150\ R^{-0.02157}$	0.9261	0.1845	0.6155
		August	$4.3180\ R^{0.05836}$	0.575	0.5189	0.3542
		September	$4.3290\ R^{0.06642}$	0.4676	0.2318	0.5308
	2014	June	$3.7760\ R^{0.11570}$	0.8056	0.5205	0.5313
		July	$4.5160\ R^{0.06397}$	0.388	0.1203	0.8024
		August	$4.0430\ R^{0.11530}$	0.7433	1.142	0.2671
		September	$3.3610\ R^{0.17420}$	0.73	0.4272	0.4885
	2015	June	$3.7530\ R^{0.12600}$	0.8868	1.174	0.2547
		July	$4.1260\ R^{0.08857}$	0.5079	0.1399	0.7611
		August	$4.2270\ R^{0.07002}$	0.7559	0.5599	0.4358
		September	$4.3720\ R^{0.05868}$	0.404	0.6666	0.3404

The obtained expression for effective path length as plotted against the rain rate as well as the empirically generated regression coefficients, $\boldsymbol{k}$ and $\boldsymbol{\alpha}$ for 19.8 GHz links in year 2013, 2014 and 2015 are tabulated in Table 5.5. The correlation coefficient, $\boldsymbol{R^2}$, is greater in 2013 which indicates the better estimation of rain attenuation from rain rate statistics. This might be due to the use of higher rain rate values at 0.01% of the time. The effective length as obtained from SAM approach is plotted against the respective month wise rain rate values whose relationship is established by the power law. In addition, the measured rain rate is divided by estimated L_{eff}, which is again plotted against the rain rate measurement so as to obtain the required regression coefficients, $\boldsymbol{k}$ and $\boldsymbol{\alpha}$ for specific attenuation, $\boldsymbol{\gamma_R}$ at different rain rate. The rain attenuation is thus calculated with the product of empirically generated $\boldsymbol{k}$ and $\boldsymbol{\alpha}$ values, with the estimated, L_{eff}. Similarly, $\boldsymbol{k}$ and $\boldsymbol{\alpha}$ are also derived from the procedure explained in ITU-R P. 838-3 which

are used to obtained attenuation values for ITU-R P. 618-12 extrapolation approach. Hence, comparison of the attenuation obtained from empirically generated $\boldsymbol{k}$ and $\boldsymbol{\alpha}$ along with the ITU-R P. 618-12 prediction method are studied for 2013, 2014 and 2015 years. The further error analyses support for the judgment of mentioned approaches.

The rain attenuation prediction model for Earth-satellite link is determined for exceeding time percentages in the range 0.001% to 1%. Hence, the percentage errors, $\boldsymbol{\varepsilon}\ (\boldsymbol{P})$, between measured Earth-satellite attenuation data ($\boldsymbol{A_{\%p,measured}}$) in dB and the model's predictions ($\boldsymbol{A_{\%p,pedicted}}$) in dB are obtained with expression exceeding time percentage of interest on link at the same probability level, $\boldsymbol{P}$, in the percentage interval 10^{-3} % < $\boldsymbol{P}$ < 1 %, whose expression is given by equation 4.5. Similarly, for standard deviation, STD and root mean square, RMS calculation, the approaches followed in[41] have been adopted. The calculated relative error probability, $\boldsymbol{\varepsilon}\ (\boldsymbol{P})$, standard deviation, STD, and root mean square, RMS values are tabulated. As per the recommendation by ITU-R P. 311-15[7], the ratio of predicted to measured attenuation is calculated and the natural logarithm of these error ratios is used as a test variable. The mean ($\boldsymbol{\mu_v}$), standard deviation ($\boldsymbol{\sigma_v}$) and root mean square ($\boldsymbol{\rho_v}$) of the test variable are then calculated to provide the statistics for prediction method comparison which are listed in Table 5.6 (a), Table 5.6 (b) and Table 5.6 (c) for 12.25, 19.8 and 20.73 GHz links for Mokdong Station respectively along with the evaluation procedures adopted for comparison of prediction methods by the recommendation ITU-R P.311-15[7].

As shown in Table 5.6 (a), in the case of 12.25 GHz, ITU-R P.618-12, Unified, DAH, SAM, Crane Global, Gracia Lopez, Karasawa and proposed technique show higher relative error

percentage when 0.05 % ≤ $\boldsymbol{P}$ ≤ 1 % which is justified from increased STD and RMS values. In the other hand, Ramachandran and Kumar show lower relative error at same time percentage which is supported by lower STD and RMS values. Thus, for higher time percentage when 0.05 % ≤ $\boldsymbol{P}$ ≤ 1 %, Ramachandran and Kumar method is suitable. In addition, for lower time percentage, when 0.001 % ≤ $\boldsymbol{P}$ < 0.01 %, ITU-R P. 618-12, SAM, Crane Global, Ramachandran and Kumar, Karasawa and proposed method give higher relative error values which overestimate the measured cumulative rain attenuation statistics. Interestingly, overestimation is observed to be lesser for ITU-R P. 618-12 and proposed method which is supported by decreased STD and RMS values. In contrast, DAH, Unified, Gracia Lopez models give underestimation against the calculated rain attenuation but less underestimation is shown by DAH method which signifies it's suitability for lower time percentage. In addition, at 0.01% of the time, ITU-R P. 618-12 and proposed method seem to provide fairly more accurate results than the other models of interest which are justified from decreased STD and RMS values. For instance, ITU-R P. 618-12 shows the relative error percentage of 53%, 4%, 24% while it is 67%, 21%, 23%; 66%, 23%, 6%; 70%, 17%, 38%; 70%, 3%, 36%; 37%, 48%, 13%; 74%, 21%, 28%; 61%, 9%, 97%; 55%, 0%, 19% for Unified, DAH, SAM, Crane Global, Ramachandran and Kumar, Gracia Lopez, Karasawa and proposed methods at 0.1%, 0.01% and 0.001% of the time respectively. Furthermore, from the calculation of $\boldsymbol{\mu_v}$, as per the recommendation of ITU-R P.311-15[7], ITU-R P. 618-12 and proposed technique show relatively fewer values which are supported by lower values of $\boldsymbol{\sigma_v}$ and $\boldsymbol{\rho_v}$ which justified their suitability for the estimation of rain attenuation in slant path for earth space communication link.

Table 5.6 (a). Percentage error obtained after testing over the interval [0.001% to 1%] for 12.25 GHz

Methods	Parameters	Time Percentage (%p)													ITU-R P.311-15		
		1	0.5	0.3	0.2	0.1	0.05	0.03	0.02	0.01	0.005	0.003	0.002	0.001	μ_v	σ_v	ρ_v
ITU-R P. 618-12	ε(P)	-0.84	-0.78	-0.72	-0.66	-0.53	-0.38	-0.26	-0.15	0.04	0.19	0.29	0.32	0.24	-0.45	0.64	0.78
	STD	0.59	0.53	0.47	0.41	0.28	0.13	0.01	0.10	0.29	0.43	0.54	0.57	0.48			
	RMS	4.70	4.98	4.94	4.79	4.17	3.23	2.40	1.49	0.44	2.27	3.89	4.77	4.49			
Unified	ε(P)	-0.94	-0.88	-0.84	-0.79	-0.67	-0.51	-0.42	-0.34	-0.21	-0.15	-0.11	-0.14	-0.23	-0.02	0.63	0.63
	STD	0.46	0.40	0.36	0.31	0.19	0.03	0.06	0.14	0.27	0.33	0.37	0.34	0.25			
	RMS	5.27	5.66	5.78	5.76	5.27	4.39	3.86	3.35	2.28	1.86	1.47	2.11	4.45			
DAH	ε(P)	-0.89	-0.85	-0.80	-0.76	-0.66	-0.55	-0.46	-0.38	-0.23	-0.12	-0.03	0.00	-0.06	-0.76	0.66	1.01
	STD	0.44	0.40	0.35	0.31	0.22	0.10	0.02	0.06	0.21	0.33	0.41	0.44	0.39			
	RMS	4.98	5.41	5.52	5.53	5.24	4.73	4.30	3.75	2.51	1.46	0.45	0.06	1.16			
SAM	ε(P)	-0.99	-0.95	-0.91	-0.86	-0.70	-0.45	-0.27	-0.12	0.17	0.36	0.49	0.47	0.38	-0.87	1.35	1.61
	STD	0.73	0.69	0.65	0.60	0.44	0.19	0.01	0.14	0.43	0.62	0.75	0.73	0.64			
	RMS	5.53	6.09	6.28	6.27	5.54	3.88	2.49	1.14	1.82	4.37	6.57	6.91	7.20			
Crane Global	ε(P)	-0.99	-0.95	-0.90	-0.85	-0.70	-0.48	-0.32	-0.20	0.03	0.18	0.28	0.26	0.36	-0.9	1.26	1.55
	STD	0.66	0.62	0.57	0.52	0.37	0.15	0.01	0.13	0.36	0.51	0.61	0.59	0.69			
	RMS	5.52	6.05	6.22	6.19	5.51	4.11	3.01	1.94	0.35	2.16	3.72	3.80	6.84			
Ramachandran and Kumar	ε(P)	-0.79	-0.71	-0.63	-0.55	-0.37	-0.12	0.13	0.42	0.48	0.45	0.43	0.36	0.13	-0.21	0.62	0.65
	STD	0.73	0.65	0.57	0.49	0.31	0.06	0.19	0.47	0.54	0.51	0.49	0.42	0.19			
	RMS	4.43	4.56	4.34	4.01	2.90	1.00	1.25	4.07	5.09	5.48	5.69	5.28	2.48			
Gracia Lopez	ε(P)	-0.99	-0.95	-0.91	-0.87	-0.74	-0.55	-0.44	-0.35	-0.21	-0.16	-0.13	-0.17	-0.28	-1.16	1.16	1.64
	STD	0.47	0.43	0.39	0.35	0.22	0.03	0.08	0.17	0.31	0.36	0.39	0.35	0.24			
	RMS	5.53	6.10	6.31	6.34	5.81	4.74	4.05	3.44	2.30	1.98	1.78	2.56	5.36			
Karasawa	ε(P)	-0.89	-0.83	-0.77	-0.72	-0.61	-0.49	-0.39	-0.29	-0.09	0.07	0.41	0.80	0.97	-0.53	0.81	0.97
	STD	0.67	0.61	0.55	0.50	0.39	0.27	0.17	0.08	0.13	0.29	0.63	1.02	1.19			
	RMS	4.97	5.30	5.32	5.25	4.83	4.18	3.61	2.87	0.98	0.83	5.47	11.76	18.45			
Proposed	ε(P)	-0.85	-0.79	-0.73	-0.67	-0.55	-0.40	-0.29	-0.19	0.00	0.14	0.24	0.28	0.19	-0.49	0.64	0.81
	STD	0.57	0.51	0.45	0.39	0.27	0.12	0.01	0.09	0.28	0.42	0.52	0.55	0.47			
	RMS	4.74	5.05	5.03	4.91	4.34	3.45	2.69	1.83	0.00	1.72	3.25	4.06	3.67			

In order to support the scientific argument for these finding, we have tested the validity of prominent rain attenuation models and proposed techniques in Ka band frequencies namely, 19.8 and 20.73 GHz whose test result are listed in Table 5.6 (b) and Table 5.6 (c) respectively.

Table 5.6 (b). Percentage error obtained after testing over the interval [0.001% to 1%] for 19.8 GHz.

Methods	Parameters	Time Percentage (%p)													ITU-R P.311-15		
		1	0.5	0.3	0.2	0.1	0.05	0.03	0.02	0.01	0.005	0.003	0.002	0.001	μ_v	σ_v	ρ_v
ITU-R P. 618-12	ε(P)	-0.29	-0.10	0.02	0.13	0.28	0.43	0.57	0.68	0.90	1.06	1.18	1.14	0.72	0.36	0.33	0.49
	STD	0.81	0.61	0.49	0.39	0.24	0.09	0.05	0.16	0.38	0.54	0.67	0.63	0.21			
	RMS	0.85	0.33	0.10	0.63	1.71	3.36	5.10	6.78	10.42	14.40	17.75	19.54	18.19			
Unified	ε(P)	-0.60	-0.34	-0.22	-0.11	0.08	0.28	0.37	0.43	0.54	0.57	0.59	0.47	0.13	0.11	0.35	0.37
	STD	0.77	0.51	0.39	0.28	0.09	0.11	0.21	0.26	0.37	0.40	0.42	0.30	0.03			
	RMS	1.75	1.19	0.93	0.53	0.50	2.15	3.36	4.29	6.30	7.71	8.88	8.08	3.37			
DAH	ε(P)	-0.38	-0.20	-0.09	0.01	0.14	0.28	0.41	0.51	0.71	0.87	0.98	0.95	0.57	0.27	0.33	0.42
	STD	0.74	0.56	0.46	0.36	0.23	0.08	0.04	0.14	0.35	0.50	0.62	0.58	0.21			
	RMS	1.09	0.69	0.37	0.04	0.86	2.20	3.67	5.10	8.28	11.76	14.74	16.23	14.40			
SAM	ε(P)	-0.90	-0.70	-0.55	-0.39	-0.03	0.41	0.68	0.87	1.22	1.42	1.57	1.42	0.95	0.14	0.82	0.83
	STD	1.36	1.16	1.01	0.85	0.49	0.05	0.22	0.41	0.76	0.96	1.11	0.96	0.49			
	RMS	2.60	2.45	2.30	1.85	0.19	3.20	6.14	8.67	14.15	19.28	23.51	24.33	23.91			
Crane Global	ε(P)	-0.89	-0.69	-0.55	-0.39	-0.09	0.26	0.47	0.60	0.86	0.99	1.10	0.98	0.93	0.05	0.75	0.75
	STD	1.17	0.97	0.82	0.67	0.36	0.01	0.19	0.33	0.58	0.72	0.82	0.70	0.66			
	RMS	2.58	2.43	2.29	1.89	0.53	2.04	4.20	6.02	9.96	13.51	16.46	16.75	23.47			
Ramachandran and Kumar	ε(P)	0.35	0.49	0.69	0.87	1.13	1.49	1.92	2.36	2.25	2.06	1.96	1.71	0.95	0.8	0.32	0.86
	STD	1.05	0.91	0.72	0.54	0.27	0.09	0.51	0.96	0.85	0.66	0.55	0.30	0.45			
	RMS	1.02	1.72	2.89	4.16	7.03	11.65	17.25	23.61	26.16	28.08	29.34	29.16	23.95			
Gracia Lopez	ε(P)	-0.90	-0.71	-0.57	-0.42	-0.14	0.14	0.28	0.35	0.45	0.45	0.44	0.32	-0.02	-0.2	0.64	0.66
	STD	0.87	0.68	0.54	0.40	0.12	0.17	0.30	0.37	0.48	0.47	0.47	0.34	0.00			
	RMS	2.61	2.48	2.38	2.03	0.87	1.12	2.51	3.47	5.27	6.10	6.61	5.41	0.52			
Karasawa	ε(P)	-0.56	-0.37	-0.25	-0.15	-0.01	0.13	0.27	0.39	0.68	0.92	1.51	2.10	1.99	0.28	0.54	0.61
	STD	1.08	0.88	0.76	0.66	0.52	0.38	0.24	0.12	0.17	0.41	1.00	1.59	1.48			
	RMS	1.64	1.30	1.04	0.70	0.05	1.05	2.40	3.87	7.86	12.48	22.60	35.89	49.91			
Proposed	ε(P)	-0.58	-0.46	-0.38	-0.31	-0.21	-0.11	-0.01	0.07	0.22	0.35	0.44	0.43	0.16	-0.1	0.33	0.34
	STD	0.55	0.43	0.35	0.28	0.18	0.08	0.02	0.10	0.25	0.38	0.47	0.46	0.19			
	RMS	1.70	1.61	1.61	1.50	1.33	0.83	0.11	0.67	2.59	4.70	6.62	7.28	4.10			

Table 5.6 (c). Percentage error obtained after testing over the interval [0.001% to 1%] for 20.73 GHz.

Methods	Parameters	Time Percentage (%p)													ITU-R P.311-15		
		1	0.5	0.3	0.2	0.1	0.05	0.03	0.02	0.01	0.005	0.003	0.002	0.001	μ_v	σ_v	ρ_v
ITU-R P. 618-12	ε(P)	0.00	0.21	0.38	0.50	0.67	0.89	1.03	1.15	1.31	1.60	1.63	1.73	1.66	0.61	0.33	0.7
	STD	0.98	0.77	0.60	0.48	0.31	0.10	0.05	0.17	0.33	0.62	0.65	0.75	0.68			
	RMS	0.01	0.66	1.43	2.19	3.83	6.29	8.55	10.68	14.79	20.29	23.84	27.16	31.47			
Unified	ε(P)	-0.49	-0.18	0.00	0.14	0.40	0.70	0.82	0.88	0.95	1.08	1.04	1.00	0.88	0.38	0.38	0.53
	STD	1.04	0.73	0.56	0.42	0.15	0.14	0.26	0.33	0.40	0.53	0.48	0.44	0.33			
	RMS	1.22	0.56	0.01	0.61	2.29	4.94	6.77	8.19	10.77	13.72	15.11	15.69	16.71			
DAH	ε(P)	-0.12	0.06	0.21	0.32	0.48	0.67	0.81	0.92	1.06	1.33	1.37	1.46	1.41	0.51	0.33	0.6
	STD	0.89	0.71	0.56	0.45	0.29	0.09	0.04	0.15	0.30	0.56	0.60	0.69	0.64			
	RMS	0.30	0.19	0.80	1.40	2.73	4.78	6.69	8.51	12.03	16.91	19.99	22.95	26.67			
SAM	ε(P)	-0.87	-0.62	-0.41	-0.20	0.28	0.89	1.24	1.47	1.82	2.22	2.29	2.29	2.25	0.41	0.85	0.95
	STD	1.84	1.59	1.39	1.18	0.70	0.08	0.27	0.50	0.85	1.25	1.32	1.32	1.27			
	RMS	2.17	1.98	1.57	0.90	1.57	6.34	10.30	13.71	20.60	28.19	33.42	36.03	42.46			
Crane Global	ε(P)	-0.86	-0.59	-0.38	-0.18	0.25	0.75	1.02	1.19	1.44	1.74	1.77	1.78	2.18	0.35	0.78	0.86
	STD	1.64	1.37	1.16	0.96	0.53	0.03	0.24	0.42	0.66	0.96	1.00	1.00	1.40			
	RMS	2.15	1.89	1.44	0.78	1.42	5.34	8.47	11.11	16.30	22.13	25.91	27.94	41.18			
Ramachandran and Kumar	ε(P)	0.68	1.01	1.29	1.49	1.82	2.31	2.79	3.31	2.98	2.90	2.60	2.48	2.06	1.04	0.33	1.09
	STD	1.45	1.12	0.84	0.64	0.31	0.17	0.66	1.18	0.84	0.76	0.46	0.35	0.07			
	RMS	1.71	3.23	4.89	6.56	10.38	16.38	23.20	30.82	33.64	36.77	37.92	39.00	38.95			
Gracia Lopez	ε(P)	-0.87	-0.63	-0.44	-0.26	0.12	0.53	0.70	0.78	0.85	0.93	0.85	0.79	0.63	0.11	0.66	0.67
	STD	1.18	0.94	0.75	0.56	0.18	0.22	0.39	0.48	0.54	0.62	0.54	0.49	0.33			
	RMS	2.17	2.02	1.67	1.13	0.70	3.77	5.81	7.29	9.61	11.84	12.41	12.47	11.96			
Karasawa	ε(P)	-0.37	-0.14	0.03	0.16	0.34	0.55	0.71	0.85	1.14	1.55	2.20	3.19	3.93	0.57	0.57	0.81
	STD	1.46	1.23	1.05	0.93	0.75	0.54	0.38	0.23	0.05	0.46	1.11	2.11	2.84			
	RMS	0.93	0.46	0.12	0.69	1.94	3.89	5.86	7.94	12.88	19.71	32.12	50.14	74.30			
Proposed	ε(P)	-0.39	-0.25	-0.14	-0.06	0.07	0.22	0.32	0.41	0.54	0.75	0.79	0.87	0.85	0.22	0.33	0.4
	STD	0.69	0.56	0.45	0.36	0.24	0.09	0.02	0.11	0.23	0.44	0.48	0.57	0.54			
	RMS	0.96	0.81	0.53	0.25	0.38	1.55	2.69	3.83	6.06	9.54	11.55	13.68	16.07			

As noted from Table 5.6 (b) and Table 5.6 (c), in the case of 19.8 and 20.73 GHz, similar statistical results are obtained where SAM, Crane Global, Ramachandran and Kumar, Gracia Lopez, Karasawa and proposed approach show higher relative error percentage when 0.1 % < $\boldsymbol{P}$ ≤ 1 % which is justified from increased STD and RMS values. In the other hand, ITU-R P. 618-12, Unified and DAH show lower relative error at same time percentage which is supported by lower STD and RMS values. Thus, for higher time percentage when 0.1 % < $\boldsymbol{P}$ ≤ 1 %, ITU-R P. 618-12, Unified and DAH methods are suitable. In addition, for lower time percentage, ITU-R P. 618-12, Unified, DAH, SAM, Crane Global, Ramachandran and Kumar, Gracia Lopez, Karasawa and proposed approach give higher relative error values which overestimate the measured cumulative rain attenuation statistics. ITU-R P. 618-12 shows the relative error percentage of 28%, 90%, 72%; 67%, 131%, 166% while it is 8%, 54%, 13%; 14%, 71%, 57%; 3%, 122%, 95%; 9%, 86%, 93%; 113%, 225%, 95%; 14%, 45%, 2%; 1%, 68%, 199%; 21%, 22%, 16% and 40%, 95%, 88%; 48%, 106%, 141%; 28%, 182%, 225%; 25%, 144%, 218%; 182%, 298%, 206%; 12%, 85%, 63%; 34%, 114%, 393%; 7%, 54%, 85% for 19.8 and 20.73 GHz respectively for Unified, DAH, SAM, Crane Global, Ramachandran and Kumar, Gracia Lopez, Karasawa and proposed approach at 0.1%, 0.01% and 0.001% of the time. This is supported by increased STD and RMS values. Hence, these models give lower effectiveness at lower time percentages. However, Unified, Gracia Lopez and proposed approach show relatively lower error percentage values which are justified from decreased STD and RMS values. Thus, these three methods are equally applicable for estimation of rain attenuation statistics at lower time percentage in slant path for earth space communication links when 0.001 % ≤ $\boldsymbol{P}$ ≤ 0.1 % of

the time. These methods suitability is further judge from the lower values of $\boldsymbol{\mu_v}$, as per the recommendation of ITU-R P.311-15 which are supported by lower values of $\boldsymbol{\sigma_v}$ and $\boldsymbol{\rho_v}$.

Furthermore, frequency scaling approach is tested for Ka-band along the same and different communication path. Frequency scaling method provide an alternative to rain attenuation models which are considered to be excellent predictors and provide a means for determining what to expect at a frequency for which there is no data. This paper analyses the approaches presented in ITU-R P. 618-12[1] where the frequency scaling formula is adopted for estimation of rain attenuation at 20.73 GHz link under circular polarization from the calculated 12.25 GHz rain attenuation values for same link while estimation in 19.8 GHz is performed for different satellite link. Further experimental analyses need to be carried out to validate the estimated rain attenuation statistics at 20.73 and 19.8 GHz under circular and vertical polarization respectively from the other locations. The predicted values are shown in Figure 5.16.

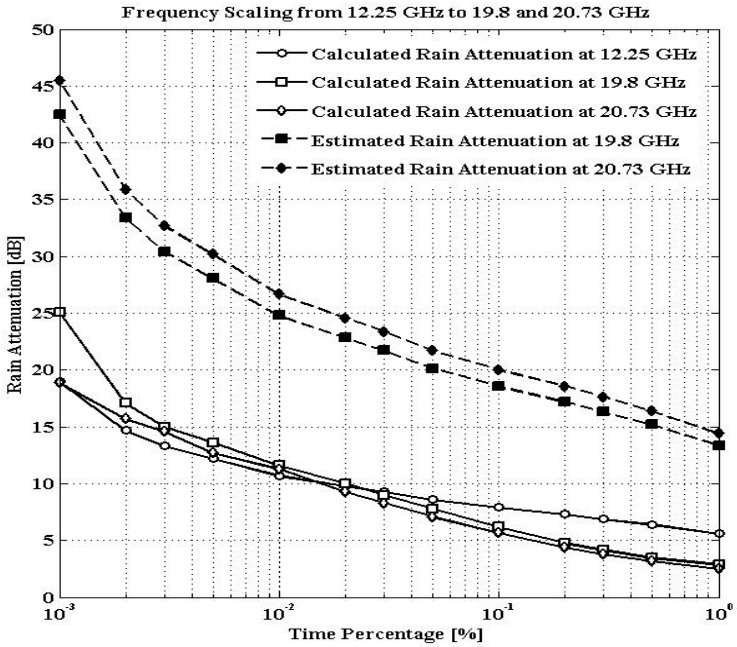

Figure 5.16: Cumulative distribution of calculated and estimated rain attenuation obtained after frequency scaling.

Figure 5.16 shows that there is the overestimation for predicted 19.8 and 20.73 GHz links which are obtained from the application of the frequency scaling method. For instance, the calculated rain attenuation at 19.8 and 20.73 GHz links are 6.2, 11.6, 25.1 dB; 5.7, 11.3, 18.9 dB respectively at 0.1%, 0.01%, 0.001% of the time and the estimated values are 18.58, 24.80, 42.48 dB; 20.06, 26.71, 45.53 dB. The better performance analyses are judge through the error matrices as presented in Table 5.7.

Table 5.7. Percentage error obtained over the interval [0.001% to 1%] after frequency scaling.

Methods	Parameters	Time Percentage (%p)													ITU-R P.311-15		
		1	0.5	0.3	0.2	0.1	0.05	0.03	0.02	0.01	0.005	0.003	0.002	0.001	μ_v	σ_v	ρ_v
ITU-R P. 618-12 (Predicted 19.8 GHz)	ε(P)	3.61	3.34	2.89	2.59	2.00	1.58	1.41	1.28	1.14	1.06	1.03	0.96	0.69	0.89	0.21	0.91
	STD	1.79	1.53	1.07	0.78	0.18	0.23	0.40	0.53	0.68	0.75	0.78	0.86	1.12			
	RMS	10.46	11.69	12.12	12.43	12.38	12.35	12.71	12.81	13.20	14.47	15.45	16.34	17.38			
ITU-R P. 618-12 (Predicted 20.73 GHz)	ε(P)	4.78	4.13	3.64	3.23	2.52	2.06	1.82	1.64	1.36	1.38	1.24	1.29	1.41	1.04	0.18	1.05
	STD	2.43	1.78	1.29	0.88	0.17	0.28	0.53	0.70	0.98	0.97	1.10	1.06	0.94			
	RMS	11.95	13.21	13.84	14.21	14.36	14.64	15.11	15.29	15.41	17.50	18.14	20.23	26.63			

As noticed from Table 5.7, the predicted 19.8 and 20.73 GHz rain attenuation statistics obtained after applying frequency scaling technique shows the higher relative error chances for all time percentage when 0.001 % ≤ $\boldsymbol{P}$ ≤ 1 % of the time. For instance, obtained relative error percentages are 200%, 114%, 69%; 252%, 136%, 141% for 19.8 and 20.73 GHz under 0.1%, 0.01% and 0.001% of the time respectively.

In addition, the calculated error matrices that are obtained after applying regional and ITU-R P. 838-3 derived regression coefficients values for $\boldsymbol{k}$ and $\boldsymbol{\alpha}$ under 12.25, 19.8 and 20.73 GHz links along with the evaluation procedures adopted for comparison of prediction methods by the recommendation ITU-R P.311-15 are shown in Table 5.8 (a), Table 5.8 (b) and Table 5.8 (c) respectively.

Table 5.8 (a). Percentage error obtained after testing over the interval [0.001% to 1%] for 12.25GHz.

Period	Methods	Parameters	Time Percentage (% p)													ITU-R P.311-15		
			1	0.5	0.3	0.2	0.1	0.05	0.03	0.02	0.01	0.005	0.003	0.002	0.001	μ_v	σ_v	ρ_v
2013	ITU-R P. 838-3	ε(P)	-0.50	-0.34	-0.24	-0.15	-0.01	0.04	0.07	0.07	0.08	0.03	0.01	-0.01	-0.08	-0.09	0.20	0.22
		STD	0.42	0.26	0.16	0.07	0.07	0.12	0.15	0.15	0.15	0.11	0.09	0.07	0.00			
		RMS	2.99	2.27	1.66	1.10	0.08	0.37	0.64	0.73	0.81	0.42	0.10	0.18	1.17			
		$\chi 2$	2.98	1.19	0.52	0.19	0.00	0.01	0.04	0.05	0.06	0.01	0.00	0.00	0.10			
	ITU-R P. 618-12	ε(P)	-0.86	-0.79	-0.73	-0.97	-0.56	-0.42	-0.30	-0.20	0.00	0.18	0.33	0.42	0.55	-0.47	0.70	0.84
		STD	0.62	0.56	0.50	0.44	0.32	0.18	0.06	0.04	0.23	0.41	0.57	0.65	0.79			
		RMS	5.14	5.23	5.11	4.99	4.51	3.71	2.84	1.97	0.02	2.11	4.16	5.58	8.10			
		$\chi 2$	30.54	20.04	13.84	10.29	5.65	2.66	1.21	0.48	0.00	0.32	1.04	1.65	2.88			
2014	ITU-R P. 838-3	ε(P)	-0.83	-0.69	-0.59	-0.51	-0.34	-0.17	-0.05	0.04	0.12	0.15	0.09	-0.05	-0.05	-0.35	0.52	0.63
		STD	0.61	0.47	0.37	0.29	0.12	0.05	0.17	0.26	0.34	0.37	0.31	0.17	0.17			
		RMS	5.06	4.75	4.38	3.95	2.84	1.56	0.50	0.46	1.42	2.24	1.73	1.08	1.29			
		$\chi 2$	24.77	10.51	6.35	4.05	1.46	0.32	0.03	0.02	0.15	0.29	0.15	0.05	0.07			
	ITU-R P. 618-12	ε(P)	-0.91	-0.87	-0.83	-0.79	-0.71	-0.62	-0.54	-0.47	-0.39	-0.34	-0.36	-0.40	-0.39	-1.02	0.59	1.17
		STD	0.32	0.28	0.24	0.21	0.13	0.03	0.04	0.11	0.20	0.25	0.22	0.19	0.20			
		RMS	5.54	6.01	6.16	6.20	5.99	5.78	5.44	4.97	4.80	5.04	6.78	9.01	10.32			
		$\chi 2$	55.07	40.45	30.49	24.01	14.90	9.51	6.51	4.48	3.07	2.57	3.88	6.02	6.47			
2015	ITU-R P. 838-3	ε(P)	-0.89	-0.74	-0.62	-0.50	-0.31	-0.07	0.06	0.09	0.13	0.04	-0.06	-0.01	0.00	-0.31	0.50	0.59
		STD	0.67	0.52	0.39	0.28	0.09	0.15	0.28	0.31	0.35	0.26	0.17	0.21	0.22			
		RMS	1.69	1.63	1.54	1.36	0.97	0.25	0.24	0.42	0.76	0.27	0.55	0.08	0.01			
		$\chi 2$	13.99	4.60	2.49	1.37	0.44	0.02	0.01	0.03	0.09	0.01	0.03	0.00	0.00			
	ITU-R P. 618-12	ε(P)	-0.76	-0.66	-0.59	-0.51	-0.35	-0.15	-0.06	-0.04	0.06	0.10	0.04	0.11	0.13	-0.25	0.37	0.45
		STD	0.55	0.46	0.38	0.30	0.14	0.05	0.15	0.16	0.27	0.30	0.24	0.31	0.34			
		RMS	1.44	1.46	1.47	1.37	1.08	0.54	0.25	0.22	0.39	0.74	0.36	1.12	1.67			
		$\chi 2$	4.52	2.89	2.08	1.40	0.58	0.10	0.02	0.01	0.02	0.07	0.01	0.11	0.20			

Table 5.8 (b). Percentage error obtained after testing over the interval [0.001% to 1%] for 19.8 GHz.

Period	Methods	Parameters	Time Percentage (% p)													ITU-R P.311-15		
			1	0.5	0.3	0.2	0.1	0.05	0.03	0.02	0.01	0.005	0.003	0.002	0.001	μ_v	σ_v	ρ_v
2013	ITU-R P. 838-3	ε(P)	-0.54	-0.33	-0.23	-0.13	0.01	0.02	0.04	0.04	0.01	0.00	-0.01	0.01	-0.02	-0.10	0.19	0.21
		STD	0.45	0.25	0.14	0.04	0.09	0.11	0.13	0.13	0.10	0.09	0.08	0.09	0.07			
		RMS	1.84	1.37	1.14	0.75	0.04	0.19	0.39	0.42	0.14	0.01	0.09	0.10	0.37			
		$\chi 2$	2.19	0.69	0.34	0.11	0.00	0.00	0.02	0.02	0.00	0.00	0.00	0.00	0.01			
	ITU-R P. 618-12	ε(P)	-0.26	-0.06	0.06	0.17	0.36	0.55	0.73	0.88	1.12	1.42	1.70	1.87	2.12	0.51	0.43	0.67
		STD	1.08	0.88	0.76	0.65	0.46	0.27	0.09	0.06	0.30	0.60	0.88	1.05	1.30			
		RMS	0.90	0.25	0.32	0.97	2.51	4.75	7.11	9.33	13.73	19.32	24.16	27.88	34.18			
		$\chi 2$	0.32	0.02	0.02	0.14	0.66	1.69	3.00	4.37	7.24	11.34	15.22	18.17	23.23			
2014	ITU-R P. 838-3	ε(P)	-0.98	-0.92	-0.86	-0.80	-0.68	-0.52	-0.39	-0.30	-0.12	0.13	0.34	-0.07	-0.05	-0.77	0.89	1.18
		STD	0.58	0.52	0.46	0.40	0.28	0.12	0.01	0.10	0.28	0.53	0.74	0.33	0.35			
		RMS	2.44	2.75	3.01	3.21	3.47	3.37	3.00	2.66	1.29	1.78	5.30	1.80	1.66			
		$\chi 2$	100.82	30.31	18.55	13.04	7.39	3.62	1.92	1.14	0.17	0.21	1.33	0.14	0.08			
	ITU-R P. 618-12	ε(P)	-0.33	-0.13	-0.17	0.12	0.29	0.43	0.53	0.58	0.69	0.79	0.77	0.24	0.07	0.22	0.28	0.36
		STD	0.63	0.43	0.47	0.18	0.01	0.13	0.24	0.29	0.39	0.49	0.47	0.06	0.23			
		RMS	0.83	0.40	0.61	0.49	1.46	2.82	4.12	5.20	7.61	10.49	12.13	6.14	2.52			
		$\chi 2$	0.41	0.06	0.13	0.05	0.33	0.85	1.44	1.92	3.11	4.62	5.27	1.20	0.17			
2015	ITU-R P. 838-3	ε(P)	-0.82	-0.62	-0.51	-0.45	-0.36	-0.23	-0.10	0.00	1.28	0.66	0.51	1.24	2.21	-0.28	0.39	0.48
		STD	0.60	0.40	0.29	0.23	0.14	0.01	0.12	0.23	0.32	0.28	0.27	0.28	0.16			
		RMS	1.73	1.75	1.84	2.02	2.25	1.85	0.91	0.03	1.13	0.81	0.71	1.11	1.49			
		$\chi 2$	7.96	2.89	1.91	1.64	1.28	0.57	0.10	0.00	0.10	0.04	0.03	0.06	0.09			
	ITU-R P. 618-12	ε(P)	-0.33	-0.22	-0.17	-0.16	-0.10	0.01	0.13	0.22	0.40	0.46	0.46	0.49	0.30	0.09	0.24	0.26
		STD	0.45	0.33	0.28	0.27	0.21	0.11	0.01	0.11	0.28	0.35	0.35	0.37	0.19			
		RMS	0.70	0.61	0.61	0.70	0.62	0.06	1.14	2.23	4.57	6.54	7.72	8.96	7.54			
		$\chi 2$	0.35	0.17	0.12	0.13	0.07	0.00	0.13	0.41	1.30	2.07	2.45	2.94	1.74			

Table 5.8 (c). Percentage error obtained after testing over the interval [0.001% to 1%] for 20.73 GHz.

Period	Methods	Parameters	Time Percentage (% p)													ITU-R P.311-15		
			1	0.5	0.3	0.2	0.1	0.05	0.03	0.02	0.01	0.005	0.003	0.002	0.001	μ_v	σ_v	ρ_v
2013	ITU-R P. 838-3	ε(P)	-0.64	-0.44	-0.34	-0.23	-0.04	0.00	0.04	0.04	0.05	0.03	-0.02	0.02	-0.04	-0.14	0.25	0.28
		STD	0.52	0.32	0.22	0.10	0.08	0.12	0.16	0.17	0.17	0.15	0.10	0.14	0.08			
		RMS	1.85	1.64	1.58	1.20	0.30	0.04	0.37	0.46	0.57	0.42	0.36	0.26	0.71			
		$\chi 2$	3.26	1.31	0.82	0.35	0.01	0.00	0.01	0.02	0.03	0.01	0.01	0.00	0.03			
	ITU-R P. 618-12	ε(P)	0.06	0.27	0.38	0.50	0.71	0.91	1.12	1.26	1.55	1.84	1.99	2.21	2.35	0.69	0.38	0.79
		STD	1.10	0.89	0.78	0.66	0.45	0.26	0.05	0.10	0.39	0.67	0.82	1.05	1.18			
		RMS	0.18	1.01	1.76	2.67	4.78	7.64	10.61	13.28	18.78	25.15	29.99	34.52	41.09			
		$\chi 2$	0.01	0.22	0.49	0.90	1.99	3.64	5.60	7.42	11.42	16.28	19.94	23.78	28.81			
2014	ITU-R P. 838-3	ε(P)	-0.75	-0.57	-0.47	-0.39	-0.26	-0.13	-0.06	-0.03	0.02	0.09	0.14	-0.06	-0.04	-0.23	0.33	0.40
		STD	0.56	0.37	0.28	0.20	0.07	0.06	0.13	0.16	0.21	0.29	0.33	0.13	0.15			
		RMS	1.87	1.81	1.79	1.68	1.40	0.82	0.06	0.03	0.02	0.09	0.14	0.06	0.04			
		$\chi 2$	5.56	2.36	1.59	1.08	0.51	0.12	0.03	0.01	0.00	0.10	0.23	0.06	0.03			
	ITU-R P. 618-12	ε(P)	-0.18	-0.01	0.13	0.26	0.49	0.74	0.90	1.00	1.16	1.31	1.34	1.04	1.04	0.47	0.33	0.58
		STD	0.89	0.72	0.58	0.45	0.22	0.03	0.19	0.29	0.45	0.60	0.63	0.34	0.33			
		RMS	0.46	0.04	0.50	1.13	2.60	4.75	6.69	8.37	11.80	15.88	18.72	18.70	22.04			
		$\chi 2$	0.10	0.00	0.06	0.23	0.86	2.02	3.18	4.17	6.33	9.01	10.71	9.56	11.23			
2015	ITU-R P. 838-3	ε(P)	-0.76	-0.53	-0.39	-0.30	-0.16	-0.05	0.03	0.06	0.04	-0.01	0.02	0.00	-0.01	-0.18	0.31	0.36
		STD	0.60	0.37	0.23	0.14	0.00	0.11	0.19	0.21	0.20	0.14	0.18	0.16	0.14			
		RMS	1.45	1.27	1.13	1.00	0.69	0.25	0.18	0.43	0.35	0.17	0.27	0.04	0.26			
		$\chi 2$	4.64	1.44	0.72	0.42	0.13	0.01	0.01	0.02	0.01	0.00	0.01	0.00	0.00			
	ITU-R P. 618-12	ε(P)	-0.10	0.11	0.25	0.35	0.56	0.73	0.83	0.87	0.96	1.05	1.19	1.17	1.14	0.47	0.28	0.55
		STD	0.80	0.59	0.45	0.35	0.14	0.03	0.13	0.17	0.26	0.35	0.49	0.47	0.44			
		RMS	0.19	0.26	0.73	1.19	2.41	4.01	5.47	6.69	9.27	12.44	15.45	17.21	20.16			
		$\chi 2$	0.02	0.03	0.15	0.31	0.87	1.69	2.48	3.11	4.53	6.38	8.39	9.28	10.74			

As shown in Table 5.8 (a), (b) and (c), in 12.25, 19.8 and 20.73 GHz links, the proposed empirically derived $\boldsymbol{k}$ and $\boldsymbol{\alpha}$ value when used in specific attenuation calculation so as to obtained desired attenuation values, result is lower chances of error as compared to ITU-R P. 618-12 approach when 0.001 % ≤ $\boldsymbol{P}$ ≤ 1 % which is justified from lower STD, RMS, $\boldsymbol{\chi^2}$ values. In addition, ITU-R P. 618-12 shows underestimation against the measured values in 2014 for 12.25 GHz link. Thus, for all time percentage when 0.001 % ≤ $\boldsymbol{P}$ ≤ 1 %, for 12.25 GHz, empirically derived $\boldsymbol{k}$ and $\boldsymbol{\alpha}$ value can be used. As noted from Table 5.8 (a), ITU-R P. 618-12 shows the relative error percentage of 56%, 0%, 55%; 71%, 39%, 39%; 35%, 6%, 13% for 0.1%, 0.01% and 0.001% of the time in 2013, 2014, 2015 while it is 1%, 8%, 8%; 34%, 12%, 5%;

31%, 13%, 0% respectively for ITU-R P.838-3 approach. Interestingly, ITU-R P. 618-12 shows overestimation against the measured values for mentioned three years for 19.8 and 20.73 GHz links. Thus, for all time percentage when 0.001 % ≤ $\boldsymbol{P}$ ≤ 1 %, empirically derived $\boldsymbol{k}$ and $\boldsymbol{\alpha}$ value can be used in 19.8 and 20.73 GHz links. As shown in Table 5.8 (b) and (c), in 19.8 and 20.73 GHz links, ITU-R P. 618-12 shows the relative error percentage of 36%, 112%, 212%; 29%, 69%, 7%; 10%, 40%, 30% and 71%, 155%, 235%; 49%, 116%, 104%; 56%, 96%, 114% for 0.1%, 0.01% and 0.001% of the time in 2013, 2014, 2015 while it is 1%, 1%, 2%; 68%, 12%, 5%; 36%, 128%, 221% and 4%, 5%, 4%; 26%, 2%, 4%; 16%, 4%, 1% respectively for ITU-R P.838-3 approach. Furthermore, use of proposed empirical coefficients $\boldsymbol{k}$ and $\boldsymbol{\alpha}$ result in lower values of $\boldsymbol{\mu_v}$ for 12.25, 19.8 and 20.73 GHz links, as per the recommendation of ITU-R P.311-15[42] which is justified from lower values of $\boldsymbol{\sigma_v}$ and $\boldsymbol{\rho_v}$. Thus, this emphasis on the suitability of proposed empirical coefficients for the estimation of rain attenuation in slant path for earth space communication in 12.25, 19.8, and 20.73 GHz links.

The analyses performed by applying the frequency scaling approach for year wise estimation of rain attenuation for 19.8 and 20.73 GHz are depicted in Figure 5.17 and 5.18. These show that the estimation is relatively higher against the measured values.

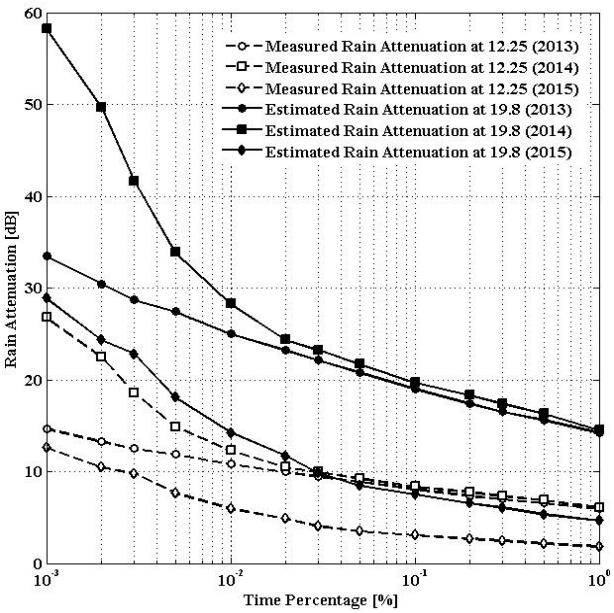

Figure 5.17: Cumulative distribution of rain attenuation obtained after frequency scaling for 19.8 GHz.

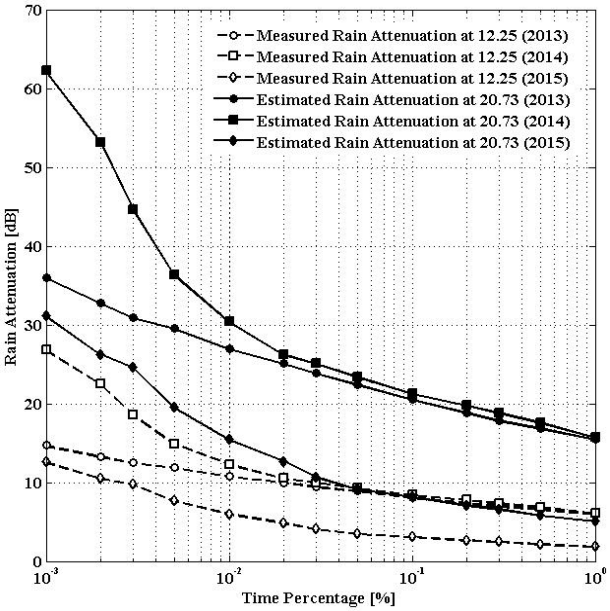

Figure 5.18: Cumulative distribution of rain attenuation obtained after frequency scaling for 20.73 GHz.

The further study shows the result of the models performance that are analyze for diurnal and monthly variation of the rain rate and rain attenuation under Ka-band link. The calculated error matrices are listed in Table 5.9 (a), (b) and (c) for 2013, 2014, 2015 in 19.8 GHz link along with the evaluation procedures adopted for comparison of prediction methods by the recommendation ITU-R P.311-15[7].The proposed empirically derived $\boldsymbol{k}$ and $\boldsymbol{\alpha}$ value when used in specific attenuation calculation so as to obtained desired attenuation values, result is lower chances of error as compared to ITU-R P. 618-12 approach when 0.001 % ≤ $\boldsymbol{P}$ ≤ 1 % which is justified from lower STD, RMS, $\boldsymbol{\chi^2}$ values. Thus, for all time percentage when 0.001 % ≤ $\boldsymbol{P}$ ≤ 1 %, for 19.8 GHz, empirically derived $\boldsymbol{k}$ and $\boldsymbol{\alpha}$ value can be used. As noted from Table 5.9 (a), ITU-R P. 618-12 shows the relative error percentage of 16%, 74%, 176%; 13%, 85%, 205%; 166%, 345%, 472%; 40%, 142%, 220% and 24%, 27%, 102%; 15%, 55%, 120%; 54%, 14%, 43%; 37%, 5%,

82% and 49%, 1%, 57%; 14%, 18%, 113%; 24%, 42%, 118%; 47%, 11%, 43% for June, July, August and September months at 0.1%, 0.01% and 0.001% of the time in 2013, 2014, 2015 respectively while it is 8%, 9%, 5%; 3%, 2%, 0%; 25%, 11%, 16%; 3%, 15%, 8% and 11%, 2%, 4%; 4%, 16%, 8%; 6%, 10%, 5%; 1%, 10%, 2% and 21%, 8%, 14%; 2%, 18%, 2%; 7%, 8%, 10%; 12%, 14%, 8% respectively for ITU-R P.838-3 approach with the use of empirically generated $\boldsymbol{k}$ and $\boldsymbol{\alpha}$ values. Furthermore, use of proposed empirical coefficients $\boldsymbol{k}$ and $\boldsymbol{\alpha}$ result in lower values of $\boldsymbol{\mu_v}$ for 19.8 GHz link, as per the recommendation of ITU-R P.311-15[7] which is justified from lower values of $\boldsymbol{\sigma_v}$ and $\boldsymbol{\rho_v}$. Thus, these emphases on the suitability of proposed empirical coefficients for the estimation of rain attenuation in slant path for earth space communication in 19.8GHz link.

Table 5.9 (a). Percentage error obtained over the interval [0.001% to 1%] for 2013.

Months	Methods	Parameters	Time Percentage (% p)													ITU-R P.311-15		
			1	0.5	0.3	0.2	0.1	0.05	0.03	0.02	0.01	0.005	0.003	0.002	0.001	μ_v	σ_v	ρ_v
June	ITU-R P. 838-3	ε(P)	-0.02	0.05	0.02	-0.02	-0.08	-0.05	0.03	0.09	0.09	0.09	-0.05	-0.05	-0.05	0.00	0.06	0.06
		STD	0.03	0.05	0.01	0.02	0.09	0.05	0.03	0.09	0.09	0.08	0.06	0.06	0.06			
		RMS	0.09	0.22	0.08	0.09	0.51	0.31	0.24	0.68	0.77	0.78	0.59	0.59	0.59			
		χ2	0.00	0.01	0.00	0.00	0.05	0.02	0.01	0.06	0.06	0.06	0.03	0.03	0.03			
	ITU-R P. 618-12	ε(P)	-0.67	-0.53	-0.42	-0.32	-0.16	0.09	0.26	0.45	0.74	1.09	1.04	1.30	1.76	0.15	0.59	0.61
		STD	1.02	0.88	0.78	0.68	0.52	0.27	0.10	0.09	0.38	0.74	0.69	0.95	1.40			
		RMS	2.53	2.22	1.98	1.64	1.00	0.58	1.89	3.43	6.30	9.95	11.49	14.34	19.31			
		χ2	5.07	2.48	1.44	0.78	0.20	0.05	0.38	1.06	2.68	5.20	5.87	8.11	12.30			
July	ITU-R P. 838-3	ε(P)	-0.02	0.04	0.05	0.03	-0.03	-0.02	-0.03	-0.04	0.02	0.03	0.00	0.00	0.00	0.00	0.03	0.03
		STD	0.02	0.04	0.05	0.03	0.03	0.03	0.03	0.04	0.02	0.03	0.00	0.00	0.00			
		RMS	0.11	0.30	0.50	0.36	0.37	0.32	0.41	0.60	0.27	0.59	0.04	0.04	0.04			
		χ2	0.00	0.01	0.03	0.01	0.01	0.01	0.01	0.03	0.00	0.02	0.00	0.00	0.00			
	ITU-R P. 618-12	ε(P)	-0.55	-0.46	-0.36	-0.28	-0.13	0.12	0.31	0.51	0.85	1.12	1.34	1.60	2.05	0.22	0.60	0.64
		STD	1.02	0.93	0.83	0.75	0.60	0.36	0.16	0.04	0.38	0.65	0.87	1.13	1.58			
		RMS	3.38	3.67	3.26	2.86	1.60	1.54	4.44	7.46	13.22	19.12	24.10	28.88	36.92			
		χ2	4.05	3.12	1.81	1.11	0.24	0.16	1.06	2.52	6.08	10.09	13.80	17.79	24.82			
August	ITU-R P. 838-3	ε(P)	-0.42	-0.24	-0.04	0.13	0.25	0.22	0.22	0.17	0.11	0.01	0.16	0.16	0.16	-0.02	0.21	0.21
		STD	0.42	0.23	0.03	0.13	0.25	0.23	0.22	0.18	0.11	0.02	0.15	0.15	0.15			
		RMS	2.28	1.55	0.28	1.03	2.38	2.46	2.54	2.20	1.58	0.23	3.09	3.09	3.09			
		χ2	1.67	0.48	0.01	0.12	0.47	0.45	0.46	0.33	0.16	0.00	0.58	0.58	0.58			
	ITU-R P. 618-12	ε(P)	0.36	0.70	1.03	1.26	1.66	2.17	2.70	2.95	3.45	3.86	3.56	4.00	4.72	1.15	0.45	1.24
		STD	2.13	1.80	1.46	1.23	0.84	0.33	0.21	0.45	0.96	1.37	1.07	1.51	2.22			
		RMS	1.97	4.53	7.43	10.11	15.90	23.83	31.35	37.42	49.34	62.19	69.77	78.46	92.47			
		χ2	0.53	1.86	3.77	5.65	9.92	16.30	22.89	27.94	38.25	49.40	54.46	62.78	76.29			
September	ITU-R P. 838-3	ε(P)	-0.34	-0.19	-0.08	0.01	0.03	0.02	0.13	0.10	0.15	0.11	-0.08	-0.08	-0.08	-0.03	0.13	0.13
		STD	0.31	0.16	0.06	0.04	0.05	0.04	0.16	0.12	0.18	0.13	0.06	0.06	0.06			
		RMS	1.17	0.79	0.40	0.06	0.21	0.17	1.26	1.01	1.72	1.30	1.38	1.38	1.38			
		χ2	0.59	0.18	0.04	0.00	0.01	0.00	0.15	0.09	0.23	0.12	0.13	0.13	0.13			
	ITU-R P. 618-12	ε(P)	-0.25	-0.04	0.14	0.28	0.40	0.57	0.87	1.02	1.42	1.81	1.45	1.73	2.20	0.55	0.43	0.70
		STD	1.14	0.93	0.75	0.62	0.49	0.32	0.02	0.13	0.53	0.92	0.56	0.84	1.31			
		RMS	0.87	0.15	0.68	1.49	2.86	5.06	8.16	10.51	15.94	22.08	23.61	28.18	35.90			
		χ2	0.28	0.01	0.08	0.32	0.82	1.84	3.79	5.31	9.36	14.23	13.97	17.85	24.69			

Table 5.9 (b). Percentage error obtained over the interval [0.001% to 1%] for 2014.

Months	Methods	Parameters	Time Percentage (% p)													ITU-R P.311-15		
			1	0.5	0.3	0.2	0.1	0.05	0.03	0.02	0.01	0.005	0.003	0.002	0.001	μ_v	σ_v	ρ_v
June	ITU-R P. 838-3	ε(P)	-0.38	-0.29	-0.18	-0.14	0.11	0.23	0.22	0.15	0.02	-0.04	-0.04	-0.04	-0.04	-0.04	0.18	0.18
		STD	0.35	0.26	0.15	0.11	0.14	0.26	0.25	0.18	0.05	0.01	0.00	0.00	0.00			
		RMS	1.77	1.56	1.06	0.92	0.81	2.08	2.39	2.16	0.33	1.04	0.89	0.89	0.89			
		χ^2	1.11	0.63	0.24	0.16	0.08	0.39	0.42	0.28	0.01	0.05	0.03	0.03	0.03			
	ITU-R P. 618-12	ε(P)	-0.47	-0.31	-0.12	0.00	0.24	0.45	0.48	0.36	0.27	0.32	0.54	0.72	1.02	0.19	0.34	0.39
		STD	0.74	0.57	0.39	0.27	0.03	0.18	0.21	0.09	0.00	0.05	0.27	0.45	0.75			
		RMS	2.16	1.65	0.72	0.00	1.77	4.02	5.31	5.17	5.43	7.80	13.14	17.48	24.85			
		χ^2	1.92	0.73	0.10	0.00	0.34	1.24	1.72	1.37	1.16	1.89	4.60	7.30	12.54			
July	ITU-R P. 838-3	ε(P)	-0.40	-0.14	-0.03	0.02	0.04	0.06	0.06	0.06	0.16	0.06	-0.08	-0.08	-0.08	-0.03	0.14	0.14
		STD	0.38	0.12	0.00	0.05	0.07	0.08	0.09	0.09	0.18	0.09	0.05	0.05	0.05			
		RMS	1.69	0.77	0.17	0.16	0.42	0.67	0.81	0.86	2.27	1.07	1.53	1.53	1.53			
		χ^2	1.13	0.13	0.00	0.00	0.02	0.04	0.05	0.05	0.31	0.06	0.13	0.13	0.13			
	ITU-R P. 618-12	ε(P)	-0.50	-0.41	-0.33	-0.27	-0.15	0.01	0.11	0.26	0.55	0.68	0.67	0.86	1.20	0.11	0.43	0.45
		STD	0.71	0.62	0.54	0.47	0.35	0.19	0.10	0.06	0.35	0.47	0.46	0.66	0.99			
		RMS	2.09	2.25	2.18	2.02	1.39	0.14	1.45	3.59	8.04	11.54	13.39	17.35	24.10			
		χ^2	2.08	1.55	1.07	0.73	0.24	0.00	0.15	0.75	2.87	4.65	5.35	8.04	13.14			
August	ITU-R P. 838-3	ε(P)	0.07	0.04	-0.01	-0.07	-0.06	-0.04	0.03	0.06	0.10	0.10	-0.05	-0.05	-0.05	0.00	0.06	0.06
		STD	0.07	0.04	0.02	0.07	0.07	0.04	0.03	0.05	0.09	0.10	0.06	0.06	0.06			
		RMS	0.24	0.19	0.08	0.42	0.46	0.35	0.30	0.62	1.15	1.27	0.83	0.83	0.83			
		χ^2	0.02	0.01	0.00	0.03	0.03	0.01	0.01	0.03	0.10	0.12	0.05	0.05	0.05			
	ITU-R P. 618-12	ε(P)	-0.76	-0.71	-0.66	-0.63	-0.54	-0.45	-0.36	-0.28	-0.14	0.06	0.04	0.18	0.43	-0.44	0.48	0.65
		STD	0.47	0.41	0.37	0.34	0.25	0.16	0.07	0.02	0.15	0.35	0.34	0.48	0.73			
		RMS	2.58	3.10	3.51	3.90	4.08	4.06	3.64	2.93	1.69	0.72	0.68	2.82	6.62			
		χ^2	8.14	7.43	6.86	6.64	4.86	3.33	2.08	1.12	0.28	0.04	0.03	0.44	2.00			
September	ITU-R P. 838-3	ε(P)	-0.10	0.02	0.02	0.07	0.01	0.02	-0.01	0.05	-0.10	0.11	-0.02	-0.02	-0.02	0.00	0.05	0.05
		STD	0.10	0.02	0.02	0.07	0.01	0.02	0.01	0.05	0.11	0.11	0.02	0.02	0.02			
		RMS	0.32	0.08	0.09	0.33	0.06	0.14	0.06	0.38	1.12	1.27	0.29	0.29	0.29			
		χ^2	0.04	0.00	0.00	0.02	0.00	0.00	0.00	0.02	0.13	0.13	0.01	0.01	0.01			
	ITU-R P. 618-12	ε(P)	-0.71	-0.62	-0.56	-0.48	-0.37	-0.22	-0.11	0.05	0.05	0.28	0.33	0.51	0.82	-0.17	0.48	0.51
		STD	0.63	0.54	0.48	0.40	0.29	0.15	0.03	0.13	0.13	0.36	0.41	0.59	0.90			
		RMS	2.19	2.36	2.52	2.37	2.24	1.57	0.84	0.39	0.54	3.20	4.34	6.64	10.69			
		χ^2	5.28	3.89	3.20	2.21	1.33	0.46	0.10	0.02	0.03	0.70	1.09	2.24	4.82			

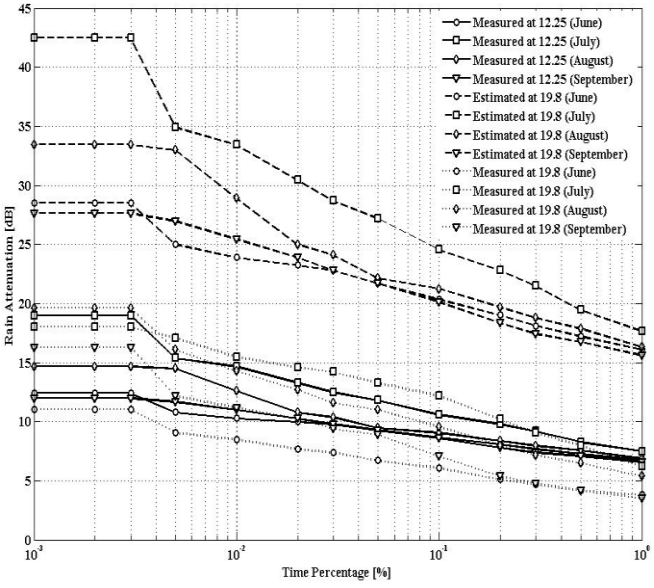

Figure 5.19(a): Cumulative distribution of rain attenuation obtained for 2013 year after frequency scaling in 19.8 GHz.

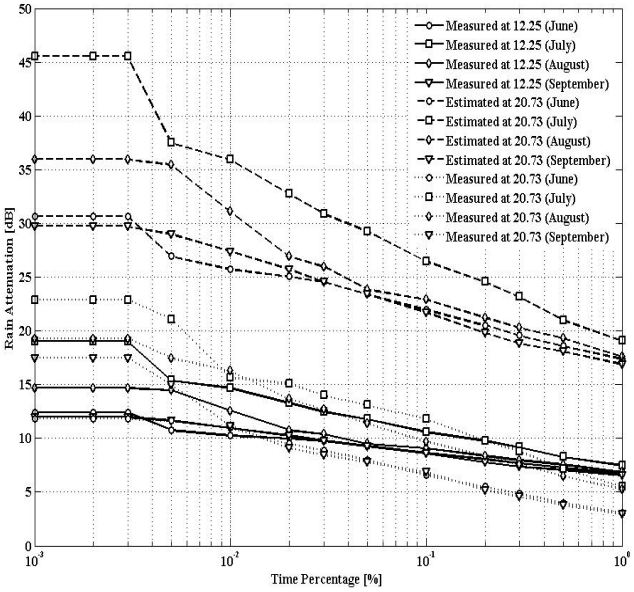

Figure 5.19(b): Cumulative distribution of rain attenuation obtained for 2013 year after frequency scaling in 20.73 GHz.

Table 5.9 (c). Percentage error obtained over the interval [0.001% to 1%] for 2015.

Months	Methods	Parameters	Time Percentage (% p)													ITU-R P.311-15		
			1	0.5	0.3	0.2	0.1	0.05	0.03	0.02	0.01	0.005	0.003	0.002	0.001	μ_v	σ_v	ρ_v
June	ITU-R P. 838-3	ε(P)	-0.12	-0.10	-0.07	-0.01	0.21	0.28	0.16	0.14	0.08	0.00	-0.14	-0.14	-0.14	0.00	0.14	0.14
		STD	0.13	0.11	0.08	0.02	0.20	0.27	0.15	0.13	0.07	0.01	0.15	0.15	0.15			
		RMS	0.71	0.70	0.61	0.09	2.21	3.17	2.12	1.95	1.17	0.02	2.90	2.90	2.90			
		χ2	0.10	0.07	0.05	0.00	0.39	0.70	0.29	0.24	0.08	0.00	0.49	0.49	0.49			
	ITU-R P. 618-12	ε(P)	-0.77	-0.72	-0.65	-0.60	-0.49	-0.33	-0.29	-0.17	0.01	0.18	0.16	0.31	0.57	-0.38	0.57	0.68
		STD	0.56	0.50	0.44	0.38	0.27	0.11	0.08	0.04	0.22	0.40	0.38	0.53	0.78			
		RMS	4.48	5.23	5.36	5.39	5.09	3.72	3.94	2.43	0.16	3.05	3.29	6.23	11.33			
		χ2	15.12	13.19	10.12	8.06	4.88	1.82	1.61	0.51	0.00	0.47	0.46	1.48	4.10			
July	ITU-R P. 838-3	ε(P)	-0.18	0.05	0.14	0.06	0.02	0.07	0.00	0.03	-0.18	0.01	0.02	0.02	0.02	0.00	0.08	0.08
		STD	0.19	0.04	0.13	0.06	0.01	0.06	0.00	0.02	0.18	0.01	0.01	0.01	0.01			
		RMS	0.48	0.16	0.57	0.34	0.14	0.63	0.01	0.34	2.95	0.18	0.36	0.36	0.36			
		χ2	0.11	0.01	0.07	0.02	0.00	0.04	0.00	0.01	0.64	0.00	0.01	0.01	0.01			
	ITU-R P. 618-12	ε(P)	-0.32	-0.19	-0.11	-0.14	-0.14	0.01	0.12	0.26	0.18	0.39	0.60	0.79	1.13	0.14	0.31	0.34
		STD	0.52	0.39	0.31	0.34	0.34	0.19	0.08	0.06	0.02	0.20	0.40	0.59	0.93			
		RMS	0.83	0.65	0.45	0.75	1.16	0.13	1.35	3.05	2.96	7.06	10.98	14.53	20.62			
		χ2	0.38	0.15	0.05	0.12	0.20	0.00	0.15	0.63	0.45	2.00	4.12	6.43	10.93			
August	ITU-R P. 838-3	ε(P)	-0.54	-0.28	-0.17	-0.17	-0.07	0.29	0.29	0.28	0.08	-0.03	-0.10	-0.10	-0.10	-0.07	0.23	0.24
		STD	0.49	0.24	0.12	0.12	0.02	0.34	0.34	0.32	0.12	0.02	0.05	0.05	0.05			
		RMS	1.93	1.37	1.01	1.13	0.58	3.10	3.64	3.92	1.52	0.71	2.50	2.50	2.50			
		χ2	2.23	0.55	0.21	0.23	0.04	0.69	0.81	0.85	0.11	0.02	0.28	0.28	0.28			
	ITU-R P. 618-12	ε(P)	-0.22	-0.10	0.00	0.11	0.24	0.37	0.46	0.55	0.42	0.55	0.67	0.86	1.18	0.30	0.27	0.40
		STD	0.61	0.49	0.39	0.28	0.15	0.02	0.07	0.16	0.03	0.16	0.28	0.47	0.79			
		RMS	0.79	0.49	0.02	0.72	2.06	3.99	5.88	7.80	8.53	12.81	16.88	21.64	29.67			
		χ2	0.22	0.06	0.00	0.07	0.40	1.08	1.86	2.76	2.54	4.54	6.79	10.02	16.07			
September	ITU-R P. 838-3	ε(P)	-0.76	-0.22	-0.01	0.05	0.12	0.07	0.05	0.12	0.14	0.15	-0.08	-0.08	-0.08	-0.07	0.30	0.31
		STD	0.72	0.18	0.03	0.09	0.17	0.11	0.09	0.16	0.18	0.19	0.04	0.04	0.04			
		RMS	1.75	0.62	0.04	0.17	0.50	0.35	0.26	0.67	0.82	1.17	0.87	0.87	0.87			
		χ2	5.65	0.17	0.00	0.01	0.05	0.02	0.01	0.07	0.10	0.15	0.08	0.08	0.08			
	ITU-R P. 618-12	ε(P)	-0.79	-0.72	-0.65	-0.59	-0.47	-0.38	-0.27	-0.14	0.11	0.12	0.02	0.16	0.43	-0.33	0.46	0.57
		STD	0.55	0.48	0.41	0.34	0.23	0.14	0.02	0.10	0.36	0.36	0.26	0.41	0.67			
		RMS	1.82	2.02	2.01	2.00	1.88	1.90	1.47	0.80	0.68	0.91	0.20	1.72	4.46			
		χ2	6.80	5.25	3.73	2.84	1.67	1.16	0.53	0.13	0.07	0.09	0.00	0.24	1.34			

In addition, frequency scaling approach is tested for monthly variation of rain attenuation in Ka-band along the same and different communication paths. The analyses performed for month wise estimation of rain attenuation for 19.8 and 20.73 GHz is depicted in Figure 5.19 (a) and 5.19 (b) for 2013 year only because of better arrangement of data measurement in this year as compared to other two years. These show that the estimation for 19.8 and 20.73 GHz are relatively higher against the measured values. For instance, the calculated rain attenuation at 19.8 and 20.73 GHz links are 6.1, 8.5, 11.0 dB; 12.2, 15.5, 18.0 dB; 9.6, 14.3, 19.6 dB; 7.1, 11.2, 16.3 dB and 6.6,

11.0, 11.8 dB; 11.8, 15.7, 22.9 dB; 9.7, 16.3, 19.3 dB; 6.9, 11.2, 17.5 dB respectively at 0.1%, 0.01%, 0.001% of the time and the estimated values are 20.4, 23.9, 28.5 dB; 24.6, 33.4, 42.5 dB; 21.3, 28.9, 33.4 dB; 20.2, 25.5, 27.6 dB and 21.9, 25.8, 30.7 dB; 26.5, 35.9, 45.5 dB; 22.9, 31.1, 35.9 dB; 21.7, 27.4, 29.7 dB.

E. Conclusions

The rain attenuation and rain rate, collected over three years during 2013-2015 in the 12.25 and 20.73 GHz from Koreasat 6 and 19.8 GHz from COMS1 for Mokdong Station were analyzed to observe the statistical characteristics. In this study, the local environmental propagation effects in slant path attenuation for Ku and Ka bands have been investigated. The suitable statistical analysis has been proposed to predict the time series of rain attenuation at Ku and Ka band over an earth space path in the South Korea. The measured rain attenuation distribution at 0.01% of the time in Ka band is higher than Ku band and the rain rate is found to be 50.35 mm/hr which is taken as a basis for the estimation of rain attenuation for other time percentages by using proposed approach. It has been found that for Ku-band communication link, at higher time percentage when 0.01 % $\leq \boldsymbol{P} \leq$ 1 %, ITU-R P.618-12, Ramachandran and Kumar, proposed approach shows the better estimation of rain attenuation and most preferable is noted from the application of ITU-R P. 618-12, Ramachandran and Kumar methods. Similarly, for lower time percentages when 0.001 % $\leq \boldsymbol{P} \leq$ 0.1 %, ITU-R P. 618-12 and proposed approach show fair good estimation while DAH method gives the very closer estimation for the measured rain attenuation series. Hence, DAH method can be better applied for lower time instances. Similarly, for Ka-band communication link, it has been found that at higher time percentage when 0.1 % $< \boldsymbol{P} \leq$ 1

%, ITU-R P. 618-12, Unified and DAH methods shows the better estimation of rain attenuation. Similarly, for lower time percentages when 0.001 % ≤ $\boldsymbol{P}$ ≤ 0.1 %, Unified, Gracia Lopez and proposed approach are equally applicable for estimation of rain rate statistics. The predictive capabilities of the models are judge through the relative error analyses, standard deviation, root mean square values as well as through the recommendation of ITU-R P.311-15 method. It has been found that the empirically derived $\boldsymbol{k}$ and $\boldsymbol{\alpha}$ shows suitability in the calculation of attenuation series for all time percentage when 0.001 % ≤ $\boldsymbol{P}$ ≤ 1 % of the time against the measured values as studied for the year wise distribution of rain rate and rain attenuation where the effective path length and specific attenuation at Ku and Ka band are used over an earth space path. Similarly, the diurnal and monthly variations of slant path rain attenuation are presented for Mokdong Station in the South Korea. The corresponding effective path length is calculated with the application of Simple Attenuation Model at 19.8 GHz for COMS1 satellite. It is obtained that higher fade margin is needed for reliable link availability and the rain attenuation probability is lower in late night time and higher in morning hours. In addition, frequency scaling scheme are analyzed for the yearly and monthly variation of rain rate and rain attenuation statistics as per the recommendation of ITU-R P. 618-12 where the validation of this approach is performed by comparing with experimental data through error matrices.

VI. Conclusions and Recommendation for Future Work

The knowledge of various propagation impairments such as rain is of ultimate importance for terrestrial and satellite communication service at frequencies above 10 GHz for planning, budgeting and predicting the transmission and reception of radio waves signals. The experimental studies indicate the significance of local climatic factor on microwave signals on these communication services. The rain rate distribution of 1-min. interval have been studied for nine prime location of the South Korea region out of 93 stations database of experimental 1-min. rainfall accumulation. Furthermore, propagation impairments of radio wave signals due to rain on terrestrial and earth-space path have been investigated.

A.Conclusions

In the initial part of the study, the rain rate estimation is discussed using both the ITU-R model and measured regional 1-min. rainfall amount data collected over 10 years (2004-2013) for nine regions of the South Korea. The comparison of rainfall rate is made against the measured data with pre-existing empirical models. The analysis of the decade rainfall data has given an appropriate indication for study of rainfall rate behavior over these regions. As noticed, empirical formulations are found to be simple yet powerful tools for determining the rainfall statistics among the available best performing models. The performance of proposed Model 1 is considered to be suitable for conversion of rainfall rate from various integration times to 1-min. equivalent because lower average error evaluation confirms the overall best performing regression fit. This model provides more realistic distributions from regional coefficients set obtained for Icheon region. The RRA database shows that rain rate is about 50 mm/hr for 0.01%

of the time. Furthermore, contour maps for 0.01% of the time have been developed for the South Korea, which was designed using advanced Geographic Information Systems (GIS) tools with the adoption of Kriging interpolation estimator. The evaluation of different error matrices emphasizes the appropriateness of the proposed Model 1, exponential and logarithmic method that can trails the nature of 1-min. rainfall rate in Icheon region. Additionally, ITU-R P. 837-6 can be used for lower time conversion especially 5-, 10- min. to 1-min. rainfall rate distribution. In contrast, for higher time conversion from 20-, 30- and 60-min. to 1-min. rainfall rate distribution, ITU-R P. 837-6 generate higher error values.

The results obtained in the second part of the research are based on the simultaneous measurement of rain attenuation and rain rate for 18, 38, 75 GHz microwave links characteristics. Similarly, the last part of this study relies on the simultaneous measurement of rain attenuation and rain rate for 12.25, 20.73 GHz for Koreasat 6 and 19.8 for COMS1 (Communication, Ocean and Meteorological Satellite).

The projection made for the estimation of attenuation for Ka band from Ku band are also studied using the frequency scaling method for satellite communication links whereas polarization and frequency scaling methods are studied for terrestrial links using ITU-R P. 618-12 and ITU-R P. 530-16 methods respectively.

In overall, for microwave terrestrial links, it can be concluded that we can adopt Moupfouma model for 18 GHz links whereas Abdulrahman et al. and ITU-R P. 530-16 are preferable for 38 and 75 GHz links respectively until the sufficient database of rain attenuation and rain rate from other locations become available for better analyses of proposed techniques. The results are vital for system designer to estimate rain degradation along the microwave links over this region. It should be noted that the results are valid for this particular climates, and its feasibility for other

regions requires more testing and analyses.

Additionally, the study performed for satellite communication links presents the comparison of the measured data with the existing eight rain attenuation prediction models and the categorization of the best fitting approach. Rain attenuation predictions are made for a number of transmission paths at a fixed set of probability levels. On the whole, we can adopt ITU-R P. 618-12 rain attenuation model in the South Korea for better prediction of rain attenuation until the sufficient database of rain attenuation and rain rate from other locations become available.

The result will be useful in the proper planning of radio links by radio network planners in the South Korea. They will enhance precision in the estimation of link availability, link performance, link budget and management of the link frequency. The studies shall be equally helpful to characterize the propagation effects on earth-satellite and terrestrial links paths in order to provide guidelines and indications to the design of future reliable system on higher frequency bands.

B.Future Works

The study of rain attenuation in both terrestrial and satellite links are still under research in the South Korea. The variable nature of the diurnal, seasonal as well as annual rain patterns presents a new frontier for the research, with regard to their impact on link performance. The future improvement for the research activities are listed below:

1. The raindrop-size distributions can be further studied for the estimation of radio wave impairments on both terrestrial and earth-space systems.
2. To determine the magnitude of signal degradation as such signal attenuation, rain-

induced signal depolarization the detailed scattering process and microphysical properties of raindrops need to be studied.

3. A study of the worst month rainfall rate and rain attenuation statistics for the South Korea can be performed for the design of any reliable terrestrial and earth space communication link.
4. Under the availability of the sufficient measurement database, mitigation techniques such as diversity can be employed for the reliable telecommunication system.
5. For system planning, the rainfall structure such as horizontal and vertical dimension of rain cells, spatial and temporal variability of rain is very important. With this information, rain attenuation and scattering can be determined and rain attenuation mitigation technique such as site diversity can be applied.
6. The nature of specific rain attenuation in the terrestrial links can be further studied so as to investigate the appropriate values of regression coefficients.
7. The study of diurnal and seasonal variation of the rain attenuation statistics in the terrestrial networks can be studied.

References

[1] ITU-R P. 618-12. Propagation data and prediction methods required for the design of Earth-space telecommunication systems, 2015.

[2] ITU-R P. 530-16, “Propagation data and prediction methods required for the design of terrestrial line-of-sight systems,” ITU, Geneva, Switzerland, 2015.

[3] R. K. Crane, Electromagnetic Wave Propagation through Rain, John Wiley & Sons, NewYork, 1996.

[4] ITU-R P.837-6, Characteristics of Precipitation for Propagation Modeling, International Telecommunication Union, Geneva, 2012.

[5] Crane, Robert K. Propagation handbook for wireless communication system design. CRC press, 2003.

[6] ITU-R, “Specific Attenuation Model for Rain for Use in Prediction Methods,” Recommendation P.838-3, ITU-R Recommendations, P Series, ITU, Geneva, International Telecommunications Union, 2005.

[7] ITU-R P. 311-15, Acquisition, presentation and analysis of data in studies of radio wave propagation, International Telecommunication Union, Geneva, 2015.

[8] Barclay, Leslie W. Propagation of radio waves, vol. 502, Iet, 2003.

[9] Allnutt, Jeremy E., “Satellite-to-ground radiowave propagation-Theory, practice and system impact at frequencies above 1 GHz,” Stevenage Herts England Peter Peregrinus Ltd IEE Electromagnetic Waves Series 29, 2011.

[10] B. Segal, "The influence of Rain gauge Integration Time on Measured Rainfall-intensity Distribution Functions," Journal of Atmospheric and Oceanic Technology, 3, pp. 662-671, December 1986.

[11] A. Burgueno, M. Puigcerver and E. Vilar, "Influence of Rain Gauge Integration Time on the Rain Rate Statistics Used in Microwave Communications," Annales Des Telecommunications, vol. 43, Issue 9, pp. 522-527, September 1988.

[12] Chebil, J., and T. A. Rahman., "Rain rate statistical conversion for the prediction of rain attenuation in Malaysia," Electronics Letters 35.12, pp. 1019-1021, 1999.

[13] Lee, J. H., et al., "Conversion of rain rate distribution for various integration time," IEEE Transactions on Microwave Theory and Techniques 42.11, pp. 2099-2106, 1994.

[14] L. D. Emiliani, L. Luini, and C. Capsoni, "Extension of ITU-R method for conversion of rain rate statistics from various integration times to 1-minute," Electronics Letters, vol. 44, no. 8, April 2008.

[15] ITU-R P.837-5, Characteristics of Precipitation for Propagation Modeling, International Telecommunication Union, Geneva, 2012.

[16] Emiliani, Luis, and Lorenzo Luini., "Evaluation of models for the conversion of T-min rainfall distributions to an equivalent one-minute distribution for Colombia," Revista Facultad de Ingeniería Universidad de Antioquia 56, pp. 99-110, 2010.

[17] C. Capsoni, L. Luini, "A physically based method for the conversion of rainfall statistics from long to short integration time," IEEE Transactions on Antennas and Propagation, vol. 57, no. 11, pp. 3692 – 3696, November 2009.

[18] Moupfouma, Fidele., “Improvement of a rain attenuation prediction method for terrestrial microwave links,” IEEE transactions on antennas and propagation32.12, pp. 1368-1372, 1984.

[19] Freeman, Roger L. Radio system design for telecommunication, John Wiley & Sons, vol. 98, 2006.

[20] Kestwal, Mukesh Chandra, Sumit Joshi, and Lalit Singh Garia., “Prediction of Rain Attenuation and Impact of Rain in Wave Propagation at Microwave Frequency for Tropical Region (Uttarakhand, India),” International Journal of Microwave Science and Technology, 2014.

[21] IO, Yussuff Abayomi, Babatunde Olusegun, and Nor Hisham Haji Khamis., “Comparative Analysis of Terrestrial Rain Attenuation at Ku band for Stations in South-Western Nigeria,” 2016.

[22] Kesavan, Ulaganathen, et al., “Comparative studies of the rain attenuation predictions for tropical regions,” Progress In Electromagnetics Research M18, pp. 17-30, 2011.

[23] Mandeep, Jit Singh., “Rain attenuation statistics over a terrestrial link at 32.6 GHz at Malaysia,” Microwaves, Antennas & Propagation, IET 3.7, pp. 1086-1093, 2009.

[24] Abdulrahman, A. Y., et al., “Rain attenuation measurements over terrestrial microwave links operating at 15 GHz in Malaysia,” International Journal of Communication Systems 25.11, pp. 1479-1488, 2012.

[25] ITU-R Databank DBSG3, http://www.itu.int/pub/R-SOFT-SG3/en

[26] da Silva Mello, L. A. R., et al., “Prediction of rain attenuation in terrestrial links using full rainfall rate distribution,” Electronics Letters 43.25, pp. 1442-1443, 2007.

[27] Mello, L., and Marlene S. Pontes., "Unified method for the prediction of rain attenuation in satellite and terrestrial links," Journal of Microwaves, Optoelectronics and Electromagnetic Applications 11.1, pp. 01-14, 2012.

[28] Moupfouma, Fidèle., "Electromagnetic waves attenuation due to rain: A prediction model for terrestrial or LOS SHF and EHF radio communication links," Journal of Infrared, Millimeter, and Terahertz Waves 30.6, pp. 622-632, 2009.

[29] Abdulrahman, A. Y., et al., "Empirically derived path reduction factor for terrestrial microwave links operating at 15 GHz in Peninsula Malaysia," Journal of Electromagnetic Waves and Applications 25.1, pp. 23-37, 2011.

[30] Lin, S. H., "11-GHz Radio: Nationwide Long-Term Rain Rate Statistics and Empirical Calculation of 11-GHz Microwave Rain Attenuation," Bell System Technical Journal 56.9, pp. 1581-1604, 1977.

[31] Abdulrahman, A. Y., et al., "Rain attenuation predictions on terrestrial radio links: differential equations approach," Transactions on Emerging Telecommunications Technologies 23.3, pp. 293-301, 2012.

[32] Hasanuddin, Zulfajri Basri, et al., "Measurement of Ku-band rain attenuation using several VSATs in Kyushu Island, Japan," IEEE antennas and wireless propagation letters 1.1, pp. 116-119, 2002.

[33] Allnutt, Jeremy E., and Fatim Haidara., "Ku-band diurnal fade characteristics and fade event duration data from three, two-year, Earth–space radiometric experiments in Equatorial Africa, " International journal of satellite communications 18.3, pp. 161-183, 2000.

[34] Elbert, Bruce R. Introduction to satellite communication. Artech house, 2008.

[35] Ippolito Jr, Louis J. Satellite communications systems engineering: atmospheric effects, satellite link design and system performance, John Wiley & Sons, vol. 6, 2008.

[36] Ippolito Jr, Louis J., "Rain Attenuation Prediction Methods," Radiowave Propagation in Satellite Communications. Springer Netherlands, pp. 64-92, 1986.

[37] Timothy, P., W. C. Bostian, and J.E. Allnutt, Satellite Communication, 2nd edition, John Wiley & Sons, 2003.

[38] Ojo, Joseph Sunday, Moses Oludare Ajewole, and Swapan Kumar Sarkar., "Rain rate and rain attenuation prediction for satellite communication in Ku and Ka bands over Nigeria," Progress In Electromagnetics Research B 5, pp. 207-223, 2008.

[39] Singh, Mandeep, and Jeremy E. Allnutt, "Rain attenuation predictions at Ku-band in South East Asia countries, " Progress In Electromagnetics Research76, pp. 65-74, 2007.

[40] Mandeep, J. S., and K. Tanaka., "Effect of atmospheric parameters on satellite link," International Journal of Infrared and Millimeter Waves 28.10, pp. 789-795, 2007.

[41] Shrestha Sujan, Jung-Jin Park, and Dong-You Choi., "Rain rate modeling of 1-min from various integration times in South Korea," SpringerPlus 5.1, 2016.

[42] Shrestha Sujan, Park Jung-Jin, Kim S.W., Kim J.J, Jung JH, Choi D.Y., " 1-minute rain rate derivation from various integration times in South Korea, " Korean Institute of Next Generation Computing, Bangkok, Thailand, January 2016.

[43] Choi, Dong You., "Rain attenuation prediction model by using the 1-hour rain rate without 1-minute rain rate conversion," Int. J. of Comput. Sci. Netw. Secur 6, pp. 130-133, 2006.

[44] D. Y. Choi, J. Y. Pyun, S. K. Noh, and S. W. Lee, "Comparison of measured rain attenuation in the 12.25-GHz band with predictions by the ITU-R model," International Journal of Antennas and Propagation, vol. 2012, Article ID 415398, pp. 1-5, 2012.

[45] Yussuff, Abayomi Isiaka, and Nor Hisham Haji Khamis., "Rain Attenuation Prediction Model for Lagos at Millimeter Wave Bands," Journal of Atmospheric and Oceanic Technology 31.3, pp. 639-646, 2014.

[46] Yussuff, Abayomi Isiaka, and Nor Hisham Khamis., "Rain Attenuation Modelling and Mitigation in The Tropics: Brief Review," International Journal of Electrical and Computer Engineering 2.6, p. 748, 2012.

[47] Mandeep, J. S., Renuka Nalinggam, and Widad Bt Ismail., "Analysis of rain attenuation models for south east Asia countries," Journal of Infrared, Millimeter, and Terahertz Waves 32.2, pp. 233-240, 2011.

[48] Chakravarty, Kaustav, and Animesh Maitra., "Rain attenuation studies over an earth–space path at a tropical location," Journal of Atmospheric and Solar-Terrestrial Physics 72.1, pp.135-138, 2010.

[49] Mandeep, J. S., "Slant path rain attenuation comparison of prediction models for satellite applications in Malaysia," Journal of Geophysical Research: Atmospheres 114.D17, 2009.

[50] Mandeep, J. S., "Comparison of rainfall models with Ku-band beacon measurement," Acta Astronautica 64.2, pp. 264-271, 2009.

[51] Mandeep, J. S., S. I. S. Hassan, and K. Tanaka., "Rainfall measurements at Ku-band satellite link in Penang, Malaysia," IET microwaves, antennas & propagation 2.2, pp. 147-151, 2008.

[52] Nalinggam, Renuka, et al., "Development of rain attenuation model for Southeast Asia equatorial climate," IET Communications 7.10, pp. 1008-1014, 2013.

[53] Mandeep, J. S., "Analysis of rain attenuation prediction models at Ku-band in Thailand, " Advances in Space Research 49.3, pp. 566-571, 2012.

[54] Dissanayake, Asoka, Jeremy Allnutt, and Fatim Haidara., "A prediction model that combines rain attenuation and other propagation impairments along earth-satellite paths," Antennas and Propagation, IEEE Transactions on 45.10, pp. 1546-1558, 1997.

[55] Stutzman, W.L., and K.M. Yon, "A simple rain attenuation model for Earth-space radio links operating at 10-35 GHz," Radio Sci. 21(1), pp. 65-75, 1986.

[56] Crane, Robert K., "Prediction of attenuation by rain," Communications, IEEE Transactions on 28.9, pp. 1717-1733, 1980.

[57] Ramachandran, Visagaperuman, and Vickal Kumar., "Modified rain attenuation model for tropical regions for Ku-Band signals," International Journal of Satellite Communications and Networking 25.1, pp. 53-67, 2007.

[58] Garcia-Lopez, J. A., J. M. Hernando, and J. M. Selga., "Simple rain attenuation prediction method for satellite radio links," IEEE transactions on antennas and propagation 36.3, pp. 444-448, 1988.

[59] Karasawa, Y., "Consideration on prediction methods or rain attenuation on earth-space paths," CCIRIWP 5.2, pp. 65-72, Japan, April 1989.

[60] Choi, Kyung Soo, et al., "Trends in rain attenuation model in satellite system," Advanced Communication Technology (ICACT), 2011 13th International Conference on. IEEE, 2011.

[61] Yeo, Jun Xiang, Yee Hui Lee, and Jin Teong Ong, "Rain attenuation prediction model for satellite communications in tropical regions," IEEE Transactions on Antennas and Propagation 62.11, pp. 5775-5781, 2014.

[62] Shrestha Sujan, and Dong-You Choi., "Study of rain attenuation in Ka band for satellite communication in South Korea," Journal of Atmospheric and Solar-Terrestrial Physics 148, pp. 53-63, 2016.

[63] ITU-R, "Rain Height Model for Prediction Methods," Recommendation P.839-4, ITU-R Recommendations, P Series, Geneva, International Telecommunications Union, 2013.

[64] Ippolito Jr, Louis J. Satellite communications systems engineering: atmospheric effects, satellite link design and system performance, John Wiley & Sons, vol. 6, 2008.

[65] Korea Meteorological Administration (KMA), web.kma.go.kr/eng/index.jsp

[66] www.mathworks.com, the mathworks, Inc. Protected by U.S. and international patents.

[67] Ojo, J. S., and P. A. Owolawi., "Development of one-minute rain-rate and rain-attenuation contour maps for satellite propagation system planning in a subtropical country: South Africa," Advances in Space Research 54.8, pp. 1487-1501, 2014.

[68] http://www.ott.com

[69] OTT, "Operating instructions: Present Weather Sensor Parsivel," 70.200.005.B.E 08-1008.

[70] Korea Meteorological Administration (KMA), web.kma.go.kr/eng/index.jsp

[71] Islam, Rafiqul MD, Yusuf A. Abdulrahman, and Tharek A. Rahman., "An improved ITU-R rain attenuation prediction model over terrestrial microwave links in tropical region," EURASIP Journal on Wireless Communications and Networking 2012.1, pp. 1-9, 2012.

[72] Downie, N. M. N. M., and Robert William Heath. Basic statistical methods. No. 04; HA29, D6 1983.

[73] National Radio Research Agency (RRA) 767, Bitgaram-ro, Naju-si, Jeollanam-do 58217, Republic of Korea http://www.rra.go.kr/en/index.jsp

[74] Shrestha Sujan, and Dong-You Choi., "Rain Attenuation statistics over Millimeter wave Bands in South Korea," Journal of Atmospheric and Solar-Terrestrial Physics vol.152-153, 2017.

Appendix

Appendix 1: Applicable formulas of rain attenuation models for terrestrial links

Model	Factors	Attenuation exceeded [0.001% to 1%]
ITU-R P. 530-16 [2]	Distance factor, r $r=\frac{1}{0.477d^{0.633}R_{0.01}^{0.073\cdot\alpha}f^{0.123}-10.579(1-\exp(-0.024d))}$	$\frac{A_p}{A_{0.01}}=C_1\,p^{-(C_2+C_3\log_{10}p)}$
Da Silva Mello [26, 27]	Path reduction factor, $r=\frac{1}{1+\left(\frac{d}{d_0(R_p)}\right)}$	$A=\gamma_R\,d_{\text{eff}}=k\,[R_{\text{eff}}\times(R_p,d)]^{\alpha}\left[\frac{1}{1+\left(\frac{d}{d_0(R_p)}\right)}\right]\times d$
Moupfouma [28]	where $\phi(a)=\left(\frac{a}{A_{0.01}}-1\right)\times ln\left(1+\frac{a}{A_{0.01}}\right)$ and $\eta(a)=\frac{1}{1+2.75\times\left(\frac{a}{A_{0.01}}\right)^{0.8}}$	$P(A_{0.01}\geq a)=0.01\times\left(\frac{A_{0.01}+1}{a+1}\right)^{\phi(a)}\times exp\left(9.21\times\left(1-\frac{a}{A_{0.01}}\right)\times\eta(a)\right)$
Abdulrahman et al. [29]	Path reduction factor, $\delta\,(R_{0.01}, d)=\frac{1}{1+\left(\frac{d}{2.6379*R_{0.01}^{0.21}}\right)}$	$A_{\%p}=\gamma_R\,d_{\text{eff}}=\{k\,(R_{\%p})^{\alpha}\}\times\frac{d}{1+\left(\frac{d}{2.6379*R_{0.01}^{0.21}}\right)}$
Lin [30]	Path reduction factor, r $r=\frac{1}{1+\left(\frac{L}{L(R)}\right)}$ where, $L(R)=\frac{2636}{R-6.2}$	$A_{\%p}=\gamma_R\,d_{\text{eff}}=\{k\,(R_{\%p})^{\alpha}\}\times\frac{d}{1+\left(\frac{L}{L(R)}\right)}$
Differential Equation Approach [31]	where $\beta=k[\alpha+b(1-r_{\%p})]d_{\text{eff}}$ and $\mu=\frac{R_{\%p}}{\alpha+b(1-r_{\%p})}$	$A_{\%p}=\mu[S(R_{\%p})]$ and, $S(R_{\%p})=\beta(R_{\%p})^{\alpha-1}$

Appendix 2: Sites pictures of Icheon station for terrestrial microwave links

Figure 2(a): Khumdang, KT Station

Figure 2(b): Icheon, RRA Station

Figure 2(c): OTT parsivel

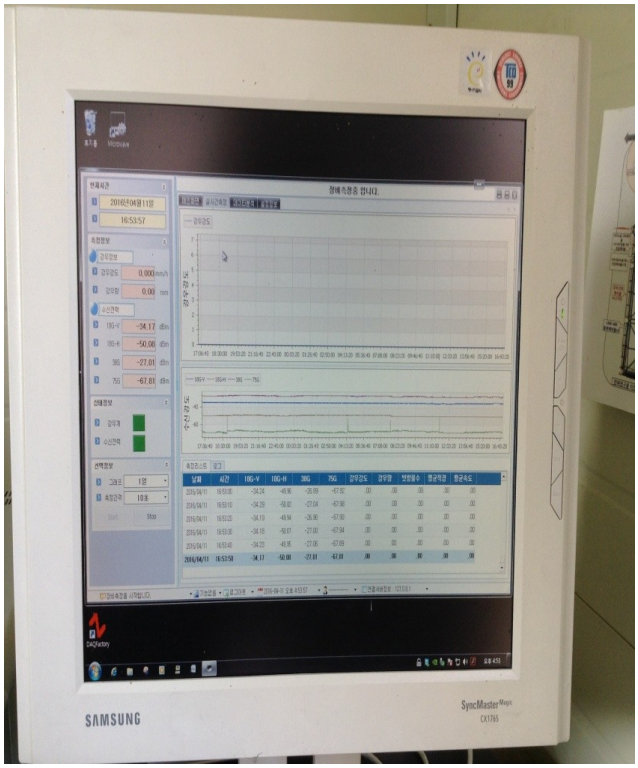

Figure 2(d): Measurement system

Appendix 3: Sites pictures of Mokdong station for satellite communication links

Figure 3(a): Parabolic antenna for 12.25 and 20.73 GHz receiving beacon signal.

Figure 3(b): Parabolic antenna for 19.8 GHz receiving beacon signal.

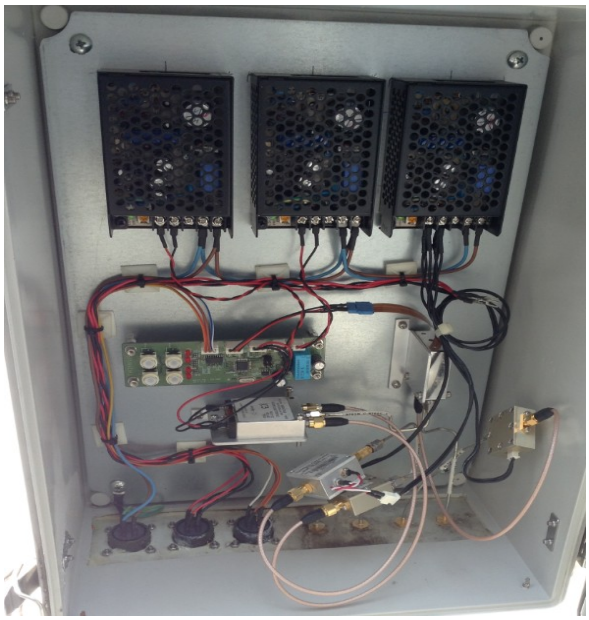

Figure 3(c): Beacon signals splitter.

Figure 3(d): Spectrum analyzer.

Contribution

The discussions mentioned in this thesis have been published in journals and conference proceeding and are mentioned below:

S.N	Manuscript	Journal	Status
1	Rain Rate Modeling of 1-min from various integration times in South Korea	SpringerPlus (SCIE)	Published
2	Study of Rain Attenuation in Ka Band for Satellite Communication in South Korea	Journal of Atmospheric and Solar Terrestrial Physics (SCI)	Published
3	Rain Attenuation statistics over Millimeter wave Bands in South Korea	Journal of Atmospheric and Solar Terrestrial Physics (SCI)	Published
4	Characterization of Rain Specific Attenuation and Frequency Scaling Method for Satellite communication in South Korea	International Journal of Antenna and Propagation (SCIE)	Published
5	Proposed One-Minute Rain Rate Conversion Method for Microwave Applications in South Korea	Journal of Information and communication convergence engineering (KCI)	Published
6	Study of Rain attenuation over Terrestrial Microwave links in South Korea	IET Microwave, Antenna and Propagation (SCI)	Minor Changes
7	Study of 1-minute rain rate integration statistic in South Korea	Journal of Atmospheric and Solar Terrestrial Physics (SCI)	Moderate Revision
8	Rain Attenuation study over 18 GHz Terrestrial Microwave link in South Korea	Journal of Atmospheric and Solar Terrestrial Physics (SCI)	Major Changes
9	Rain attenuation study at Ku Band over Earth-Space Path in South Korea	International Journal of Satellite Communications and Networking (SCIE)	Under Review
10	Diurnal and Monthly Variations of Rain Rate and Rain Attenuation on Ka-Band Satellite Communication in South Korea	KCA, KIEES competition paper (KCI)	Submitted
11	1-minute rain rate derivation from various integration times in South Korea	Conference (Thailand)	Published
12	Rain Specific Attenuation and Frequency Scaling approach in Slant-Path for Ku and Ka-Band Experiments in South Korea	Conference (Thailand)	Published

Acknowledgement

I wish to express my profound gratitude to my advisor, Professor Dong-You Choi who encouraged me and thoroughly supervised this work. His words of encouragement, guidance, his assistance in providing new books and necessary experimental database with unrelenting support have added to accomplish the successful completion to this research.

The support of Korea Meteorological Administration (KMA) is greatly acknowledged for providing the 1-min. rainfall amount data base of 93 locations of the South Korea which covers from 2004 till 2013. Similarly, the assistance of National Radio Research Agency (RRA) is also gratefully acknowledged for granting me with the terrestrial and earth-space communication links data base covering 2013 till 2015 for preparing Master Thesis.

My deep gratitude to my parent, Mr. Pradip Lal Shrestha, Mrs. Siddi Laxmi Taujale and sister Ms. Shilpa Shrestha and my family members for their love, understanding, moral support and encouragement during the period of this research.

My deepest thanks to my fellow lab mates, friends and colleagues, who helped me directly or indirectly for their continuous encouragement and support.

Finally, I thank to almighty God and further extend the acknowledgement to Basic Science Research Program through the National Research Foundation of Korea (NRF) funded by the Ministry of Education as well as to Chosun University for their support during the course of studies.